Title

PRODUCTION OF n AND w MESONS IN THE REACTION n+d-> (p)pn+n-n| BETWEEN 1.1 AND 2.4 GeV/c

Authors

Danburg, Jerome S.
Abolins, Maris A.
Dahl, Grin I.
et al.

Publication Date

1970

Submitted to Physical Review

UCRL-19272
Preprint

c. 2

PRODUCTION OF η AND ω MESONS IN THE REACTION $\pi^+ d \rightarrow (p)p\pi^+\pi^-\pi^0$ BETWEEN 1.1 AND 2.4 GeV/c

Jerome S. Danburg, Maris A. Abolins, Orin I. Dahl
Donald W. Davies, Paul L. Hoch, Janos Kirz,
Donald H. Miller, and Robert K. Rader

January 1970

AEC Contract No. W-7405-eng-48

LAWRENCE RADIATION LABORATORY
UNIVERSITY of CALIFORNIA BERKELEY

DISCLAIMER

PRODUCTION OF η AND ω MESONS IN THE REACTION $\pi^+ d \rightarrow (p)p\pi^+\pi^-\pi^0$ BETWEEN 1.1 AND 2.4 GeV/c.§ *

Jerome S. Danburg,† Maris A. Abolins,‡ Orin I. Dahl, Donald W. Davies,**
Paul L. Hoch, Janos Kirz,++ Donald H. Miller, and Robert K. Rader

Lawrence Radiation Laboratory
University of California
Berkeley, California 94720

January 1970

ABSTRACT

The reaction $\pi^+ d \rightarrow (p)p\pi^+\pi^-\pi^0$ has been studied in a bubble chamber experiment with pion beam momentum between 1.1 and 2.4 GeV/c; the exposure size was 14 events/μb.

The most significant features of the final state are production of η and ω mesons in the reactions

$$\pi^+ n \rightarrow \eta p,$$
$$\pi^+ n \rightarrow \omega p.$$

The η-production characteristics are well described by a Reggeized A_2-exchange model using Veneziano-type residue functions. The ω production and decay characteristics are presented, and it is found that a ρ-exchange model with absorptive corrections is inadequate to describe these data.

I. INTRODUCTION

The experiment reported here was performed in 1966 using a beam of π^+ mesons from the Bevatron incident on the deuterium-filled 72-inch Alvarez bubble chamber of the Lawrence Radiation Laboratory. The incident pion momentum covered the range from 1.1 to 2.4 GeV/c in eight settings. The beam used for this experiment has been described elsewhere.[1] A total of 264 000 pictures was taken; the incident momentum settings and the exposure size at each setting are given in Table I. The path-length numbers given in Table I were obtained by dividing the total number of events estimated to be on the film at each momentum setting by the total $\pi^+ d$ cross section as measured by other workers.[2] This procedure, as well as a more detailed exposition of the work discussed in this report, is given elsewhere.[3]

The main purpose of the experiment was to analyze reactions of the type

$$\pi^+ n \rightarrow pM^0,$$
$$M^0 \rightarrow \pi^+\pi^-, \text{ neutrals} \quad (1a)$$
or $$M^0 \rightarrow \pi^+\pi^+\pi^-\pi^-, \text{ neutrals}. \quad (1b)$$

Here M^0 is a neutral meson, and "neutrals" means any number of π^0's or γ's. The neutron target is obtained by filling the bubble chamber with deuterium.

This report deals primarily with the reaction

$$\pi^+ d \rightarrow pp\pi^+\pi^-\pi^0, \quad (2)$$

and in particular with the production and decay

of η and ω mesons via the reactions

$$\pi^+ d \rightarrow pp\eta, \quad \eta \rightarrow \pi^+\pi^-\pi^0, \tag{3}$$

$$\pi^+ d \rightarrow pp\omega, \quad \omega \rightarrow \pi^+\pi^-\pi^0. \tag{4}$$

Reaction (1.4) is explored beginning at threshold for ω production.

Section II discusses the scanning and measuring of the bubble chamber photographs and the fitting of the events. Section III is devoted to some of the complications arising from the use of a deuteron target. In Section IV we display various mass spectra for reaction (2) and give the cross sections for η and ω production in reactions (3) and (4). Section V gives the η production and decay characteristics in reaction (3), and Section VI presents production and decay information for ω mesons in reaction (4). Section VII is a compilation of literature on π^+d experiments performed with bubble chambers.

II. SCANNING, MEASURING, AND FITTING

The entire sample of film was scanned once for all three- and four-pronged events. A total of 128 000 four-pronged and 93 000 three-pronged events was found. A check scan of a small sample of the film revealed that the overall single-scan efficiency for finding three- and four-pronged events was 95%.

Of the events found, all but the three-pronged events at the beam momentum settings 1.70 and 1.86 GeV/c were measured, on Spiral Reader[4] measuring machines I and II of the Lawrence Radiation Laboratory. The average measuring rate for the events described here was 80 events per hour.

The track coordinates produced from the measurements by the program POOH were reconstructed in space and fitted to the hypotheses listed below by the standard Alvarez-Group program package TVGP-SQUAW.[5] Bubble density information for the tracks was provided by the Spiral Reader in the form of pulse heights; this information was used for each kinematic hypothesis to do a separate fit to the expected bubble density of all tracks. This procedure was incorporated into SQUAW with the program BUBBLE.[6]

The three- and four-pronged events were fitted to the following reaction hypotheses:

$$\pi^+ d \rightarrow pp\pi^+\pi^-, \tag{5}$$
$$pp\pi^+\pi^-\pi^0, \tag{6}$$
$$pp\pi^+\pi^-(\text{mm}), \tag{7}$$
$$pp\pi^+\pi^-\gamma, \tag{8}$$
$$ppK^+K^-, \tag{9}$$
$$np\pi^+\pi^+\pi^-, \tag{10}$$
$$p\pi^+\pi^+\pi^-(\text{mm}), \tag{11}$$
$$\pi^+\pi^+\pi^+\pi^-(\text{mm}), \tag{12}$$
$$d\pi^+\pi^+\pi^-, \tag{13}$$
$$d\pi^+\pi^+\pi^-\pi^0. \tag{14}$$

After completion of the fitting process, most events were found to have a successful fit to more than one hypothesis. The selection of the correct hypothesis was performed by the program CREE,[7] a version of the program ARROW. The details of the separation procedure are set forth in Ref. 3.

At this point we restrict our interest to those examples of reaction (6) which appear as four-pronged event topologies, i.e., those for which both the final-state protons had sufficient laboratory-frame momentum to be visible in the bubble chamber. (The lower cutoff on proton lab momentum was found to be approximately 85 MeV/c; this momentum yields a track 0.15 cm long in space, which is the practical lower limit of visibility. In the physics data that follow in this report, we use only those events which are assigned to reaction (6) and in addition fulfill the following criteria:

(a) the confidence level for the kinematic fit is greater than 1%,

(b) the confidence level for the ionization fit is greater than 1%,

(c) all track measurements were available for the kinematic fit (i.e., "constraint-reduced" events were not used),

(d) the event occurred within a preselected fiducial volume of the bubble chamber, and the dip and azimuth of the beam track for the event lay within preselected limits for each momentum setting.

Events fulfilling these criteria will be referred to as "good" events; there are about 15 500 such events.

Examination of the results of hypothesis separation shows that:[3]

(a) events assigned to reaction (6) are neither contaminated by nor lost into the four-constraint final state $pp\pi^+\pi^-$;

(b) about 4% of the events assigned to reaction (6) are actually from the final state $pp\pi^+\pi^-$(mm), but no events from reaction (6) are assigned to this zero-constraint channel;

(c) the events assigned to reaction (6) contain about half the η events from $\pi^+ d \to pp\eta$, $\eta \to \pi^+\pi^-\gamma$, and almost all the η' events from the analogous decay; these events actually belong to the channel (8). The total number of these events is less than 100, and account has been taken of them in calculating the η-production cross section. Furthermore, no events from reaction (6) are assigned to channel (8);

(d) about 4% of the events assigned to reaction (6) (at all energies) are actually events from the one-constraint reaction (10); no events from reaction (6) are lost into channel (10). Furthermore, when the "spectator" lab momentum restriction $p_{spec} < 300$ MeV/c (see below) is placed on the events assigned to reaction (6), the contamination of this sample by events from reaction (10) is only 2%, independent of energy.

Since the cross sections for η and ω production are found by comparing the number of resonant (η or ω) events in channel (6) with the total number of events in channels (5) through (8), it is important that no events from reaction (6) are assigned to other channels. In addition, the determination of the resonant cross sections is unaffected by the contamination mentioned in point (b) above, since the contaminating events should not lie preferentially inside the resonant three-pion mass bands. Furthermore, any cross-mixing among the events from channels (5), (7), and (8) does not affect the cross-section determination; hence, for instance, it is unimportant that most of the events assigned to reaction (8) probably are misassigned examples of reaction (5). However, the contamination of the $pp\pi^+\pi^-\pi^0$ events mentioned in point (d) must be considered in calculating the η and ω cross sections.

Figure 1 shows the missing-mass-squared distribution for "good" $pp\pi^+\pi^-\pi^0$ four-pronged events. In Fig. 2 are shown the confidence level distributions for the kinematic and ionization fits separately. At this point we remark again that events in the leftmost bin in Fig. 2a and in Fig. 2b are not included in the sample of "good" events.

III. THE DEUTERON TARGET

The use of deuterium in the bubble chamber in this experiment is, of course, necessitated by the need for a neutron target. The deuteron is a bound composite of a proton and a neutron, and although the binding energy is only 2.2 MeV, a number of important effects must be taken into account when the neutron in the deuteron is used as the target particle.

A. The Hulthén Wave Function and Spectator Momentum Distributions

A wave function commonly used to describe the separation r of the nucleons in the deuteron is that proposed by Hulthén.[8] It is

$$\psi(r) = C(e^{-\alpha r} - e^{-\beta r})/r.$$

Here C is a normalization constant, and

α = 45.5 MeV = (4.33 fermi)$^{-1}$ = $(2\mu B)^{1/2}$,

with

μ = reduced mass = $M_{nucleon}/2$,

B = deuteron binding energy = 2.2 MeV;

β is often taken to be $\beta = 7\alpha$ (Ref. 9) or $\beta = 5.18\alpha$ (Ref. 10). In all applications of the Hulthén wave function in this report, the average value $\beta = 6.09\,\alpha$ is used.

The Fourier transform of $\psi(r)$ gives the distribution $\phi(p)$ of the momentum of the two nucleons in the deuteron; it is

$$p^2\phi^2(p) = C'p^2[1/(p^2+\alpha^2) - 1/(p^2+\beta^2)]^2.$$

Experimentally $p^2\phi^2(p)$ can be measured when the impulse approximation for the $\pi^+ d$ collisions is assumed. This means that the π^+ is assumed to interact with only one of the nucleons in the deuteron, the other nucleon going off after the collision with the same momentum it had before the collision.

For the reaction $\pi^+ n(p) \rightarrow (p)p\pi^+\pi^-\pi^0$ the notation (p) means that one final-state proton is assumed to be a "spectator" to the collision between the π^+ and the neutron. The final-state proton with the lower lab momentum is taken to be the spectator. Figure 3 shows the experimental distribution of spectator momentum; the steep cutoff in the distribution around 85 MeV/c is due to the fact that only events with two visible protons (four-pronged events) are used. The curve is the Hulthén distribution $p^2\phi^2(p)$ normalized to have the same area as the histogram between 110 and 160 MeV/c. A deviation from the Hulthén wave function is exhibited as an excess of events with high momentum, that is, with momentum greater than 300 MeV/c, which is the practical upper cutoff of the Hulthén distribution. Forty-four per cent of the four-pronged events in Fig. 3 have momentum greater than 300 MeV/c. Reference 3 contains a discussion of some possible causes for the excess of high-momentum spectators.

B. The Flux Factor, Spectator-Beam Angle, and c.m. Energy Smearing

The internal motion of the two nucleons bound in the deuteron gives rise to two interesting effects. We discuss first the effect of this motion on the experimentally measured angle between the spectator nucleon and the incoming pion beam.

The proton and neutron bound in the deuteron move at random in opposite directions with momentum given by a function like the Hulthén distribution. Because of the random nature of the motion, some authors[11, 12] have stated incorrectly that the experimentally measured angle between the beam and the spectator nucleon should have an isotropic distribution. This statement, however, fails to take into account the fact that when the target particle is moving toward the beam, there is a greater particle flux and hence a higher reaction rate than when the target particle is receding from the beam. Let θ be the angle between the spectator and the beam. Since the target nucleon and the spectator nucleon in the deuteron move in opposite directions to conserve momentum, there will be more events for which $\cos\theta$ is greater than 0 for $\cos\theta$ less than 0 provided the cross section is constant.

The experimental distribution can be predicted by using the invariant flux factor of Møller[13] to account for the variation of particle flux with the relative motion of the beam and the target particle; it is

$$f = [(p_b \cdot p_t)^2 - m_b^2 m_t^2]^{1/2}/(m_b m_t)$$

Here the momenta p_b and p_t are four-vectors,

and the subscripts b and t refer to the beam and the target particle, respectively. The four-vector of the target particle is taken to be that of the deuteron minus that of the spectator nucleon.

In order to see what sort of distribution is predicted for the cosine of the angle between the spectator and the beam. Monte Carlo calculations were performed and $\cos\theta$ histogrammed for incoming pion momenta of 1.0, 1.5, and 2.0 GeV/c separately, assuming the nucleons in the deuteron are moving in a random direction with equal and opposite momenta described by the Hulthén distribution. Figure 4 shows the results of the Monte Carlo experiment performed for a beam momentum of 2.0 GeV/c. Figure 4a is the histogram of $\cos\theta$ for all events, and Fig. 4b is that for proton spectator lab momentum greater than 85 MeV/c, corresponding to the four-pronged events of this report. The nonisotropy of the distributions is evident. In fact, very similar histograms are obtained for all three Monte Carlo experiments. The histograms for incident momentum between 1.0 and 2.0 GeV/c are well approximated by a linear dependence on $\cos\theta$; it is $f(\cos\theta) = 1 + 0.10\cos\theta$ for all events, and for only those events with spectator momentum greater than 85 MeV/c,

$$f(\cos\theta) = 1 + 0.16\cos\theta \qquad (15)$$

Figure 5 displays the comparison between the experimental distribution in $\cos\theta$ (the angle between the spectator and the beam) and the distribution given by the flux factor. Figure 5a shows the distribution in $\cos\theta$ for all "good" events of the final state $pp\pi^+\pi^-\pi^0$; the straight line is Eq. (15) normalized to have the same area as the histogram. In Fig. 5b only the events with spectator momentum less than 300 MeV/c are included, and here it is seen that the agreement between the data and the flux-factor prediction is good. The spectator distribution of Fig. 3 and the $\cos\theta$ distribution of Fig. 5b indicate that events with spectator momentum less than 300 MeV/c conform well to the expectations of the impulse model.

It should be emphasized that the above prediction for the distribution of $\cos\theta$ holds only if the cross section is assumed to be constant over the range of c. m. energies produced in the collisions. This is because the number of events is proportional to the particle flux times the cross section. However, the assumption of roughly constant cross section is valid for the $pp\pi^+\pi^-\pi^0$ channel, as is discussed in Ref. 3.

Another important effect arising from the motion of the nucleons in the deuteron is the smearing of the center-of-mass energy distribution. In a collision of a beam with a stationary target nucleon, there is a unique c. m. energy corresponding to the beam momentum. When one of the nucleons in the deuteron is the target, however, there results a broad spectrum of c. m. energies due to the fact that the target nucleon has a range of momentum and is moving in a random direction with respect to the beam. The c. m. energy for the collision is

$$E_{c.m.} = [(p_b + p_d - p_s)^2]^{1/2}.$$

The momenta here are four-vectors, and the subscripts b, d, and s refer to the beam, deuteron, and spectator, respectively. The motion of the target nucleon results in a c. m. energy spectrum with a total width of 300 MeV from a monoenergetic beam with a momentum typical for this experiment (p = 1.5 GeV/c).

Figure 6 shows the c. m. energy spectrum for all "good" four-pronged events in the final state $pp\pi^+\pi^-\pi^0$ with spectator momentum less than 300 MeV/c. It is seen that the eight incident momenta between 1.1 and 2.4 GeV/c yield a continuous coverage of the c. m. energy range from 1.7 to 2.3 GeV.

C. Glauber Screening

In a very intuitive sense one can understand that the cross section for a beam colliding with a deuteron is less than the sum of the cross sections for a collision with each of the two nucleons in the deuteron separately. If the target deuteron is imagined to be two hard spheres close together, clearly part of the time one of the spheres occludes the other, reducing the effective cross section. Glauber[14] has derived the expression

$$\sigma(\pi d) = \sigma(\pi n) + \sigma(\pi p) - \sigma(\pi n)\sigma(\pi p)/4\pi\langle r^2\rangle, \quad (16)$$

where $\langle r^2\rangle$ is the average squared separation between the two nucleons. Wilkin[15] has since derived a modified formula which exhibits charge independence; he shows that the correction term should be

$$\left[\sigma(\pi n)\,\sigma(\pi p) - (1/4)[\sigma(\pi p) - \sigma(\pi n)]^2\right]/(4\pi\langle r^2\rangle) \quad (17)$$

for a charged-pion beam.

Recently accurate cross sections have been published[2] for π^+ and π^- incident on protons and deuterium over a wide range of energies. From Ref. 2 it is seen that over the range of incident momenta of this report, we have the total cross sections

$\sigma(\pi^{\pm}p) \approx 30$ mb,

$\sigma(\pi^- p) \approx 35$ mb $= \sigma(\pi^+ n)$, by charge symmetry.

Since $[\sigma(\pi^+ p) - \sigma(\pi^+ n)]^2 \approx (5\text{ mb})^2$ is small compared with $\sigma(\pi^+ p)\,\sigma(\pi^+ n)$, the correction factor of Wilkin (Eq. 17) is almost the same as the non-charge-independent correction factor of Eq. (16). From Ref. 2 it is also seen that over our range of incident momentum, $\langle r^{-2}\rangle \approx 0.02\text{ mb}^{-1}$. The typical value of the cross-section defect in this experiment due to Glauber screening is, from Eq. (16), approximately 1.7 mb; that is, the sum of the $\pi^+ n$ and $\pi^+ p$ cross sections is more than the $\pi^+ d$ cross section by about 1.7 mb, or 2.4% of the total $\pi^+ d$ cross section.

How this cross-section defect is to be applied to the various final-state channels is unknown. The method of Section IV for obtaining cross section for η and ω production in the final state $pp\pi^+\pi^-\pi^0$ is valid if the final states (5) through (8) are each depleted by the same fraction. But even if these channels are not all depleted due to Glauber screening in the same proportion, the difference in fractional depletion should not be more than the total depletion itself. Since a difference in depletion among channels (5) through (8) of $\approx 2.4\%$ is much smaller than the statistical cross-section errors obtained, the Glauber screening correction has no effect on the η and ω cross-section determination.

D. The Pauli Exclusion Principle and Final States With Two Protons

One can easily see that the Pauli exculsion principle has an effect on final states containing two protons. In particular, imagine a very glancing ($t \approx 0$) charge-exchange collision of the π^+ beam with the neutron in the deuteron in which the neutron spin is not flipped. After this hypothetical charge-exchange collision there are two protons close together in a spatially symmetric spin-1 configuration. Since this configuration of two identical fermions is symmetric, it is forbidden by the Pauli exclusion principle. Thus it is seen that in the limit of no momentum transfer, such a charge-exchange collision cannot occur in the absence of nucleon spin flip.

The effect of the Pauli exclusion principle on charge-exchange scattering on the neutron in the deuteron has been calculated for $K^+ d$ scattering.[16,17] The expression for the measured cross section when there are two final-state protons is[17]

$$d\sigma/d\Omega = [1 - H(q)]\,(d\sigma/d\Omega)_{nf} + [1 - H(q)/3]\,(d\sigma/d\Omega)_{sf}. \quad (18)$$

Here the subscripts nf and sf denote the non-spin-flip and spin-flip cross sections respectively, $q = (-t)^{1/2}$ is the momentum transfer in the collision, and H(q) is the deuteron form factor, defined as

$$H(q) = \int |\psi(r)|^2 e^{-iq\cdot r} dr.$$

Equation (18) applies to the final state $pp\pi^+\pi^-\pi^0$ discussed here; it tells us how to correct the production angular distribution of the three pions for the suppression due to the Pauli principle. Let us restrict our attention to the specific reactions

$$\pi^+ d \rightarrow pp\eta \text{ (or } \omega),$$
$$\eta \text{ (or } \omega) \rightarrow \pi^+\pi^-\pi^0,$$

since it is the production angular distributions for only the resonance events whose exact form form we are interested in.

Figure 7 shows the deuteron form factor H(q), calculated using the Hulthén wave function; it has the functional form[16]

$$H(q) = \left[2\alpha\beta(\alpha+\beta)/(\beta-\alpha)^2 q\right] \times \left[\tan^{-1} q/2\alpha + \tan^{-1} q/2\beta - 2\tan^{-1} q/(\alpha+\beta)\right].$$

From the figure it is seen that H(q) is appreciably different from zero only for $-t < 0.1$ GeV^2, and it is only for this range of momentum transfer squared that the effects of the Pauli exclusion principle are important. In Sections V and VI of this report, where η and ω production are discussed, the production angular distributions are presented as distributions of 20 bins in production cosine; in all the production angular distribution histograms, the two forwardmost of the 20 bins, $(0.8 < \cos\theta < 0.9)$ and $(0.9 < \cos\theta < 1.0)$, cover the momentum-transfer-squared range out to at least 0.1 GeV^2. Thus it is only the forwardmost two bins that are affected noticeably by the Pauli principle, and the calculation of the effect is, for simplicity, restricted to this angular region. We define the suppression factors $f_{nf} = 1 - H(q)$, $f_{sf} = 1 - H(q)/3$ taken from Eq. (18). Table II gives the values of these factors averaged over the production cosines of the forwardmost two bins (each bin is 0.1 wide in production cosine) separately for the reactions $\pi^+ d \rightarrow pp\eta$ and $\pi^+ d \rightarrow pp\omega$. It is seen that f_{nf} is significantly less than unity in the production cosine interval (0.9, 1.0) for the energies encountered in this experiment, and thus implies a large correction. The suppression factors are to be treated as detection efficiencies in the production cosine interval indicated, the events in that interval being divided by the appropriate factor (or combination of factors) to get the number of events that would be found if the beam had collided with a free neutron. To make the correction, however, one must know the relative sizes of the spin-flip and non-spin-flip cross sections. For this reason the application of Table II in correcting the η and ω production angular distributions is deferred until Sections V and VI, where we infer from the shapes of the production angular distributions the relative importance of the spin-flip and non-spin-flip contributions.

The upward corrections obtained above are not expected to increase the η and ω cross sections obtained in Section IV, however. This is because in Section IV these resonance cross sections are obtained by normalizing to the sum of the known cross sections for the charge-symmetric counterparts to reactions (5) through (8). All these reactions have two protons in the final state, however, and depending upon the particular form of the production angular distribution in each final state, all should be corrected upward to account for the Pauli principle. The forwardmost two production bins, which contain not more than 20% of the events for any of reactions (5) through (8), would be corrected upward typically by about 15%, so that there would be in general a correction of less than about 3% to the total number of events in any channel. This percentage probably does not vary much for the four final states used for

normalization, so the cross section obtained for the resonant part of reaction (6) would not be significantly affected by the Pauli principle.

IV. THE FINAL STATE $(p)p\pi^+\pi^-\pi^0$: GENERAL CHARACTERISTICS

In this section attention is focused on resonance production in the final state $(p)p\pi^+\pi^-\pi^0$, in which it is explicitly assumed that one of the final-state protons, designated as (p), is a spectator to the reaction

$$\pi^+ n \rightarrow p\pi^+\pi^-\pi^0. \qquad (19)$$

In order to help assure that this is the case, only those "good" examples of final state (6) which have at least one proton with lab momentum less than 300 MeV/c are used in the discussion of this section and the two following sections on η and ω production. Spectator protons with momentum less than 300 MeV/c do indeed conform well to the predictions of the impulse model, as was seen in the preceding section, particularly from Fig. 3 and 5b. There are 8710 events satisfying the above criteria.

A. Mass Spectra

Figure 8 shows the most important features of reaction (19). Figure 8a is a scatter plot of c.m. energy vs the three-pion mass; a prominent η band at mass 549 MeV/c^2 and a very strong ω band at about 785 MeV/c^2 characterize the data. The resonant signals show up as large peaks in the three-pion mass spectrum of Fig. 8b, the lower histogram of which shows the spectrum for events in which -t (from the beam to the three pions) is less than 0.6 GeV^2. It will be seen below that this mass spectrum and all others are well described by a fit which includes η and ω production in the three-pion mass spectrum as the only resonances present.

The three-pion mass spectrum is now investigated more closely. In order to find the amounts of η and ω as a function of c.m. energy, the data were divided into six c.m. energy intervals, each of which is 100 MeV wide, centered at the values $E_{c.m.}$ = 1.8, 1.9 2.0, 2.1, 2.2, and 2.3 GeV. For each interval a separate maximum-likelihood fit to the data was performed using the program MURTLEBERT.[18] The amount, mass, and width of the two resonances were determined by the fit; the values obtained are given in Table III. Because the η and ω widths are larger than the established values of the widths of these resonances,[19] the line shape used in the fits was Gaussian, and the widths in Table III are full width at half maximum. Inclusion of $\Delta^{++}(1236)$ in the maximum-likelihood fitting procedure was found to indicate production of only a few per cent of this resonance, with large errors on its amount and width; in addition, the η and ω parameters were the same whether or not $\Delta^{++}(1236)$ was included in the fit, so for simplicity this resonance is ignored in Table III.

Each of Fig. 9 through 18 shows a mass spectrum from reaction (19) at the six c.m. energy intervals; the curves are the Monte Carlo predictions of the maximum-likelihood fits summarized in Table III. With the exception of the $p\pi^+$ spectrum, all the mass distributions are well described by a fit involving only η and ω signals in the three-pion mass spectrum.

The momentum transfer squared between the beam and the three pions in reaction (19) is plotted vs three-pion mass in Fig. 19. All c.m. energies are combined in the plot, so that there is not a well-defined boundary, as there would be if the c.m. energy had a single value. Therefore the distribution of points in the vertical direction is not equivalent to the production angular distribution. However, it is apparent from the figure that ω's are produced out to -t of more than 1.5 GeV^2, whereas

η production occurs only out to about $-t = 1\ \mathrm{GeV}^2$.

Although there is no obvious structure in the three-pion mass spectra of Fig. 8 and 9 above the ω mass, we have examined the possibility of the presence of the H(990), ϕ(1019), and A mesons, all of which have $\pi^+\pi^-\pi^0$ modes reported. However, it was found that whether or not the mass of any two of the pions was constrained to lie in the ρ band, no evidence for any of these mesons was found. In the case of the three-pion decay of the ϕ, limited statistics prevented a conclusive determination. See Ref. 3 for a description of this analysis.

B. Cross Sections for the Reactions $\pi^+n \to p\eta$, $\pi^+n \to p\omega$

The cross sections for η and ω production were obtained by calculating the ratio R_{res} of the number of resonance (η or ω) events to the number of events fitting reactions (5) through (8), the sum of whose cross sections is required by charge symmetry to be equal to the sum of the cross sections (call this sum σ_{sum}) for the processes

$$\pi^-p \to \pi^+\pi^-n, \qquad (20a)$$

$$\to \pi^+\pi^-(\mathrm{mm}). \qquad (20b)$$

The resonance cross section is then $R_{res}\,\sigma_{sum}$. The cross sections for reactions (20) have been measured elsewhere[20] over the energy range of this experiment; the values of σ_{sum} used here are given in Table IV. Identical "event goodness" and spectator momentum cuts were made on all of reactions (5) through (8), and the fraction of η and ω events in reaction (6) was determined in 13 different c.m. energy intervals, each 50 MeV wide, centered at the values 1.75, 1.80, 1.85, $\cdots$, 2.35 GeV. The maximum-likelihood method was applied to find the fraction of η and ω events; in this series of fits the resonance masses were set at the average values seen from Table III ($m_\eta = 549\ \mathrm{MeV/c^2}$, $m_\omega = 785\ \mathrm{MeV/c^2}$), and the widths as a function of c.m. energy were also obtained from Table III (interpolating where necessary). The cross section σ_{sum} was calculated by interpolating from Table IV.

To find cross sections for the processes

$$\pi^+n \to p\eta, \qquad (21a)$$

$$\to p\omega, \qquad (21b)$$

the data were corrected for the branching ratios[19]

$$[\eta \to \pi^+\pi^-\pi^0(\mathrm{or}\ \gamma)]/(\eta \to \mathrm{all}) = 0.29, \qquad (22a)$$

$$(\omega \to \pi^+\pi^-\pi^0)/(\omega \to \mathrm{all}) = 0.90. \qquad (22b)$$

In the calculation account was taken of the fact that most but not all of the events with a $\pi^+\pi^-\gamma$ decay of the η were included in the events assigned to reaction (6). In fact, from the $\pi^+\pi^-\gamma$ mass spectrum of the "good" events with $p_{spec} < 300$ MeV/c assigned to reaction (8) we estimated that 26 $\eta \to \pi^+\pi^-\gamma$ events are assigned to this reaction. The maximum-likelihood fits described above showed that there are about 318 η events in reaction (6), so a correction factor of 344/318 = 1.08 must be applied to the η cross section, since the branching ratio (22a) is used in the calculation. Furthermore, an examination of the $\pi^+\pi^-\gamma$ mass spectrum as a function of c.m. energy shows that the correction factor of 1.08 is independent of $E_{c.m.}$, and so it has been applied at each c.m. energy value.

As is discussed in Section III, the Glauber screening of the target neutron by the spectator proton and the effect of the Pauli exclusion principle in suppressing low-momentum-transfer processes should affect the cross section determination only insignificantly. The reason for this is basically that all the reactions (5) through (8), which serve as the normalization cross section, are affected in similar proportions, so that the ratio of the number of resonant events to the number of normalization events is unaffected to a first approximation; in Section III a more complete discussion is presented.

The main uncertainty in the method arises from the spectator momentum cut ($p_{spec} < 300$ MeV/c) applied to all the events used in the cross-section determination. Each of reactions (5) through (8) has a somewhat different fraction of events with spectator momentum above 300 MeV/c, so that a different fraction of events is excluded from each reaction. However, as was stressed at the beginning of this section, events with spectator momentum less than 300 MeV/c conform well to the expectations of the impulse model, so that for each of the normalization reactions only those events are used for which it is likely that the target particle is a neutron rather than the entire deuteron. Still, if scattering of the final-state pions on the spectator nucleon in reactions (5)–(8) is the cause of most of the high-momentum spectators, then differences in the amount of this scattering among the normalization reactions will lead to a systematic error caused by excluding different fractions of events for the different reactions (5)–(8). This systematic error could not be large, however, since the normalization reactions all have similar fractions of high-momentum spectators.

It was noted in Section II that about 2% of reaction (6) is actually contamination from reaction (10), independent of energy. Reaction (6) accounts for about 40% of the normalization reactions (5)–(8), so that this contamination is about 0.8% of the normalization events. Therefore the cross sections for η and ω production have been increased by this percentage.

Table V shows the cross sections obtained as described above for reactions (21). The errors take into account the uncertainty in the resonance fractions and the errors in the normalization cross section of Table IV. As stated above, the cross sections are corrected for unseen η and ω decay modes.

The cross section for η production has been measured elsewhere, both for reaction (21a) itself (by Bacon et al.[21] and by Litchfield[22]) and for its charge-symmetric counterpart, $\pi^- p \to \eta n$ (by Jones et al.,[23] Bulos et al.,[24] Richards et al.,[25] Deinet et al.,[26] Crouch et al.,[27] Wahlig and Mannelli,[28] and Guisan et al.[29]), which should have the same cross section. Likewise the cross section for reaction (21b) has been measured at other energies, although much less extensively, both for process (21b) itself (by Kraemer et al.,[30] Bacon et al.,[21] Miller et al.,[11] and Benson[12]) and for its charge-symmetric version (by Boyd et al.[31]). Figure 20a is a logarithmic plot of the η cross section measured in this experiment, along with the data points of Bulos et al., Bacon et al., and Guisan et al. For the sake of clarity, the other measurements listed above are not included in the figure. In general all the experiments listed, including the one described here, agree as to the total cross section where they overlap with one another; an exception is the discrepancy between the total cross-section values reported by Crouch et al. and Guisan et al. Figure 20b shows the ω cross-section points of this experiment along with the data of Kraemer et al., Bacon et al., Boyd et al., Miller et al., and Benson, which for the most part do not overlap with those of this report.

V. η PRODUCTION AND DECAY IN THE REACTION $\pi^+ n \to \eta p$

The discussion of η production and decay presented in this section is based on 349 low-background events in the η mass band that decay as $\eta \to \pi^+\pi^-\pi^0$ (or $\pi^+\pi^-\gamma$). (About 10% are estimated to be $\pi^+\pi^-\gamma$ decays; see Section IV.) The mass cut for the η selection is $530\ \text{MeV/c}^2 < m(\pi^+\pi^-\pi^0) < 570\ \text{MeV/c}^2$. These events also satisfy the "goodness" criteria defined in Section II and have spectator proton

momentum less than 300 MeV/c. The cross section for η production as a function of c.m energy is given in the preceding section.

A. The η-Decay Dalitz Plot

Figure 21 is the Dalitz plot for the three-pion decay of 349 η-band events. The x axis is $\sqrt{3}(T_+ - T_-)/Q$, and the y axis is $(3T_0/Q) - 1$, where T_+, T_-, and T_0 are, respectively, the kinetic energies (in the three-pion rest frame) of the π^+, π^-, and π^0, and $Q = m_\eta - m_{\pi^+} - m_{\pi^-} - m_{\pi^0}$.

A topic of current interest is the violation of C-conjugation invariance in η decay into $\pi^+\pi^-\pi^0$ and $\pi^+\pi^-\gamma$;[32-34] an excess of events on either side of the vertical bisector of the η-decay Dalitz plot of the form of Fig. 21 is an indication of C violation. The fractional right-left asymmetry,

$$A = (R - L)/(R + L),$$

of the $\eta \to \pi^+\pi^-\pi^0$ Dalitz plot has been measured by many groups.[35-39] The asymmetry for the $\pi^+\pi^-\gamma$ decay of the η has also been measured (although with less precision than for the $\pi^+\pi^-\pi^0$ decay).[40-43]

The right-left asymmetry in the decay Dalitz plot of the η events in this report is $A = +0.032 \pm 0.054$.

The variation along the vertical direction in the density of points in the $\eta \to \pi^+\pi^-\pi^0$ Dalitz plot of Fig. 21 is a well-known feature of this decay, and it has been discussed as evidence for the existence of an intermediate $\pi^+\pi^-$ resonance in the decay.[44]

When the η decay into $\pi^+\pi^-\pi^0$ is fitted with a matrix element of the form

$$M(\eta \to \pi^+\pi^-\pi^0) = 1 + b(3T_0/Q - 1), \quad (23)$$

Price and Crawford[45] find $b = -0.45 \pm 0.05$, and Cnops et al.[46] find $b = -0.55 \pm 0.02$.

Figure 22 shows the variation of density of points with the y coordinate $3T_0/Q - 1$ for the Dalitz plot of Fig. 21. The y axis of Fig. 22 is the density of points relative to that expected for uniform population of the Dalitz plot. The density was calculated under the assumption that of the events in the η-mass cut, 86% are true η events, and the rest are background uniformly distributed over the Dalitz plot. The background estimate is explained below in the discussion of the η-production angular distributions. No account has been taken of the estimated 10% of the η events which are really $\pi^+\pi^-\gamma$ decays. The straight line is a good fit to the points in the figure and has a slope of -1. Since, from Eq. (23), we have $|M(\eta \to \pi^+\pi^-\pi^0)|^2 \approx 1 + 2b(3T_0/Q - 1)$ (assuming that b is real), this gives roughly $b = -0.50 \pm 0.05$ for the density variation factor for the η events in this experiment.

B. Production Angular Distributions for $\pi^+ n \to \eta p$

The production angle in this reaction is defined in the $\pi^+ n$ rest frame [the rest frame of the four-vector $p_{\pi^+} + p_d - p_{(p)}$] as the angle between the incoming π^+ beam and the outgoing $\pi^+\pi^-\pi^0$ momentum vector.

Appreciable numbers of events in the η band are found in the six 100-MeV-wide c.m. energy intervals centered at $E_{c.m.} = 1.7, 1.8, \cdots, 2.2$ GeV; the first interval has 19 events, and the rest contain between 40 and 80 events apiece. From the assumed Gaussian line shape of the $\pi^+\pi^-\pi^0$ mass spectrum in the η-mass region it is possible to estimate the fraction of background events in the η-mass cut in each c.m. energy interval, using the widths for the η signal given in Table III. The background fraction estimates are 0.15, 0.07, 0.13, 0.17, 0.11, and 0.19, for the c.m. energy intervals centered at 1.7, 1.8, 1.9, 2.0, 2.1 and 2.2 GeV, respectively. The overall background fraction for all the events in the η mass cut is 0.14. The three-pion production cosine distributions for three-pion masses somewhat above the η mass cut (there are very few events with three-pion mass below

the η band) are fairly flat at all c.m. energies. Assuming that the production angular distributions in this control region are the same as those of the background events in the η mass region, the background events (whose fractions are given above) were subtracted isotropically in production cosine from the production distributions for all events in the η band.

Figure 23 shows the production cosine distributions in the c.m. energy intervals mentioned above for events in the η band, with isotropic background subtracted in the amounts given above. The variable in the distributions is production cosine and not momentum transfer squared (-t), because the 100-MeV range of c.m. energies in each plot means that the maximum value of -t varies by typically 25% over the plot. As an aid in estimating the t distributions, Table VI shows $(-t)_{min}$ and $(-t)_{max}$ for the reaction $\pi^+ n \rightarrow \eta p$ at a series of c.m. energy values. In Fig. 23 the shaded areas in the forwardmost two bins are the estimated correction for the loss of events due to the Pauli exclusion principle. Section III contains a discussion of this effect; in particular, see Table IIb. From the presence of the forward dip in the η production cosine distributions, and from the fact that the nucleon spin-flip amplitude must vanish in the forward direction, whereas the non-spin-flip amplitude need not, it is assumed that the Pauli principle correction factors to be used for the η production cosine distributions are those for the spin-flip amplitude.

The sharpness of the forward dip in the η production cosine distributions suggests that the dip may be due to an experimental bias in the sample of events.[47] Because only four-pronged events (events with two visible final-state protons) are used for this report, it is plausible that events with low momentum transfer may be lost into the sample of three-pronged events in the following way: Since the target neutron, when it collides with an incoming π^+ and becomes a proton, is moving with a Fermi momentum of around 100 MeV/c in the laboratory system, it is possible that for low-momentum-transfer collisions many target neutrons are given just enough three-momentum to make the lab momentum of the final-state proton below 85 MeV/c. Such a proton does not produce a visible track, and the event, which would normally appear as a four-pronged event, is a three-pronged event and does not appear in the sample of η's shown here. A Monte Carlo experiment was programmed to investigate this effect over a few values of c.m. energies covering the c.m. energy range of this experiment. It was found that this bias affects only the forwardmost bin of any of the η production cosine distributions presented, and that the correction for events lost from this ben into the three-pronged events and into other production cosine bins due to identification of the wrong proton as spectator was at most 4%, and typically 2%. This correction cannot account for the sharpness of the forward dips seen in Fig. 23, and it is ignored because of its smallness. It is thus felt that the sharp forward dips seen in the figure are a real attribute of the data.

C. A Regge Description of the Reaction $\pi^+ n \rightarrow \eta p$ Using Veneziano-Type Residue Functions

A briefer account of the work in this section has appeared elsewhere.[48] The concentration of events near the forward direction ($\cos\theta = 1$) in Fig. 23 suggests a description of the production process in terms of a t-channel pole, that is, in terms of particle or Regge-pole exchange. The only known particle which can be exchanged in this reaction is the $A_2(1300)$ meson with spin-parity of 2^+.

The differential cross section for this reaction, in terms of the invariant amplitudes A and B,[49] is

$$\frac{d\sigma}{d(\cos\theta)}\ (\text{mb}) = \frac{0.3895\ M^2}{8\pi s}\ \frac{q_f}{q_i}\left\{\frac{p^2}{M^2}\,|A|^2 + \left[\left(\frac{s-u}{4M}\right)^2 + \frac{k^2 t}{4M^2}\right]|B|^2 - \left(\frac{s-u}{2M}\right)\mathrm{Re}(A^* B)\right\}.$$

Here s, t, and u are the usual Mandelstam variables, and

q_i = initial-state c.m. three-momentum,

q_f = final-state c.m. three-momentum,

k = t-channel meson momentum
$= \left\{[t-(m_\pi+m_\eta)^2][t-(m_\pi-m_\eta)^2]\right\}^{\frac{1}{2}}/2(-t)^{\frac{1}{2}}$,

p = t-channel baryon momentum
$= (M^2 - t/4)^{\frac{1}{2}}$,

M = nucleon mass.

All masses and momenta are in GeV. The Regge form of the invariant amplitudes A and B is the leading term in s of a Veneziano parameterization:[49]

$$A\ (\text{GeV}^{-1}) = a_0\Gamma[1-\alpha(t)]\left[1+e^{-i\pi\alpha(t)}\right](b's)^{\alpha(t)}, \qquad (24a)$$

$$B\ (\text{GeV}^{-2}) = b_0\Gamma[1-\alpha(t)]\left[1+e^{-i\pi\alpha(t)}\right](b''s)^{\alpha(t)-1}; \qquad (24b)$$

$\alpha(t)$ is the A_2 trajectory function, which is taken to be the straight-line form $\alpha(t) = 2 + b\,(t - m_{A_2}^2) = 2 + b\,(t - 1.69)$. This parameterization is similar to the standard Regge treatment of t-channel helicity amplitudes,[50] but the Veneziano model demands that $b'' = b' = b$ be the universal slope of the linear trajectories. Hence, when the universal slope b is taken from experiment to be 1 GeV^{-2}, A and B are prescribed up to the real constants a_0 and b_0, the only parameters of our fit.

A least-squares fit to the shape only of the η production angular distributions results in the choice

$$b_0/a_0 = 2.4 \qquad (25)$$

as the ratio of magnitudes giving the best fit, which is displayed upon the six production cosine distributions in Fig. 23. The curves on the production distributions all satisfy Eq. (25), but they are normalized separately to have the same area as the respective histogram in Fig. 23. It will be seen below, however, that a single choice of scale factor, i.e., a unique choice of a_0 and b_0, fits both the shape and absolute scale of all distributions. The zero in the curves at t = -1.3 GeV^2 occurs because the signature factors in amplitudes (24) go to zero when $\alpha(t)$ passes through -1.

The energy dependence of the total cross section for this reaction and its charge-symmetric counterpart has also been compared with the model. The cross sections of Ref. 21, 24, and 29, as well as the data points of this experiment, were used to test the validity of the energy dependence of the total cross section predicted by the model; these data points span the c.m. energy interval from threshold for the reaction up to almost 6 GeV, the highest energy at which it has been studied. Figure 24 is a plot of the total cross section for reaction (21a) and its charge-symmetric equivalent vs c.m. energy, along with the prediction of the Reggeized A_2-exchange model. With $b_0/a_0 = 2.4$, and the value of a_0 chosen so that the curve passes through the arbitrarily selected data point at $E_{c.m.} = 3.46$ GeV, the fit is seen to be very good over the entire range of energies. The energy dependence of the curves is seen to be quite sensitive to the value of b_0/a_0; agreement with the total-cross-section data is obtained only for the ratio b_0/a_0 within ± 5% of the value 2.4, which is the same ratio needed, within ± 10%, in order to fit the shape of the production angular distributions! Furthermore an A_2 trajectory slope of 1 GeV^{-2} ± 10% is necessary to fit the width of the experimental production cosine distributions, and this is in accordance with a universal trajectory slope of 1 GeV^{-2}.

The parameter values used to obtain the fit to the shape of our production angular distributions and to the total cross section over a wide range of energies are $a_0 = 28.7$, $b_0 = 68.8$.

Figure 25 shows the differential cross section $d\sigma/dt$ for

$$\pi^- p \rightarrow n\eta, \quad \eta \rightarrow \gamma\gamma \qquad (26)$$

from Ref. 29 at c.m. energies above 2.50 GeV, along with the predictions of the Reggeized A_2-exchange model; the curves are normalized to have the same area as the histograms. The agreement between most of the experimental distributions and the model is seen to be satisfactory; the total-cross-section points of this reference are in excellent agreement with the model, as is seen from Fig. 24. Figure 26 shows differential cross section measurements from two more experiments. In Fig. 26a the differential cross section measured by Benson[12, 51] is compared with the model. Here the agreement is quite good except for the greater number of events at large values of -t than is predicted by the model. However, it should be noted that the experimental distribution of Fig. 26a includes events from reaction (6) with spectator proton momentum greater than 300 MeV/c. These are events which are suspected not to arise from π^+ collisions with only one of the nucleons in the deuteron, and they are at the same time events which are likely to have large momentum transfer values, since both final-state protons have lab momentum greater than 300 MeV/c. It is further noted that the sharp forward dip in Fig. 26a is in disagreement with the equivalent distribution of Ref. 29 shown in Fig. 25b. Figure 26b is the differential cross section for reaction (26) determined by Wahlig and Mannelli[28] at $E_{c.m.} = 4.43$ GeV. The distribution is broader than the model predicts; in this connection it is noted that the equivalent distribution of Ref. 29 seen in Fig. 25d is narrower than that of Wahlig and Mannelli and more in agreement with the model, although both these sources obtain the same total cross section.

At the lower end of the energy spectrum Richards et al.[25] have measured differential cross sections for reaction (26) which are in excellent agreement with those of this report at the energy values where they overlap. Only in the differential cross section measurements of this reference around $E_{c.m.} = 1.55$ GeV, the mass value of the $N_{1/2}(1550)$ resonance,[19] do the data differ markedly from the predictions of the Reggeized A_2-exchange model.

The simple two-parameter Regge exchange model described here is thus sufficient to describe both the production angular distributions and the total cross section for reaction (21a) over a wide range of energies; this indicates that the t-channel process of A_2 exchange dominates the reaction from near threshold up to the highest energy for which data are available.

Reference 52 is a list of other Regge fits to this reaction, using different parameterizations.

VI. ω PRODUCTION AND DECAY IN THE REACTION $\pi^+ n \rightarrow \omega p$

The $\pi^+\pi^-\pi^0$ decay mode of the ω is the only one considered in this report, and an ω event is defined as one for which $750\ \text{MeV}/c^2 < m(\pi^+\pi^-\pi^0) < 820\ \text{MeV}/c^2$. Only those events are used which satisfy the "goodness" requirements of Section II and have proton spectator momentum less than 300 MeV/c. About 3100 such events lie in the ω mass band defined above; the background fraction in this cut is estimated to be 17%. The reader is reminded that the cross section for ω production as a function of c.m. energy is given in Section IV.

A. The ω-Decay Dalitz Plot

The Dalitz plot for the three-pion decay of 3116 ω-band events is shown in Fig. 27. T_+, T_-, and T_0 are the kinetic energies in the ω rest frame of the π^+, π^-, and π^0, respectively. The prominent feature of this Dalitz plot is the concentration of events near the center and the paucity of events near the boundary. This characteristic distribution of events in the Dalitz plot was used to determine the spin-parity of the ω as 1^- in the analysis of the experiment in which this meson was discovered and all its quantum numbers determined.[53] Since then Flatté et al.[54] have made a thorough analysis of more than 4600 three-pion ω decays and also conclude that the spin-parity of the ω is 1^-. The simplest matrix element for the decay of a 1^- particle into $\pi^+\pi^-\pi^0$ is $\underset{\sim}{p}_+ \times \underset{\sim}{p}_-$, where $\underset{\sim}{p}_+$ and $\underset{\sim}{p}_-$ are the momentum vectors of the π^+ and the π^- in the three-pion rest frame.[55] The prediction of this matrix element is displayed on the Dalitz plot of Fig. 27. The contours are lines of constant intensity; the center of the Dalitz plot has maximum probability, and the boundary is the contour of zero probability.

The fractional left-right asymmetry of the events on the ω Dalitz plot in this report is $A = (R - L)/(R + L) = -0.024 \pm 0.018$.

B. Production Angular Distributions for $\pi^+ n \to \omega p$

The production angle is the angle between the π^+ beam and the final-state $\pi^+\pi^-\pi^0$ momentum vector, in the initial-state $\pi^+ n$ rest frame.

Production cosine distributions were obtained for six 100-MeV-wide c.m. energy intervals centered at $E_{c.m.} = 1.8, 1.9, \cdots, 2.3$ GeV; the intervals contain between 200 and 750 events each. Using the Gaussian widths of the ω signals in these intervals (see Table III), we have estimated the background fraction in the ω mass cut for each interval of c.m. energy. The background estimates for the intervals centered at $E_{c.m.} = 1.8$, 1.9, 2.0, 2.1, 2.2, and 2.3 GeV are 0.18, 0.17, 0.20, 0.16, 0.11, and 0.14, respectively. The shape of the background production cosine distribution was presumed to be the same as that for three-pion combinations with masses above and below the ω mass. The sum of production cosine distributions for three-pion masses above ($830\ \text{MeV}/c^2 < m(3\pi) < 930\ \text{MeV}/c^2$) and below ($640\ \text{MeV}/c^2 < m(3\pi) < 740\ \text{MeV}/c^2$) the ω mass was found to be forward-peaked at all c.m. energies except 1.8 GeV. The shape of the production cosine distribution for these three-pion mass cuts is well approximated by the empirical function $b(\cos\theta) = 1 + h\,e^{-(1-\cos\theta)/0.25}$, where h varied between 1 and 5 (except h = 0 at 1.8 GeV). A background with this shape was subtracted from each production cosine distribution in the amount given by the fractions stated above.

Figure 28 gives the ω production distributions for six 100-MeV-wide c.m. energy intervals after subtraction of the estimated background. We note that the energy interval of Fig. 28a lies just above threshold for ω production. The shaded area in the forwardmost two bins is the estimated number of events suppressed at low momentum transfer by the Pauli exclusion principle. This effect is discussed in Section III. The fact that the production cosine distributions at the three highest energies have a somewhat flat forward peak suggests that the spin-flip as well as the non-spin-flip amplitude contributes. It was thus decided to take the average of the spin-flip and non-spin-flip Pauli suppression factors of Table IIa in making an upward correction to the two forwardmost production cosine bins at each energy. Table VII shows $(-t)_{min}$ and $(-t)_{max}$ for this reaction at a number of c.m. energy values so that the t-distributions can be estimated.

C. Decay Angular Distributions for $\omega \to \pi^+\pi^-\pi^0$

The decay of ω mesons from the reaction $\pi^+ n \to \omega p$ is described in the rest frame of the ω. The decay direction is the direction of the normal to the plane of the three decay pions. Correlation data for ω decay are given for two reference frames.

a. Jackson frame:[56]

Here the axes in the ω rest frame are defined as follows:

$\underset{\sim}{z}$ = direction of incoming beam,

$\underset{\sim}{y}$ = normal to production plane,

$\underset{\sim}{x} = \underset{\sim}{y} \times \underset{\sim}{z}$.

b. Helicity frame:

The axes in the ω rest frame are

$\underset{\sim}{z}$ = direction of flight of the ω,

$\underset{\sim}{y}$ = normal to the production plane,

$\underset{\sim}{x} = \underset{\sim}{y} \times \underset{\sim}{z}$.

In both definitions the normal to the production plane is taken to be $\underset{\sim}{b} \times \underset{\sim}{\omega}$, where $\underset{\sim}{b}$ is the three-momentum of the incident beam and $\underset{\sim}{\omega}$ is that of the outgoing ω meson.

The distribution of the normal to the three-pion plane in these two frames is given by[57]

$$W(\theta,\phi) = \frac{3}{4\pi}\left[\rho_{0,0}\cos^2\theta + \frac{1}{2}(1-\rho_{0,0})\sin^2\theta - \rho_{1,-1}\sin^2\theta\cos 2\phi - \sqrt{2}\,\mathrm{Re}(\rho_{1,0})\sin 2\theta\cos\phi\right] \quad (27)$$

Here $\rho_{i,j}$ are the elements of the ω spin density matrix.

The method of moments was used to determine the values of the density matrix elements. If the fraction of ω events in the ω mass cut is f, then under the assumption that the background events in the cut produce no decay correlations of the form given in Eq. (27), the density matrix elements are given by

$$\rho_{0,0} = \frac{1}{3} + \frac{1}{3}\left(\frac{5}{4\pi}\right)^{1/2} a_{20}/f,$$

$$\rho_{1,-1} = -\frac{1}{12}\left(\frac{30}{4\pi}\right)^{1/2} a_{22}/f,$$

$$\mathrm{Re}(\rho_{1,0}) = \frac{1}{12}\left(\frac{15}{4\pi}\right)^{1/2} a_{21}/f.$$

Here

$$a_{20} = \langle Y_2^0(\theta,\phi)\rangle = \left\langle \left(\frac{5}{4\pi}\right)^{1/2}\left(\frac{3}{2}\cos^2\theta - \frac{1}{2}\right)\right\rangle,$$

$$a_{21} = 2\langle \mathrm{Re}[Y_2^1(\theta,\phi]\rangle = 2\left\langle -\left(\frac{15}{8\pi}\right)^{1/2}\sin\theta\cos\theta\cos\phi\right\rangle,$$

$$a_{22} = 2\langle \mathrm{Re}[Y_2^2(\theta,\phi)]\rangle = 2\left\langle \frac{1}{4}\left(\frac{15}{2\pi}\right)^{1/2}\sin^2\theta\cos 2\phi\right\rangle,$$

where the $\langle Y_\ell^m\rangle$ are the averages of the spherical harmonics over the decay distribution.

At each c.m. energy the events were divided into production cosine intervals such that each interval contained about 100 resonance events. In each production cosine interval the maximum-likelihood fitting program MURTLEBERT[18] was used to estimate the fraction of ω events; the fit was performed leaving the ω mass and width to be found as well as its fraction. The assumption that only the ω events (and not the background) contribute to the moments of Y_2^0, $\mathrm{Re}(Y_2^1)$, and $\mathrm{Re}(Y_2^2)$ was strengthened by taking moments in the nonresonant mass band 830 MeV/c^2 < m(3π) < 930 MeV/c^2 for each c.m. energy interval and noting that these moments are consistent with zero. Since only ω events and background events, whose three-pion "decay" should be isotropic, are assumed to be present in the ω mass cut, only the three moments listed above should be nonvanishing. To check this prediction, all the moments of Y_ℓ^0, $\mathrm{Re}(Y_\ell^m)$, and $\mathrm{Im}(Y_\ell^m)$ for $\ell = 1, 2, 3$ were calculated, and it was seen that all moments, except the allowed ones, are consistent with zero in the ω band.

An independent check on the method was supplied by a series of maximum-likelihood fits, in which the decay correlation ceoefficients a_{20}, a_{21}, and a_{22} were included in addition to the ω amount, mass, and width. In a few production cosine intervals no solution could be obtained, since a few events

yielded negative likelihoods, but in all cases in which a solution was found, the coefficients were in excellent agreement with those determined from the moments analysis.

The density matrix elements quoted in this report are the ones found from the moments analysis.

Table VIII gives the density matrix elements in the Jackson frame found as described above, and Table IX gives those in the helicity frame. The errors take into account the uncertainty in the coefficients a_{20}, a_{21}, and a_{22} as well as that in the ω fraction. Figures 29, 30, and 31 show the density matrix elements $\rho_{0,0}$, $\rho_{1,-1}$, and $\mathrm{Re}(\rho_{1,0})$, respectively, in the Jackson frame. The curves in these figures are discussed below. Figures 32 through 34 display these density matrix elements in the helicity frame.

It is noted that the density-matrix values in the Jackson frame for $E_{c.m.} = 2.0$ GeV agree well with the values given by Bacon et al.[21] averaged over all production cosine. The Jackson frame values of $\rho_{0,0}$ are also similar to those found by Miller et al.,[11] Cohn et al.,[58] and Benson[12,51] at higher energies: typically $\rho_{0,0} \approx 0.5$, which implies a $1+\cos^2\theta$ decay distribution.

D. An Attempt to Describe the Reaction $\pi^+ n \to \omega p$ Using a ρ-Exchange Model With Absorption

The forward peaking of the production cosine distributions of Fig. 28 at the higher c.m. energies suggests that in this energy region, say for $E_{c.m.} > 1.9$ GeV, a description of the production process might be obtained in terms of particle or Regge-pole exchange. An exchanged meson must have I = 1, and of the four I = 1 possibilities (π, ρ, A_2, B), π and A_2 have the incorrect G parity. The ρ meson has a lower mass than the B meson and might at first consideration be expected to contribute more than the B.

The postulate of ρ exchange leads to the conclusion that $\rho_{0,0} = \mathrm{Re}(\rho_{1,0}) = 0$ in the Jackson frame.

It is clear from the nonvanishing values of $\rho_{0,0}$ in the Jackson frame in this and other experiments that the simple ρ-exchange process discussed above does not agree with the data. A way around the difficulty is the inclusion of absorptive corrections, that is, the inclusion of diffractive scattering of the initial- and final-state particles along with the ρ exchange. J. D. Jackson and his co-workers have developed a theory of particle exchange, including the effects of absorption; Ref. 56 is a list of papers expounding the theory and summarizing its comparisons with many experiments. The initial- and final-state absorption (diffractive scattering) not only change the value of $\rho_{0,0}$ from that expected according to simple ρ exchange, but also predict production angular distributions narrower than those predicted by the ρ propagator factor alone.

In essence, the initial- and final-state diffraction scattering processes each contribute to the overall process with a phase shift $\delta(\ell)$ given by $e^{2i\delta(\ell)} = 1 - C\, e^{-\gamma \ell^2}$, where, by analogy with diffraction scattering on a "gray" disk, C gives the "darkness" of the disk (C = 1 gives an opaque disk, C = 0 means no disk at all); and $\gamma = 2/k^2R^2$, where k is the particle momentum, R is the radius of the diffracting disk, and ℓ is the angular momentum. The parameters γ and C are known for the initial-state scattering ($\pi^+ n$ scattering in our example), and for the final-state scattering the usual choice[56] of parameters is C = 1, and $\gamma_{\mathrm{final}} = 0.75\, \gamma_{\mathrm{initial}}$.

A fit to the reaction $\pi^+ n \to \omega p$ at our c.m. energies using a ρ-exchange model with absorption has been attempted.[59] With the absorption parameters γ and C fixed as stated in the above paragraph, fits were tried for three values of the ratio G_T/G_V, the ratio of tensor

to vector coupling at the ρnp vertex.[56] The model was compared with the data of this report for G_T/G_V = 1, 2, and 3; at all these values the agreement is in general poor, so that no more detailed fitting was attempted. Although vector-meson dominance of the nucleon form factor predicts G_T/G_V = 3.7,[56] this value was not tried, since the agreement between the model and the data, where present, occurred for a ratio of 1.

The total cross section for this reaction cannot be described by the model, since the experimental cross section drops after reaching a peak near threshold (see Fig. 20), whereas the model predicts a cross section rising uniformly with energy from threshold. In order to ignore this basic discrepancy between experiment and the theory, the differential cross-section curves predicted by the model have been normalized to have the same area as the histograms of Fig. 35, which shows the differential cross section and the theoretical curves for G_T/G_V = 1. The curves agree with the experimental production distributions only for $E_{c.m.}$ = 2.2 and 2.3 GeV. The curves in Figs. 29–31 show the predictions of the ρ-exchange model with absorption for the ω-decay density matrix elements. The value G_T/G_V = 1 was selected for graphical comparison with the data primarily because it yields a fairly good fit to $\rho_{0,0}$. However, the agreement with $\rho_{1,-1}$ and $\mathrm{Re}(\rho_{1,0})$ is poor, as it is for the other values of G_T/G_V. Similar difficulties in comparing this ρ-exchange model with experiment have been met by other authors.[11, 12, 21, 58]

An attempt to understand the reaction $\pi^+ n \to \omega p$ in terms of a Regge pole-exchange model involving both B and ρ trajectory exchanges has also been attempted by some authors,[11, 12, 21] with little success.

VII. LITERATURE ON π^+d EXPERIMENTS

The following is a compilation of literature sources on π^+d experiments performed in bubble chambers; it is hoped that the compilation is complete up to about September 1969.

The exposure reported here (beam momentum of 1.1 to 2.4 GeV/c) was done along with a higher-energy exposure (beam momentum of about 3 and 4 GeV/c). References on both parts of this experiment are listed first, followed by references to other experiments, in order of increasing beam momentum.

π^+d at 1.1 to 2.4 GeV/c (this experiment)
Gerald A. Smith and Robert J. Manning, Phys. Rev. 171, 1399 (1968); Jerome S. Danburg, Donald W. Davies, Orin I. Dahl, Paul L. Hoch, Janos Kirz, Donald H. Miller, Robert K. Rader, Maris A. Abolins, Thalis Delikaris, and Gerald A. Smith, Phys. Rev. Letters 23, 41 (1969); Gerald A. Smith and Robert J. Manning, Phys. Rev. Letters 23, 335 (1969); J. S. Danburg, M. A. Abolins, R. C. Brower, O. I. Dahl, D. W. Davies, P. L. Hoch, J. Kirz, D. H. Miller, and R. K. Rader, Phys. Letters 30B, 270 (1969); R. J. Manning, UCRL-19343, 1969; Jerome S. Danburg (Ph. D. thesis), UCRL-19275, July 1969; Donald W. Davies (Ph. D. thesis), UCRL-19263, July 1969; Robert J. Manning (Ph. D. thesis), UCRL-19339, Sept. 1969; Robert K. Rader (Ph. D. thesis), UCRL-19431, Dec. 1969.

π^+d at 3 and 4 GeV/c (this experiment)
J. Gezelter, S. Lichtman, F. J. Loeffler, R. J. Miller, and R. B. Willmann, Nuovo Cimento 53A, 213 (1968); Maris A. Abolins, Orin I. Dahl, Jerome Danburg, Donald Davies, Paul Hoch, Donald H. Miller, Robert Rader, and Janos Kirz, Phys. Rev. Letters 22, 427 (1969); J. H. Campbell, S. Lichtman, F. J. Loeffler, D. H. Miller, R. J. Miller,

W. J. Miller, and R. B. Willmann, Phys. Rev. Letters 22, 1204 (1969); R. J. Miller S. Lichtman, and R. B. Willmann, Phys. Rev. 178, 2061 (1969); G. S. Abrams, B. Eisenstein, and H. Gordon, Phys. Rev. Letters 23, 673 (1969); P. M. Dauber, P. Hoch, R. J. Manning, D. M. Siegel, M. A. Abolins, and G. A. Smith, Phys. Letters 29B, 609 (1969).

π^+d at 0.65 to 0.85 GeV/c

E. Pauli, A. Muller, R. Barloutaud, L. Cardin, J. Meyer, M. Beneventano, G. Gialanella, L. Paoluzi, and R. Finzi, in Proceedings of the Siena International Conference on Elementary Particles, Vol. I, 92 (1963); A. Muller, E. Pauli, R. Berloutaud, L. Cardin, J. Meyer, M. Beneventano, G. Gialanella, and L. Paoluzi, ibid., Vol. I, 99 (1963); E. Pauli and A. Muller, Phys. Letters 13, 351 (1964).

π^+d at 0.82 GeV/c

C. Baltay, P. Franzini, J. Kim, L. Kirsch, D. Zanello, J. Lee-Franzini, R. Loveless, J. McFadyen, and H. Yarger, Phys. Rev. Letters 16, 1224 (1966); C. Baltay, P. Franzini, J. Kim, R. Newman, N. Yeh, and L. Kirsch, Phys. Rev. Letters 19, 1495 (1967); C. Baltay, P. Franzini, J. Kim, L. Kirsch, R. Newman, N. Yeh, J. A. Cole, J. Lee-Franzini, and H. Yarger, Phys. Rev. Letters 19, 1498 (1967).

π^+d at 0.82 GeV/c

A. Larribe, A. Leveque, A. Muller, E. Pauli, D. Revel, T. Tallini, P. J. Litchfield, L. K. Rangan, A. M. Segar, J. R. Smith, P. J. Finney, C. M. Fisher, and E. Pickup, Phys. Letters 23, 600 (1966); P. J. Litchfield, L. K. Rangan, A. M. Segar, J. R. Smith, A. Larribe, A. Leveque, A. Muller, E. Pauli, D. Revel, and B. Tallini, Phys. Letters 24B, 486 (1967); P. J. Litchfield, Nuovo Cimento 58A, 468 (1968); P. J. Litchfield, Phys. Rev. 183, 1152 (1969).

π^+d at 0.82 GeV/c

M. Bazin, A. T. Goshaw, R. Zacher, H. Blumenfeld, T. Kitagaki, and C. R. Sun, Phys. Rev. Letters 19, 1157 (1967).

π^+d at 1.23 GeV/c

A. Pevsner, R. Kraemer, M. Nussbaum, P. Schlein, T. Toohig, M. Block, A. Kovacs, and C. Meltzer, in Proceedings of International Conference on Elementary Particles, Aix-en-Provence, 277 (1961); A. Pevsner, R. Kraemer, M. Nussbaum, C. Richardson, P. Schlein, R. Strand, T. Toohig, M. Block, A. Engler, R. Gessaroli, and C. Meltzer, Phys. Rev. Letters 7, 421 (1961); C. Richardson, R. Kraemer, M. Meer, M. Nussbaum, A. Pevsner, R. Strand, T. Toohig, and M. Block, in Proceedings of 1962 CERN Conference, 96 (1962); T. Toohig, R. Kraemer, L. Madansky, M. Meer, M. Nussbaum, A. Pevsner, C. Richardson, and M. Block, ibid., 99 (1962); M. Meer, R. Strand, R. Kraemer, L. Madansky, M. Nussbaum, A. Pevsner, C. Richardson, T. Toohig, M. Block, S. Orenstein, and T. Fields, ibid., 103 (1962); T. Fields, S. Orenstein, R. Kraemer, L. Madansky, M. Meer, A. Pevsner, C. Richardson, and T. Toohig, in Proceedings of Athens Topical Conference on Resonant Particles, 185 (1963); R. Kraemer, L. Mandansky, M. Meer, M. Nussbaum, A. Pevsner, C. Richardson, R. Strand, R. Zdanis, T. Fields, S. Orenstein, and T. Toohig, Phys. Rev. 136B, 496 (1964).

π^+d at 1.7 GeV/c

T. C. Bacon, H. W. K. Hopkins, D. K. Robinson, D. G. Hill, E. O. Salant, A. Engler, H. E. Fisk, C. M. Meltzer, and

J. B. Westgard, in Proceedings of Dubna Conference, Vol. I, 532 (1964); T. C. Bacon, W. J. Fickinger, D. G. Hill, H. W. K. Hopkins, D. K. Robinson, and E. O. Salant, in Proceedings of Athens Conference on Newly Discovered Resonances, 129 (1965); T. C. Bacon, W. J. Fickinger, D. G. Hill, H. W. K. Hopkins, D. K. Robinson, and E. O. Salant, Phys. Rev. 157, 1263 (1967).

π^+d at 2.15 GeV/c

K. J. Braun, D. Cline, and V. Scherer, Phys. Rev. Letters 21, 1275 (1968).

π^+d at 2.15 GeV/c

D. Cline, J. English, R. Terrell, W. Wilke, B. Chaudhary, H. Courant, E. Marquit, and K. Ruddick, Phys. Rev. Letters 23, 491 (1969)

π^+d at 3.29 GeV/c

N. Gelfand, G. Lütjens, and J. Steinberger, in Proceedings of Dubna Conference , Vol. I, 437 (1964); N. Gelfand, G. Lütjens, M. Nussbaum, J. Steinberger, H. O. Cohn, W. M. Bugg, and G. T. Condo, Phys. Rev. Letters 12, 567 (1964); H. O. Cohn, W. M. Bugg, and G. T. Condo, Phys. Letters 15, 344 (1965); H. O. Cohn, W. M. Bugg, G. T. Condo, R. D. McCulloch, G. Lütjens, and N. Gelfand, Phys. Rev. Letters 15, 906 (1965); H. O. Cohn, R. D. McCulloch, W. M. Bugg, and G. T. Condo, Phys. Letters 21, 347 (1966); H. O. Cohn, R. D. McCulloch, W. M. Bugg, and G. T. Condo, Nucl. Phys. 82, 690 (1966); H. O. Cohn, R. D. McCulloch, W. M. Bugg, and G. T. Condo, Nucl. Phys. B1, 57 (1967); W. M. Bugg, G. T. Condo, J. T. Humphreys, R. D. McCulloch, and H. O. Cohn, Nucl. Phys. B6, 246 (1968).

π^+d at 3.65 GeV/c

G. Benson, L. Lovell, E. Marquit, B. Roe, D. Sinclair, J. Vander Velde, and K. Weaver, Phys. Rev. Letters 12, 600 (1964); G. Benson, L. Lovell, E. Marquit, B. Roe, D. Sinclair, and J. Vander Velde, Phys. Rev. Letters 16, 1177 (1966); G. Benson, E. Marquit, B. Roe, D. Sinclair, and J. Vander Velde, Phys. Rev. Letters 17, 1234 (1966); George C. Benson (Ph. D. thesis), University of Michigan, 1966; G. C. Benson, B. P. Roe, D. Sinclair, and J. C. Vander Velde, Phys. Rev. Letters 22, 1074 (1969).

π^+d at 4.5 GeV/c

A. Forino et al. (Saclay-Orsay-Bologna Collaboration), in Proceedings of Dubna Conference, Vol. I, 445 (1964); A. Forino et al. (Saclay-Orsay-Bari-Bologna Collaboration), Phys. Letters 11, 347 (1964); A. Forino et al. (Saclay-Orsay-Bologna Collaboration), Phys. Letters 19, 65 (1965); A. Forino et al. (Saclay-Orsay-Bari-Bologna-Firenze Collaboration), Phys. Letters 19, 68 (1965).

π^+d at 5.1 GeV/c

N. Armenise et al. (Bari-Bologna-Firenze-Orsay Collaboration), Phys. Letters 25B, 53 (1967); N. Armenise et al. (Bari-Bologna-Firenze-Orsay Collaboration), Phys. Letters 26B, 336 (1968); N. Armenise et al. (Bari-Bologna-Firenze-Orsay Collaboration), Nuovo Cimento 54A, 999 (1968); N. Armenise et al. (Bari-Bologna-Firenze Collaboration), Lettere al Nuovo Cimento 2, 501 (1969); R. Vanderhaghen, G. de Rosny, N. Armenise, B. Ghidini, A. Romano, A. Forino, and M. Goldberg, Nucl. Phys. B13, 329 (1969).

π^+d at 6 GeV/c

F. Bruyant, M. Goldberg, G. Vegni, H. Winzeler, P. Fleury, J. Huc, R. Lestienne, G. de Rosny, and R. Vanderhaghen, in Proceedings of Dubna Conference, Vol. I, 180 (1964); F. Bruyant, M. Goldberg, G. Vegni, H. Winzeler, P. Fleury, J. Huc, R. Lestienne,

G. de Rosny, and R. Vanderhaghen, ibid., Vol. I, 442 (1964); F. Bruyant, M. Goldberg, M. Holder, M. Krammer, J. V. Major, G. Vegni, H. Winzeler, P. Fleury, J. Huc, R. Lestienne, G. de Rosny, and R. Vanderhaghen, Phys. Letters 10, 232 (1964); F. Bruyant, M. Goldberg, G. Vegni, H. Winzeler, P. Fleury, J. Huc, R. Lestienne, G. de Rosny, and R. Vanderhaghen, Phys. Letters 12, 278 (1964); M. Goldberg et al. (CERN-Ecole Polytechnique Collaboration), Phys. Letters 17, 354 (1965); G. Vegni, H. Winzeler, P. Zaniol, P. Fleury, and G. de Rosny, Phys. Letters 19, 526 (1965); G. de Rosny and P. Fleury, Nuovo Cimento 48A, 1137 (1967).

$\pi^+ d$ at 7 GeV/c

B. Y. Oh et al. (Wisconsin-Toronto Collaboration), Phys. Rev. Letters 23, 331 (1969).

$\pi^+ d$ at 8 GeV/c

A. M. Cnops, P. V. C. Hough, F. R. Huson, I. R. Kenyon, J. M. Scarr, I. O. Skillicorn, H. O. Cohn, R. D. McCulloch, W. M. Bugg, G. T. Condo, and M. M. Nussbaum, Phys. Rev. Letters 21, 1609 (1968); A. M. Cnops, P. V. C. Hough, F. R. Huson, I. R. Kenyon, J. M. Scarr, I. O. Skillicorn, H. O. Cohn, R. D. McCulloch, W. M. Bugg, G. T. Condo, and M. M. Nussbaum, Phys. Letters 29B, 45 (1969); I. R. Kenyon, J. B. Kinson, J. M. Scarr, I. O. Skillicorn, H. O. Cohn, R. D. McCulloch, W. M. Bugg, G. T. Condo, and M. M. Nussbaum, Phys. Rev. Letters 23, 146 (1969).

ACKNOWLEDGMENTS

We wish to thank all those whose support, knowledge, and inspiration have helped in the completion of this work.

Thanks are due to the crews of the Bevatron and the 72-inch bubble chamber.

The scanning and measuring efforts, as well as the handling of the many large computer jobs associated with the preliminary data reduction, were supervised by our competent experiment librarians Wally Hendricks, Betty Armstrong, Maureen Nassiri, and Meredeth Vogler. We also owe thanks to the many scanners, and to the supervisors and operators of the Spiral Reader measuring machines.

The staff of the LRL computer center deserve thanks for their constant cooperation throughout the months of data analysis in ensuring fast, reliable processing of hundreds of computer jobs.

We acknowledge the support and encouragement of Professor Luis W. Alvarez.

FOOTNOTES AND REFERENCES

§Based on a thesis submitted by Jerome S. Danburg to the University of California — Berkeley in partial fulfillment of the requirements for the degree of Ph. D.

*Work supported by the U. S. Atomic Energy Commission.

†Now at Brookhaven National Laboratory, Department of Physics, Upton, New York 11973

‡Now at Michigan State University, Department of Physics, East Lansing, Michigan 48823

**Now at University of California–Los Angeles, Department of Physics, Los Angeles, California 90024

++Now at State University of New York at Stony Brook, Department of Physics, Stony Brook, New York 11790

1. W. Chinowsky, G. Smith, and J. Kirz, Bevatron Secondary Beam 1B, in Bevatron Experimenters' Handbook, Sec. C, Dec. 1965.

2. A. A. Carter, K. F. Riley, R. J. Tapper, D. V. Bugg, R. S. Gilmore, K. M. Knight, D. C. Salter, G. H. Stafford, E. J. N. Wilson, J. D. Davies, J. D. Dowell, P. M. Hattersley, R. J. Homer, and A. W. O'Dell, Phys. Rev. 168, 1457 (1968).
3. Jerome S. Danburg (Ph. D. thesis), Lawrence Radiation Laboratory report UCRL-19275, July 1969.
4. Gerald R. Lynch, Lawrence Radiation Laboratory report UCRL-17328, Jan. 1967.
5. F. T. Solmitz, A. D. Johnson, and T. B. Day, Alvarez Group (Lawrence Radiation Laboratory) Programming Note P-117, June 1966.
6. J. S. Danburg and G. R. Lynch, Alvarez Group (Lawrence Radiation Laboratory) Programming Note P-160, May 1967.
7. Orin Dahl and Don Davies, Alvarez Group (Lawrence Radiation Laboratory) Programming Note P-154, Nov. 1966.
8. Lamek Hulthén and Masao Sugawara, in Hanbuch der Physik (Springer-Verlag, Berlin, 1957), Vol. 39, Chap. 1.
9. R. L. Gluckstern and H. A. Bethe, Phys. Rev. 81, 761 (1951).
10. M. Moravcsik, Nucl. Phys. 7, 113 (1958).
11. R. J. Miller, S. Lichtman, and R. B. Willmann, Phys. Rev. 178, 2061 (1969).
12. George C. Benson (Ph. D. thesis), University of Michigan, 1966.
13. R. G. Newton, Scattering Theory of Waves and Particles (McGraw-Hill Book Company, 1966), Chap. 8.
14. R. J. Glauber, Phys. Rev. 100, 242 (1955).
15. Colin Wilkin, Phys. Rev. Letters 17, 561 (1966).
16. V. J. Stenger, W. E. Slater, D. H. Stork, H. K. Ticho, G. Goldhaber, and S. Goldhaber, Phys. Rev. 134B, 1111 (1964).
17. I. Butterworth, J. L. Brown, G. Goldhaber, S. Goldhaber, A. A. Hirata, J. A. Kadyk, B. M. Schwarzschild, and G. H. Trilling, Phys. Rev. Letters 15, 734 (1965).
18. J. Friedman, Alvarez Group (Lawrence Radiation Laboratory) Programming Note P-156, Nov. 1966.
19. N. Barash-Schmidt, A. Barbaro-Galtieri, L. R. Price, A. H. Rosenfeld, P. Söding, C. G. Wohl, M. Roos, and G. Conforto, Lawrence Radiation Laboratory report UCRL-8030, Jan. 1969.
20. (a) E. Pickup, D. K. Robinson, E. O. Salant, F. Ayer, and B. A. Munir, Phys. Rev. 132, 1819 (1963);
(b) T. C. Bacon, W. J. Fickinger, D. G. Hill, H. W. K. Hopkins, D. K. Robinson, and E. O. Salant, Phys. Rev. 157, 1263 (1967);
(c) L. D. Jacobs, (Ph. D. thesis), Lawrence Radiation Laboratory report UCRL-16877, Aug. 1966.
21. T. C. Bacon, W. J. Fickinger, D. G. Hill, H. W. K. Hopkins, D. K. Robinson, and E. O. Salant, Phys. Rev. 157, 1263 (1967).
22. P. J. Litchfield, Phys. Rev. 183, 1152 (1969).
23. W. G. Jones, D. M. Binnie, A. Duane, J. P. Horsey, D. C. Mason, J. A. Newth, I. U. Rahman, J. Walters, N. Horwitz, and P. Palit, Phys. Letters 23, 597 (1966).
24. F. Bulos et al. (Brown-Brandeis-Harvard-M.I.T.-Padua Collaboration), Phys. Rev. Letters 13, 486 (1964).
25. W. B. Richards, C. B. Chiu, R. D. Eandi, A. C. Helmholz, B. W. Kenney, B. J. Moyer, J. A. Poirier, R. J. Cence, V. Z. Peterson, N. K. Sehgal, and V. J. Stenger, Phys. Rev. Letters 16, 1221 (1966).
26. W. Deinet, H. Müller, D. Schmitt, H.-M. Staudenmaier, S. Buniatov, and E. Zavattini, Nuclear Phys. B11, 495 (1969).
27. H. R. Crouch et al. (Brown-Harvard-Padua-Weizmann Institute-M.I.T. Collaboration), Phys. Rev. Letters 21, 845 (1968).
28. M. A. Wahlig and I. Mannelli, Phys. Rev. 168, 1515 (1968).

29. O. Guisan, J. Kirz, P. Sonderegger, A. V. Stirling, P. Borgeaud, C. Bruneton, P. Falk-Vairant, B. Amblard, C. Caversasio, J. P. Guillaud, and M. Yvert, Phys. Letters 18, 200 (1965).
30. R. Kraemer, L. Madansky, M. Meer, M. Nussbaum, A. Pevsner, C. Richardson, R. Strand, R. Zdanis, T. Fields, S. Orenstein, and T. Toohig, Phys. Rev. 136B, 496 (1964).
31. J. H. Boyd, A. R. Erwin, W. D. Walker, and E. West, Phys. Rev. 166, 1458 (1968).
32. T. D. Lee, Phys. Rev. 139B, 1415 (1965).
33. H. Yuta and S. Okubo, Phys. Rev. Letters 21, 781 (1968).
34. P. K. Kabir, Phys. Rev. 178, 2486 (1969).
35. Columbia-Berkeley-Purdue-Wisconsin-Yale Collaboration, Phys. Rev. 149, 1044 (1966).
36. A. M. Cnops, J. Finocchiaro, J. C. Lassalle, P. Mittner, P. Zanella, J. P. Dufey, B. Gobbi, M. A. Pouchon, and A. Muller, Phys. Letters 22, 546 (1966).
37. A. Larribe, A. Leveque, A. Muller, E. Pauli, D. Revel, T. Tallini, P. J. Litchfield, L. K. Rangan, A. M. Segar, J. R. Smith, P. J. Finney, C. M. Fisher, and E. Pickup, Phys. Letters 23, 600 (1966).
38. C. Baltay, P. Franzini, J. Kim, L. Kirsch, D. Zanello, J. Lee-Franzini, R. Loveless, J. McFadyen, and H. Yarger, Phys. Rev. Letters 16, 1224 (1966).
39. M. Gormley, E. Hyman, W. Lee, T. Nash, J. Peoples, C. Schultz, and S. Stein, Phys. Rev. Letters 21, 402 (1968).
40. Frank S. Crawford, Jr., and LeRoy R. Price, Phys. Rev. Letters 16, 333 (1966).
41. P. J. Litchfield, L. K. Rangan, A. M. Segar, J. R. Smith, A. Larribe, A. Leveque, A Muller, E. Pauli, D. Revel, and B. Tallini, Phys. Letters 24B, 486 (1967).
42. R. A. Bowen, A. M. Cnops, G. Finocchiaro, P. Mittner, J. P. Dufey, B. Gobbi, M. A. Pouchon, and A. Muller, Phys. Letters 24B, 206 (1967).
43. M. Gormley, E. Hyman, W. Lee, T. Nash, J. Peoples, C. Schultz, and S. Stein, Phys. Rev. Letters 21, 399 (1968).
44. Laurie M. Brown and Paul Singer, Phys. Rev. Letters 8, 460 (1962); Laurie M. Brown and Paul Singer, Phys. Rev. 133B, 812 (1964).
45. LeRoy R. Price and Frank S. Crawford, Jr., Phys. Rev. 167, 1339 (1968).
46. A. M. Cnops, G. Finocchiaro, P. Mittner, J. P. Dufey, B. Gobbi, M. A. Pouchon, and A. Müller, Phys. Letters 27B, 113 (1968).
47. This possible bias was suggested by J. D. Jackson (Lawrence Radiation Laboratory), private communication, 1969.
48. J. S. Danburg et al., Phys. Letters 30B, 270 (1969).
49. This parameterization of the cross section was suggested by Richard C. Brower (Lawrence Radiation Laboratory), private communication, 1969; see also K. Igi, Phys. Letters 28B, 330 (1968) for an example of such a parameterization for the reaction $\pi N \rightarrow \pi N$.
50. F. Arbab, N. F. Bali, and J. W. Dash, Phys. Rev. 158, 1515 (1967). Our kinematical factors are identical to those in this reference when A and B are written in terms of helicity amplitudes.
51. G. C. Benson, B. P. Roe, D. Sinclair, and J. C. Vander Velde, Phys. Rev. Letters 22, 1074 (1969).
52. Roger J. N. Phillips and William Rarita, Phys. Rev. 140B, 200 (1965); Roger J. N. Phillips and William Rarita, Phys. Rev. Letters 15, 807 (1965); R. J. N. Phillips and W. Rarita, Phys. Letters 19, 598 (1965); R. J. N. Phillips, Nucl Phys. B1, 573 (1967); Farzam Arbab, Naren F. Bali, and Jan W. Dash, Phys. Rev. 158, 1515 (1967); D. D. Reeder and K. V. L. Sarma, Nuovo Cimento 51A, 169 (1967); D. D. Reeder and K. V. L. Sarma, Phys. Rev. 172, 1566 (1968);

Maurice L. Blackmon, Phys. Rev. 178, 2385 (1969).
53. B. C. Maglić, L. W. Alvarez, A. H. Rosenfeld, and M. L. Stevenson, Phys. Rev. Letters 7, 178 (1961); M. L. Stevenson, L. W. Alvarez, B. C. Maglić, and A. H. Rosenfeld, Phys. Rev. 125, 687 (1962).
54. S. M. Flatté, D. O. Huwe, J. J. Murray, J. Button-Shafer, F. T. Solmitz, M. L. Stevenson, and C. Wohl, Phys. Rev. 145, 1050 (1966).
55. Charles Zemach, Phys. Rev. 133B, 1201 (1964).
56. K. Gottfried and J. D. Jackson, Phys. Letters 8, 144 (1964); K. Gottfried and J. D. Jackson, Nuovo Cimento 33, 309 (1964); J. D. Jackson and H. Pilkuhn, Nuovo Cimento 33, 906 (1964); K. Gottfried and J. D. Jackson, Nuovo Cimento 34, 735 (1964); J. D. Jackson, J. T. Donohue, K. Gottfried, R. Keyser, and B. E. Y. Svensson, Phys. Rev. 139B, 428 (1965); J. D. Jackson, Rev. Mod. Phys. 37, 484 (1965).
57. J. D. Jackson, Particle and Polarization Angular Distributions for Two and Three Body Decays, in High Energy Physics, 1965 Les Houches Lectures, edited by C. Dewitt and M. Jacob (Gordon and Breach Science Publishers, Inc. New York 1965).
58. H. O. Cohn, W. M. Bugg, and G. T. Condo, Phys. Letters 15, 344 (1965).
59. We are grateful to J. D. Jackson and C. Quigg for providing the computer programs used in this fitting process.

Table I. Momentum settings and exposure size.

Beam momentum (GeV/c)	Number of pictures (approximately)	Exposure size (events/μb)
1.10	13 000	0.44
1.30	13 000	0.44
1.53	50 000	2.55
1.58	13 000	0.45
1.70	50 000	3.00
1.86	50 000	2.92
2.15	50 000	2.97
2.37	26 000	0.84

Table II. Spin-flip and non-spin-flip suppression factors due to the Pauli principle for the two forwardmost production cosine bins.

$E_{c.m.}$ (GeV)	$(0.8 < \cos\theta < 0.9)$		$(0.9 < \cos\theta < 1.0)$	
	f_{nf}	f_{sf}	f_{nf}	f_{sf}
For $\pi^+ d \to pp\omega$				
1.8	0.93	0.98	0.91	0.97
1.9	0.93	0.98	0.87	0.96
2.0	0.93	0.98	0.85	0.95
2.1	0.94	0.98	0.83	0.95
2.2	0.95	0.98	0.83	0.94
2.3	0.96	0.99	0.83	0.94
2.4	0.96	0.99	0.84	0.95
For $\pi^+ d \to pp\eta$				
1.7	0.87	0.96	0.74	0.91
1.8	0.89	0.96	0.73	0.91
1.9	0.91	0.97	0.73	0.91
2.0	0.93	0.98	0.74	0.91
2.1	0.94	0.98	0.76	0.92
2.2	0.95	0.98	0.78	0.93
2.3	0.96	0.99	0.79	0.93
2.4	0.97	0.99	0.81	0.94

Table III. Number of events, and the amount, mass, and width of η and ω, in each of six 100-MeV-wide c. m. energy intervals.

$E_{c.m.}$ (GeV)	Number of events	η fraction	m_η (MeV)	Γ_η (MeV)	ω fraction	m_ω (MeV)	Γ_ω (MeV)
1.8	509	0.083±0.023	548±3	24±19	0.503±0.058	784± 1	31±10
1.9	1 278	0.059±0.008	547±3	39± 7	0.432±0.019	786± 1	38± 3
2.0	1 972	0.033±0.004	549±1	19± 3	0.314±0.015	784± 1	37± 3
2.1	1 976	0.037±0.005	549±1	25± 3	0.287±0.013	786± 1	39± 3
2.2	1 611	0.024±0.004	549±1	11± 2	0.274±0.014	785± 1	47± 3
2.3	954	0.012±0.004	550±2	14± 3	0.202±0.015	785± 2	39± 4

Table IV. Sum of cross sections for the reactions $\pi^-p\to\pi^+\pi^-n$ and $\pi^-p\to\pi^+\pi^-$ (mm) as a function of c. m. energy.

$E_{c.m.}$ (GeV)	σ_{sum} (mb)	Source
1.618	11.5±0.6	a
1.716	11.4±0.6	b
1.726	10.4±0.8	a
1.795	10.4±0.8	b
1.872	11.1±0.3	b
2.030	12.0±0.7	b
2.181	11.6±0.6	c
2.232	11.8±0.6	c
2.309	10.7±0.6	c
2.405	10.4±0.5	c
2.504	9.0±0.4	c

a. E. Pickup et al., Phys. Rev. 132, 1819 (1963).

b. T. C. Bacon et al., Phys. Rev. 157, 1263 (1967).

c. L. D. Jacobs, Ph. D. thesis, UCRL-16877, 1966.

Table V. Cross sections for $\pi^+ n \to \eta p$ and $\pi^+ n \to \omega p$ as a function of c.m. energy in 50-MeV intervals centered at the values given.

$E_{c.m.}$ (GeV)	$\sigma(\pi^+ n \to \eta p)$ (mb)	$\sigma(\pi^+ n \to \omega p)$ (mb)
1.75	1.30±0.44	1.50±0.29
1.80	1.09±0.35	2.46±0.35
1.85	1.66±0.33	2.51±0.25
1.90	0.87±0.20	2.11±0.20
1.95	0.90±0.19	1.99±0.19
2.00	0.50±0.13	1.52±0.17
2.05	0.59±0.14	1.68±0.19
2.10	0.55±0.14	1.58±0.18
2.15	0.60±0.14	1.40±0.16
2.20	0.55±0.14	1.70±0.19
2.25	0.29±0.12	1.19±0.17
2.30	0.30±0.12	1.08±0.16
2.35	0.16±0.11	1.04±0.19

Table VI. Limits on momentum transfer squared as a function of c.m. energy for the reaction $\pi^+ n \to \eta p$.

$E_{c.m.}$ (GeV)	$(-t)_{min}$ (GeV^2)	$(-t)_{max}$ (GeV^2)
1.65	0.032	0.79
1.70	0.025	0.95
1.75	0.020	1.12
1.80	0.016	1.29
1.85	0.014	1.47
1.90	0.011	1.65
1.95	0.010	1.84
2.00	0.008	2.03
2.05	0.007	2.23
2.10	0.006	2.43
2.15	0.006	2.64
2.20	0.005	2.85
2.25	0.004	3.07

Table VII. Limits on momentum transfer squared as a function of c.m. energy for the reaction $\pi^+ n \rightarrow \omega p$.

$E_{c.m.}$ (GeV)	$(-t)_{min}$ (GeV^2)	$(-t)_{max}$ (GeV^2)
1.75	0.183	0.555
1.80	0.121	0.790
1.85	0.091	0.999
1.90	0.071	1.203
1.95	0.058	1.406
2.00	0.048	1.610
2.05	0.041	1.817
2.10	0.035	2.028
2.15	0.030	2.243
2.20	0.026	2.462
2.25	0.023	2.686
2.30	0.020	2.914
2.35	0.018	3.147

Table VIII. ω-decay density matrix elements in the Jackson frame as a function of c.m. energy and production cosine interval.

$E_{c.m.}$ (GeV)	cos θ	$\rho_{0,0}$	$\rho_{1,-1}$	$Re(\rho_{1,0})$
1.8	(-1, 0)	0.53±0.12	-0.05±0.08	0.12±0.08
	(0, 0.5)	0.60±0.14	-0.04±0.09	-0.05±0.08
	(0.5, 1)	0.49±0.13	0.07±0.10	-0.08±0.08
1.9	(-1, -0.3)	0.62±0.18	-0.06±0.10	-0.01±0.08
	(-0.3, 0.1)	0.61±0.11	-0.19±0.08	-0.07±0.06
	(0.1, 0.4)	0.58±0.11	0.01±0.07	-0.10±0.06
	(0.4, 0.7)	0.63±0.11	0.09±0.07	-0.16±0.06
	(0.7, 1)	0.33±0.11	-0.06±0.10	-0.06±0.08
2.0	(-1, -0.3)	0.52±0.13	0.00±0.08	-0.06±0.07
	(-0.3, 0.1)	0.80±0.13	-0.08±0.07	-0.15±0.07
	(0.1, 0.4)	0.53±0.10	-0.03±0.07	-0.24±0.08
	(0.4, 0.7)	0.51±0.10	-0.03±0.07	-0.21±0.06
	(0.7, 1)	0.31±0.09	0.04±0.07	-0.18±0.06
2.1	(-1, -0.2)	0.40±0.10	-0.12±0.09	-0.16±0.08
	(-0.2, 0.2)	0.55±0.11	-0.09±0.08	-0.16±0.07
	(0.2, 0.6)	0.37±0.09	0.05±0.08	-0.21±0.07
	(0.6, 0.8)	0.20±0.08	0.07±0.09	-0.17±0.06
	(0.8, 1)	0.42±0.09	0.08±0.08	-0.05±0.06
2.2	(-1, 0)	0.30±0.11	-0.29±0.13	-0.16±0.09
	(0, 0.6)	0.34±0.11	-0.09±0.10	-0.27±0.09
	(0.6, 0.85)	0.27±0.08	0.09±0.07	-0.12±0.05
	(0.85, 1)	0.49±0.09	-0.11±0.07	-0.01±0.05
2.3	(-1, 0.7)	0.42±0.12	-0.11±0.10	-0.16±0.09
	(0.7, 1)	0.49±0.10	0.08±0.07	-0.16±0.06

Table IX. ω-decay density matrix elements in the helicity frame as a function of c.m. energy and production cosine interval.

$E_{c.m.}$ (GeV)	cos θ	$\rho_{0,0}$	$\rho_{1,-1}$	$Re(\rho_{1,0})$
1.8	(-1, 0)	0.53±0.13	-0.04±0.08	-0.07±0.07
	(0, 0.5)	0.23±0.12	-0.22±0.12	0.01±0.08
	(0.5, 1)	0.40±0.12	0.03±0.10	0.12±0.08
1.9	(-1, -0.3)	0.46±0.15	-0.14±0.12	-0.11±0.09
	(-0.3, 0.1)	0.36±0.09	-0.31±0.09	-0.03±0.05
	(0.1, 0.4)	0.18±0.09	-0.20±0.09	0.02±0.06
	(0.4, 0.7)	0.15±0.09	-0.15±0.08	0.18±0.06
	(0.7, 1)	0.43±0.13	0.00±0.09	0.07±0.08
2.0	(-1, -0.3)	0.38±0.11	-0.07±0.09	-0.08±0.07
	(-0.3, 0.1)	0.23±0.09	-0.36±0.10	-0.17±0.07
	(0.1, 0.4)	0.08±0.10	-0.26±0.10	0.13±0.07
	(0.4, 0.7)	0.29±0.08	-0.14±0.08	0.20±0.06
	(0.7, 1)	0.60±0.11	0.19±0.08	0.07±0.06
2.1	(-1, -0.2)	0.15±0.10	-0.24±0.11	-0.06±0.07
	(-0.2, 0.2)	0.20±0.09	-0.26±0.10	-0.05±0.06
	(0.2, 0.6)	0.12±0.10	-0.07±0.08	0.16±0.06
	(0.6, 0.8)	0.42±0.10	0.18±0.08	0.15±0.06
	(0.8, 1)	0.43±0.09	0.08±0.08	0.12±0.07
2.2	(-1, 0)	0.17±0.13	-0.36±0.14	0.01±0.07
	(0, 0.6)	0.13±0.12	-0.19±0.12	0.15±0.09
	(0.6, 0.85)	0.33±0.07	0.12±0.07	0.10±0.05
	(0.85, 1)	0.45±0.09	-0.13±0.08	0.04±0.06
2.3	(-1, 0.7)	0.30±0.11	-0.18±0.12	0.09±0.08
	(0.7, 1)	0.43±0.10	0.05±0.07	0.15±0.06

Figure Captions

Fig. 1. Missing-mass-squared distribution for 14 829 "good" $pp\pi^+\pi^-\pi^0$ events. Approximately 700 events lie outside the limits of the histogram.

Fig. 2. (a) Kinematic confidence level and (b) ionization confidence level for 20 924 events assigned to the final state $pp\pi^+\pi^-\pi^0$.

Fig. 3. Laboratory-system momentum of lower-momentum proton in the final state $pp\pi^+\pi^-\pi^0$ for four-pronged events; the curve is the Hulthén distribution normalized to have the same area as the histogram in the interval (110 MeV/c < p < 160 MeV/c).

Fig. 4. Distribution of cosine between beam and spectator nucleon for a $\pi^+ d$ Monte Carlo experiment of 100 000 events with beam momentum of 2.0 GeV/c, taking the Møller flux factor into account. (a) All events, and (b) events with spectator momentum greater than 85 MeV/c.

Fig. 5. Distribution of cosine between beam and spectator proton for "good" four-pronged events from the final state $pp\pi^+\pi^-\pi^0$. (A) All events, and (B) events with spectator momentum less than 300 MeV/c. The curves are Eq. (15) normalized to have the same area as the histograms in (A) and (B).

Fig. 6. Distribution of c.m. energy for "good" four-pronged events from the final state $(p)p\pi^+\pi^-\pi^0$ with spectator momentum less than 300 MeV/c.

Fig. 7. Deuteron form factor vs momentum transfer squared, calculated using the Hulthén wave function.

Fig. 8. (a) $m(\pi^+\pi^-\pi^0)$ vs c.m. energy; (b) $m(\pi^+\pi^-\pi^0)$. The lower histogram has events with $-t(\text{beam to } \pi^+\pi^-\pi^0) < 0.6\ \text{GeV}^2$.

Fig. 9. $m(\pi^+\pi^-\pi^0)$ in six 100-MeV-wide c.m. energy intervals centered at (a) 1.8, (b) 1.9, (c) 2.0, (d) 2.1, (e) 2.2, and (f) 2.3 GeV; the curves are from maximum-likelihood fits.

Fig. 10. $m(p\pi^+)$ in six 100-MeV-wide c.m. energy intervals centered at (a) 1.8, (b) 1.9, (c) 2.0, (d) 2.1, (e) 2.2, and (f) 2.3 GeV; the curves are from maximum-likelihood fits.

Fig. 11. $m(p\pi^-)$ in six 100-MeV-wide c.m. energy intervals centered at (a) 1.8, (b) 1.9, (c) 2.0, (d) 2.1 (e) 2.2, and (f) 2.3 GeV; the curves are from maximum-likelihood fits.

Fig. 12. $m(p\pi^0)$ in six 100-MeV-wide c.m. energy intervals centered at (a) 1.8, (b) 1.9, (c) 2.0, (d) 2.1, (e) 2.2, and (f) 2.3 GeV; the curves are from maximum-likelihood fits.

Fig. 13. $m(\pi^+\pi^-)$ in six 100-MeV-wide c.m. energy intervals centered at (a) 1.8, (b) 1.9, (c) 2.0, (d) 2.1, (e) 2.2, and (f) 2.3 GeV; the curves are from maximum-likelihood fits.

Fig. 14. $m(\pi^+\pi^0)$ in six 100-MeV-wide c.m. energy intervals centered at (a) 1.8, (b) 1.9, (c) 2.0, (d) 2.1, (e) 2.2, and (f) 2.3 GeV; the curves are from maximum-likelihood fits.

Fig. 15. $m(\pi^-\pi^0)$ in six 100-MeV-wide c.m. energy intervals centered at (a) 1.8, (b) 1.9, (c) 2.0, (d) 2.1, (e) 2.2, and (f) 2.3 GeV; the curves are from maximum-likelihood fits.

Fig. 16. $m(p\pi^+\pi^-)$ in six 100-MeV-wide c.m. energy intervals centered at (a) 1.8, (b) 1.9, (c) 2.0, (d) 2.1, (e) 2.2, and If) 2.3 GeV; the curves are from maximum-likelihood fits.

Fig. 17. $m(p\pi^+\pi^0)$ in six 100-MeV-wide c.m. energy intervals centered at (a) 1.8, (b) 1.9, (c) 2.0, (d) 2.1, (e) 2.2, and (f) 2.3 GeV; the curves are from maximum-likelihood fits.

Fig. 18. $m(p\pi^-\pi^0)$ in six 199-MeV-wide c.m. energy intervals centered at (a) 1.8, (b) 1.9, (c) 2.0, (d) 2.1, (e) 2.2, and (f) 2.3 GeV; the curves are from maximum-likelihood fits.

Fig. 19. $m(\pi^+\pi^-\pi^0)$ vs $-t$(beam to $\pi^+\pi^-\pi^0$).

Fig. 20. (a) Logarithm of cross section for $\pi^+n \to \eta p$ and $\pi^-p \to \eta n$ vs c.m. energy, data from this and three other experiments; (b) cross section for $\pi^+n \to \omega p$ and $\pi^-p \to \omega n$ vs c.m. energy, data from this and five other experiments.

Fig. 21. Dalitz plot of 349 events in the η-mass band (530 MeV/c^2 ($530\ \text{MeV}/c^2 < m(3\pi) < 570\ \text{MeV}/c^2$).

Fig. 22. Relative density of points on the η Dalitz plot vs $3T_0/Q - 1$. The straight line has slope -1.

Fig. 23. η production cosine distributions for six 100-MeV-wide c.m. energy intervals centered at the values indicated. The shaded events are added to account for the effect of the Pauli exclusion principle. The curves are the predictions of the Reggeized A_2-exchange model with $b_0/a_0 = 2.4$; they are normalized to have the same area as the histograms.

Fig. 24. Cross section for $\pi^+ n \to \eta p$ or $\pi^- p \to \eta n$ vs c.m. energy. Three predictions of the Reggeized A_2-exchange model are plotted; all curves are normalized to pass through the data point at $E_{c.m.} = 3.46$ GeV.

Fig. 25. Differential cross sections for $\pi^- p \to \eta n$ from Guisan et al., Phys. Letters 18, 200 (1965). The curves are the Reggeized A_2-exchange model predictions with $b_0/a_0 = 2.4$, and are normalized to have the same area as the histograms.

Fig. 26. Differential cross section for (a) $\pi^+ n \to \eta p$ from Benson, Ph. D. thesis, University of Michigan, 1966, and (b) $\pi^- p \to \eta n$ from Wahlig and Mannelli, Phys. Rev. 168, 1515 (1968). The curves are the predictions of the Reggeized A_2-exchange model with $b_0/a_0 = 2.4$ and are normalized to have the same area as the histograms.

Fig. 28. ω production cosine distributions for six 100-MeV-wide c.m. energy intervals. The shaded events are added to account for the effect of the Pauli exclusion principle.

Fig. 29. $\rho_{0,0}$ for ω decay in the Jackson frame; the curves are the predictions of the ρ-exchange model with absorption for $G_T = G_V$.

Fig. 30. $\rho_{1,-1}$ for ω decay in the Jackson frame; the curves are the predictions of the ρ-exchange model with absorption for $G_T = G_V$.

Fig. 31 $\mathrm{Re}(\rho_{1,0})$ for ω decay in the Jackson frame; the curves are the predictions of the ρ-exchange model with absorption for $G_T=G_V$.

Fig. 32. $\rho_{0,0}$ for ω decay in the helicity frame.

Fig. 33. $\rho_{1,-1}$ for ω decay in the helicity frame.

Fig. 34. $\mathrm{Re}(\rho_{1,0})$ for ω decay in the helicity frame.

Fig. 35. ω production cosine distributions for six 100-MeV-wide c. m. energy intervals. The forward two bins of each distribution have been corrected upward to account for the effect of the Pauli exclusion principle. The curves are the predictions of the ρ-exchange model with absorption; they are normalized to have the same area as the histograms.

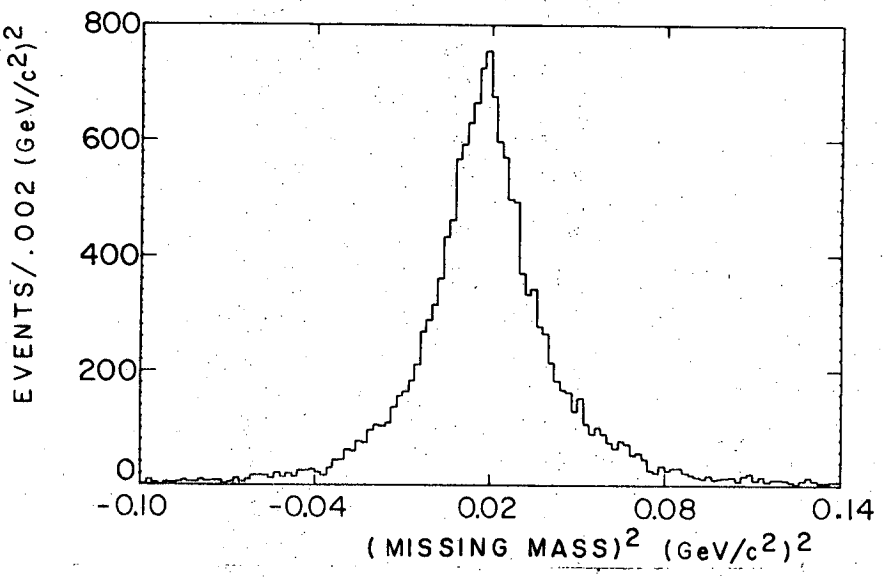

Figure 1.

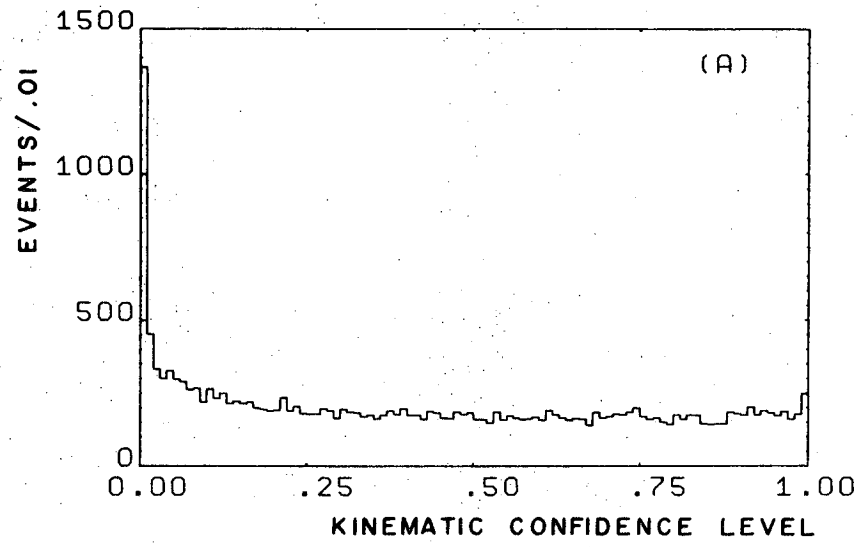

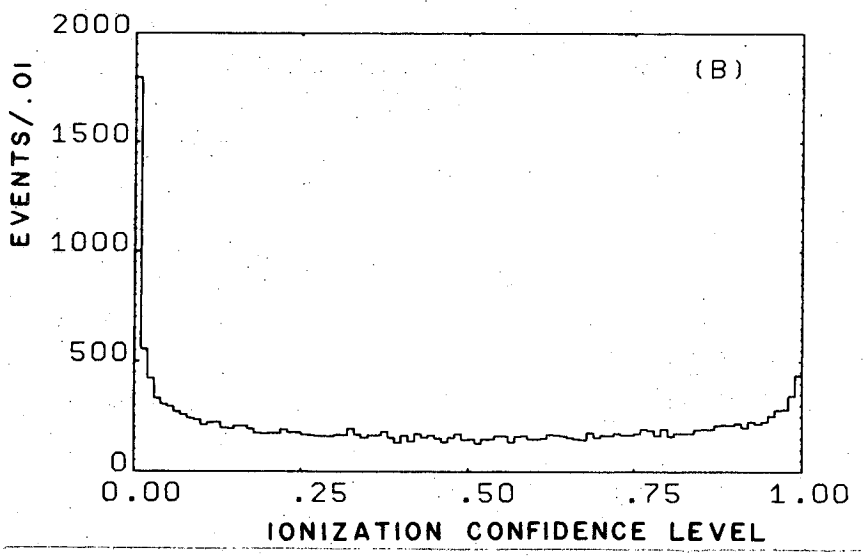

Figure 2.

XBL 695-587

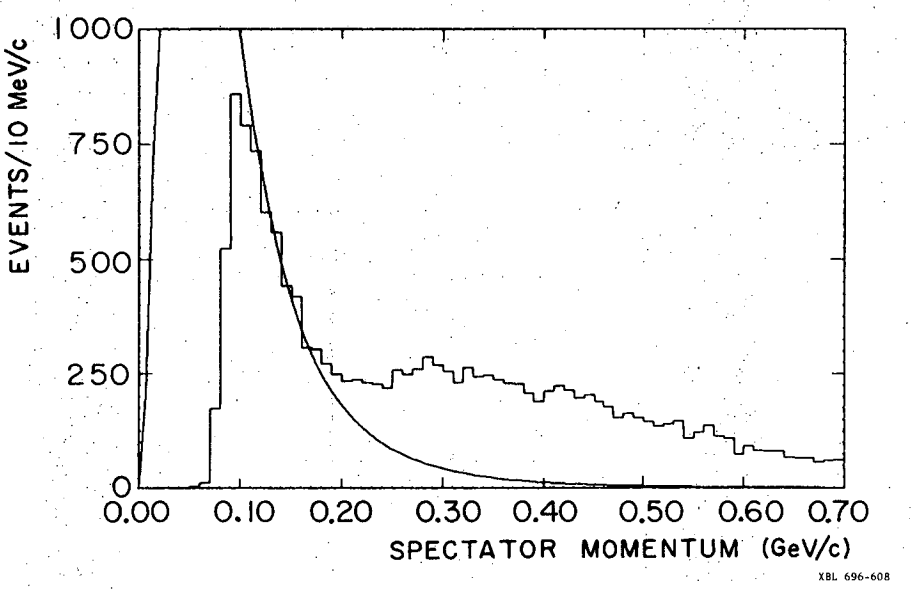

Figure 3.

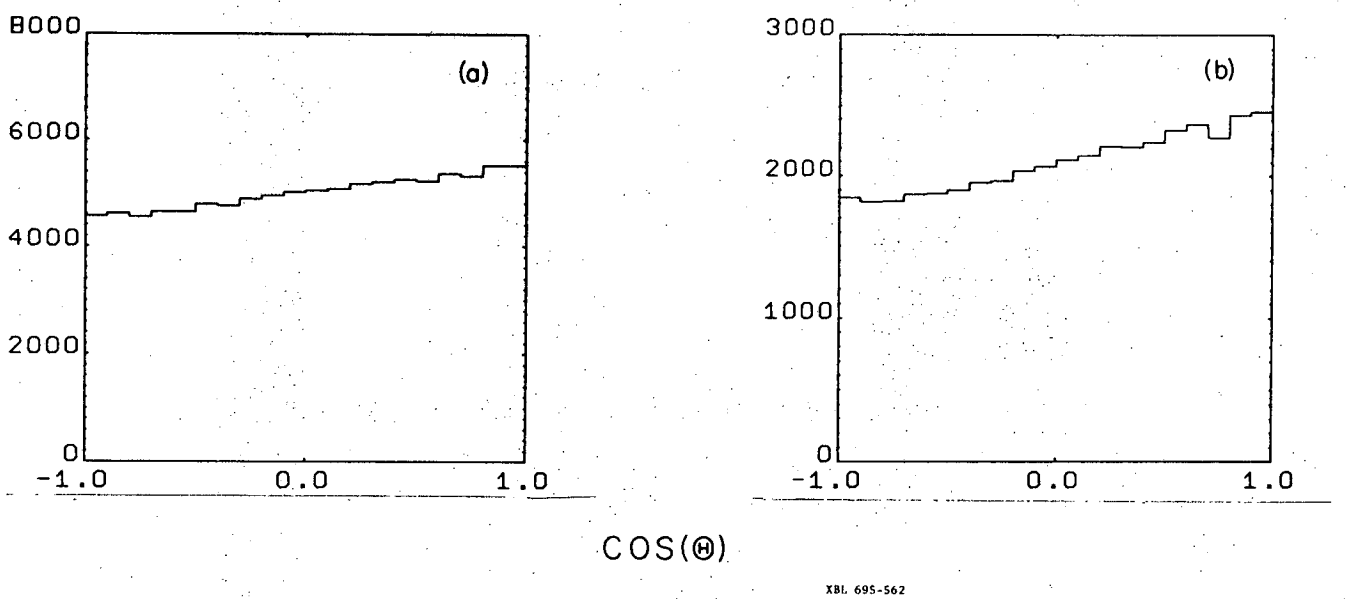

Figure 4.

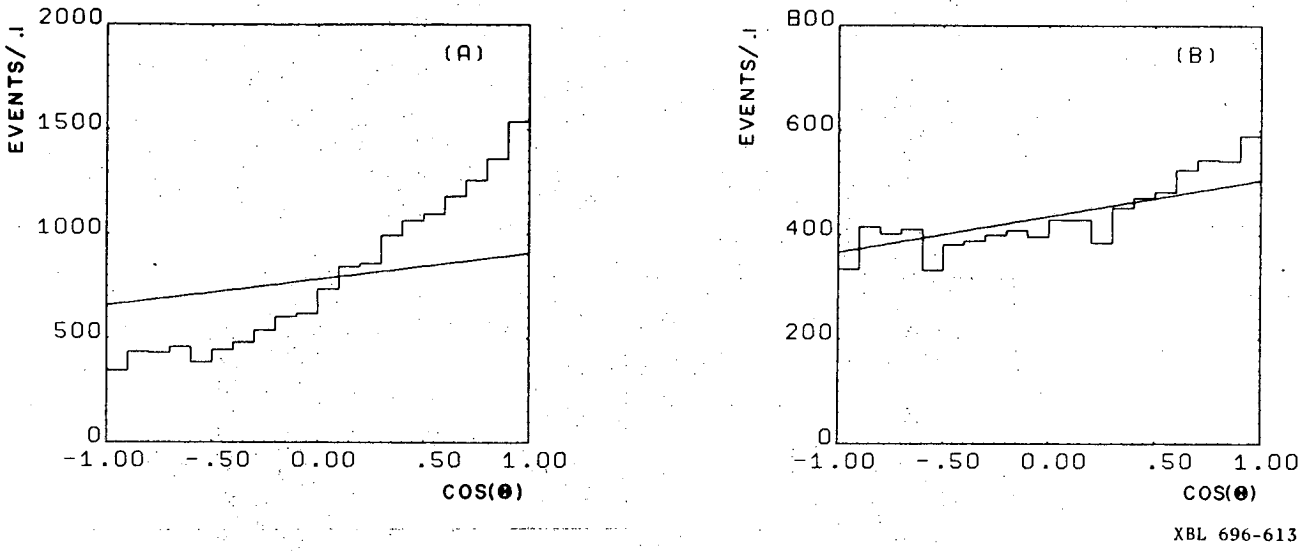

Figure 5.

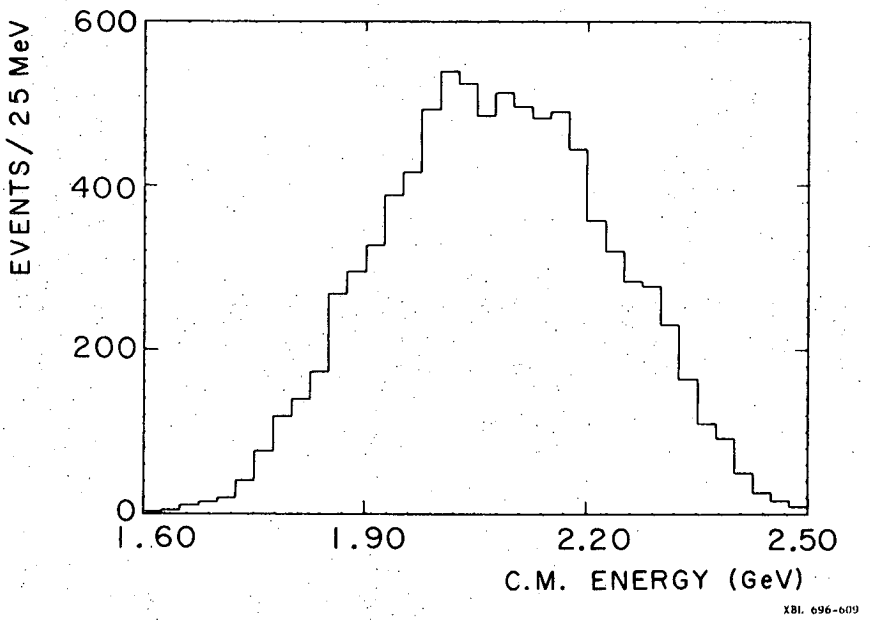

Figure 6.

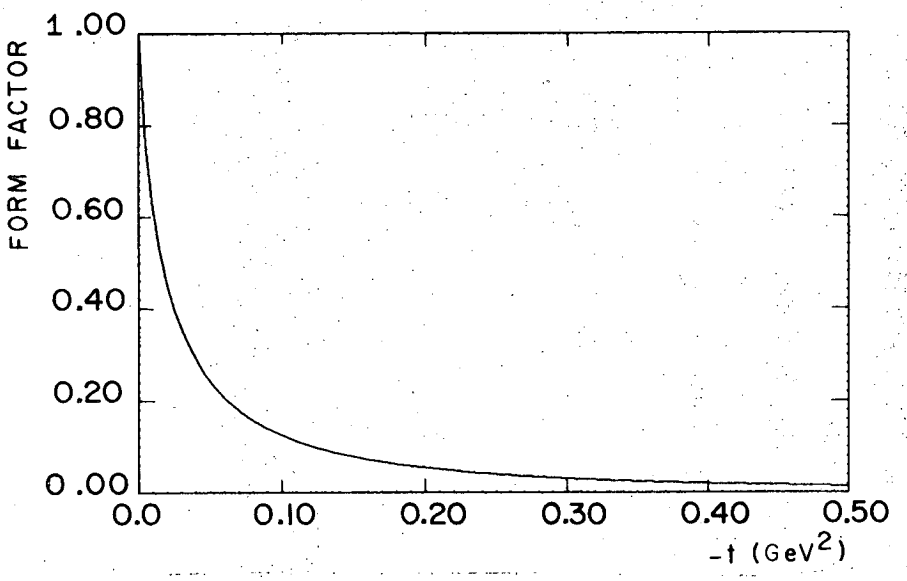

Figure 7.

XBL 696-610

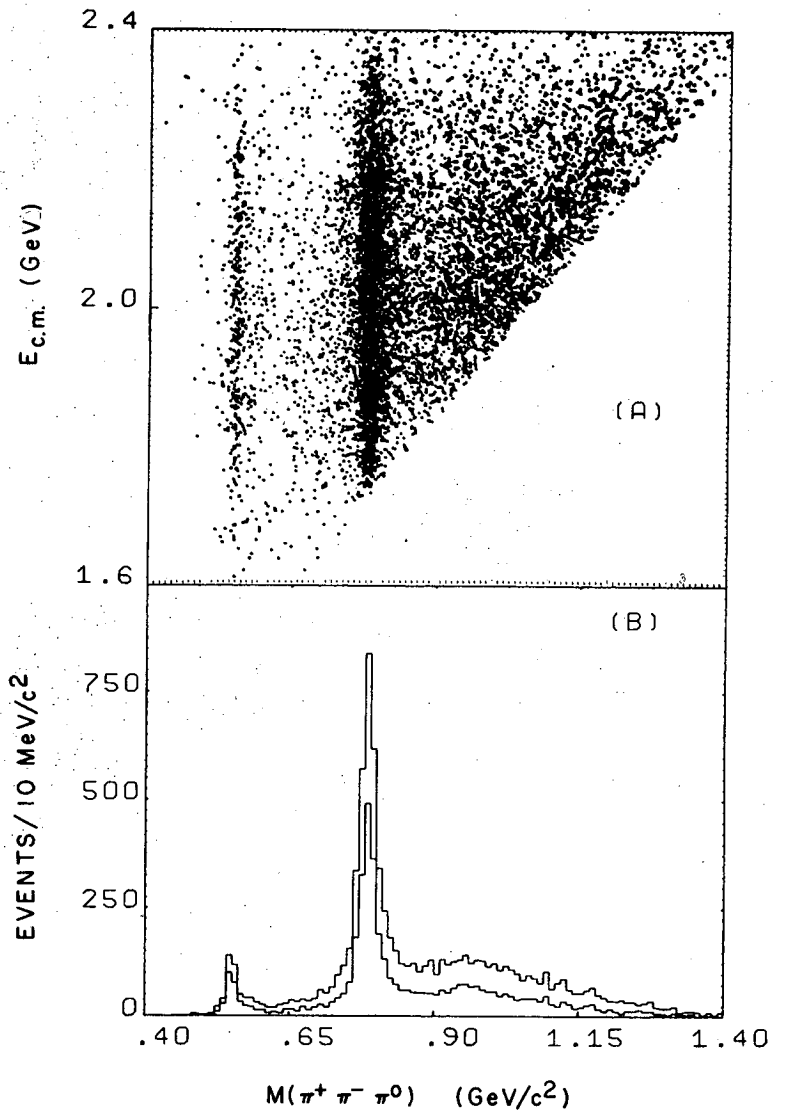

Figure 8.

XBL 696-740

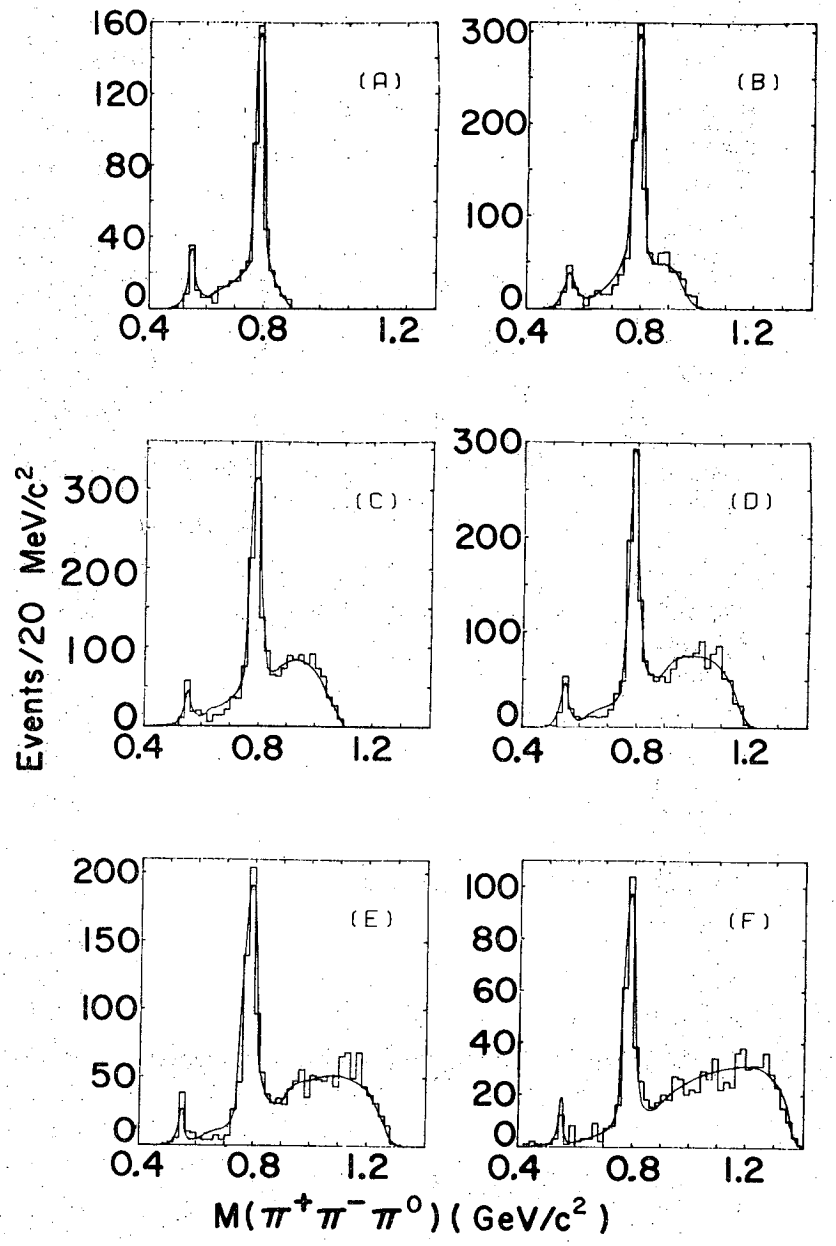

Figure 9.

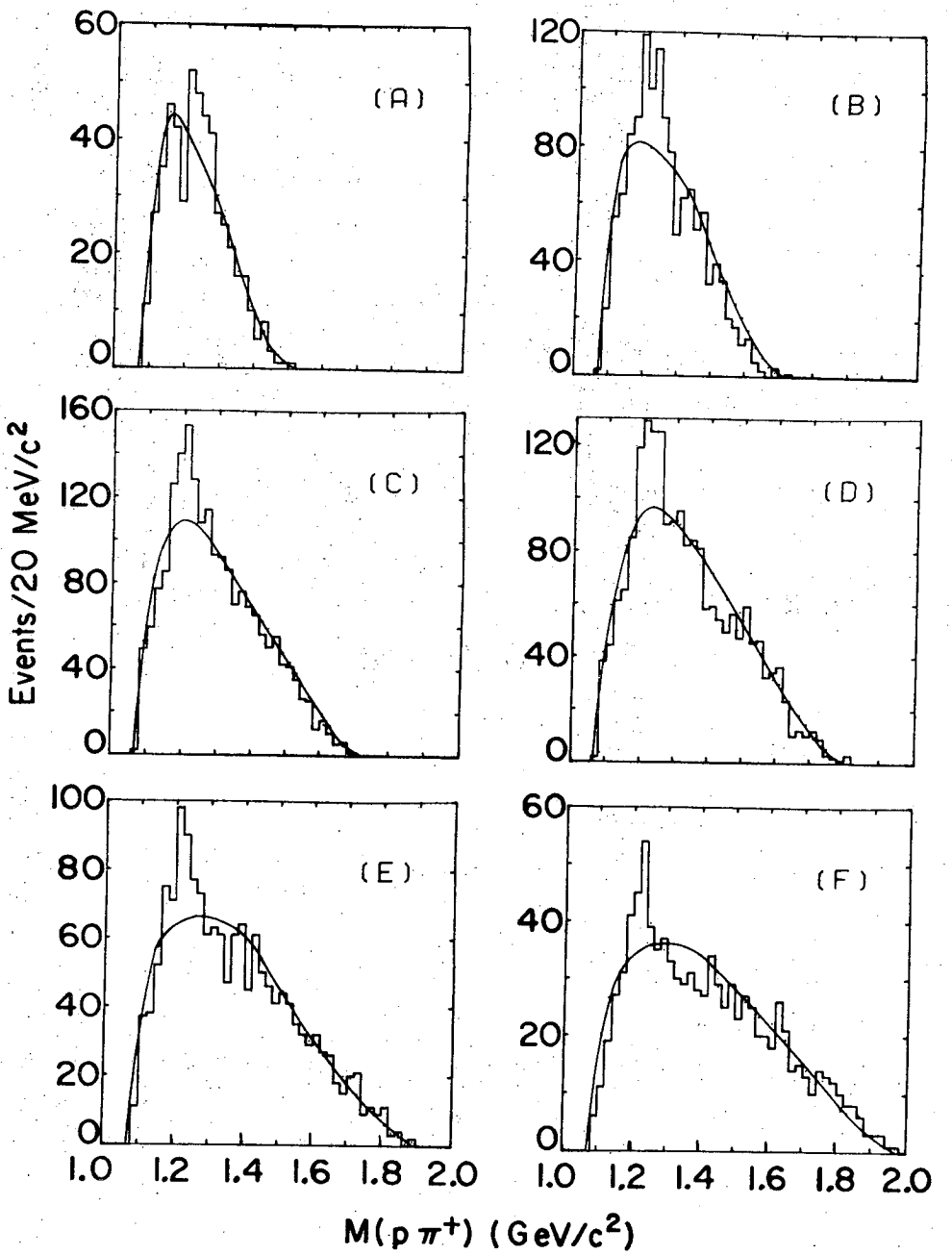

XBL 696-752

Figure 10.

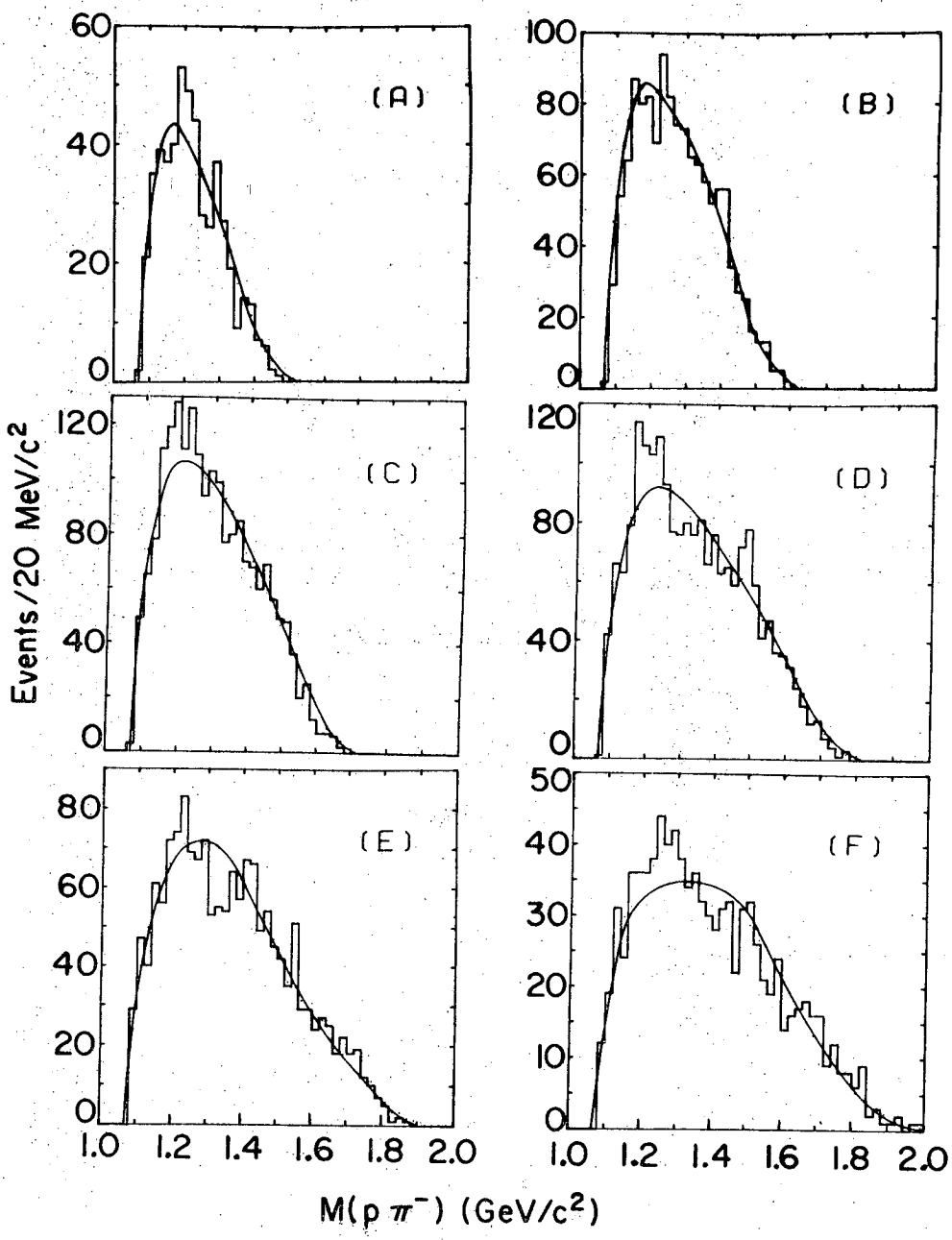

XBL 696-766

Figure 11.

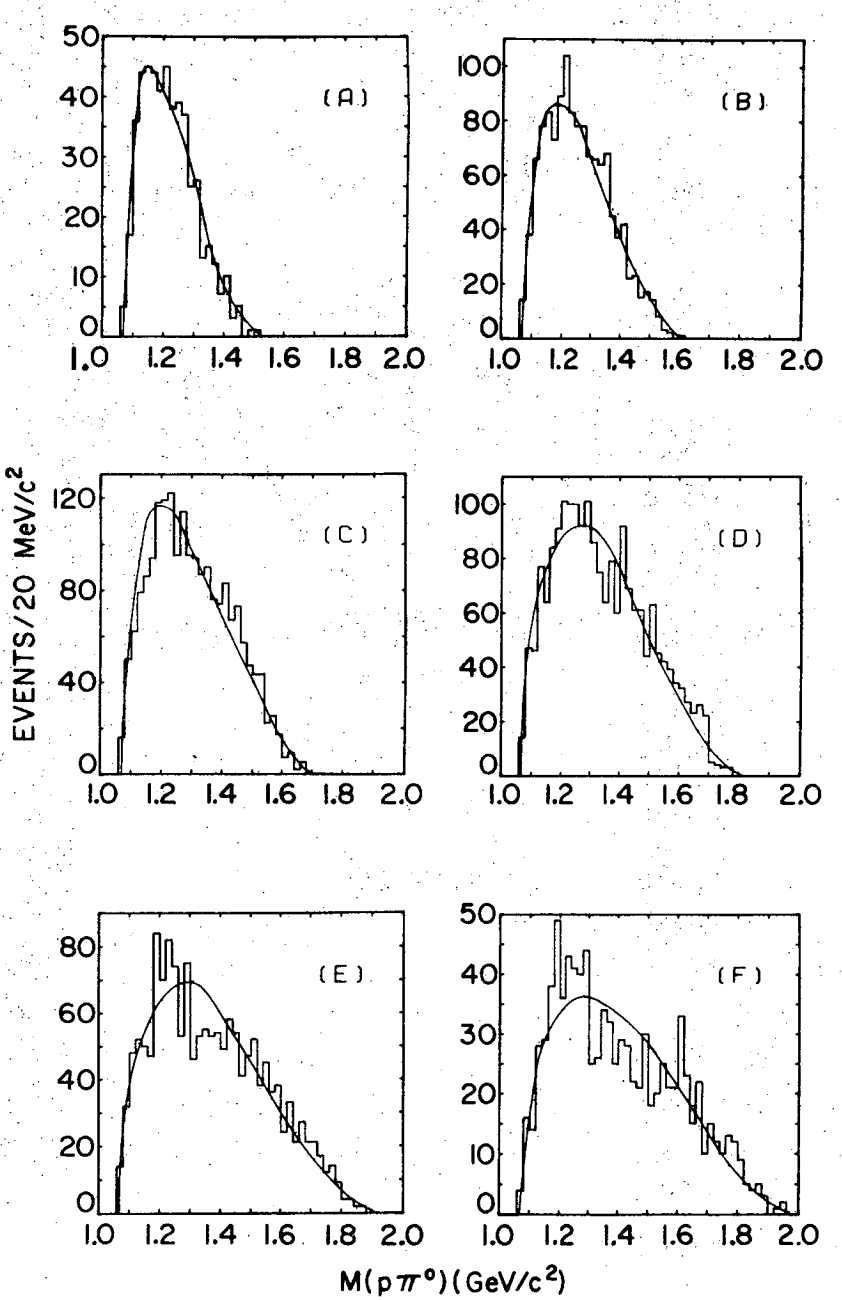

Figure 12.

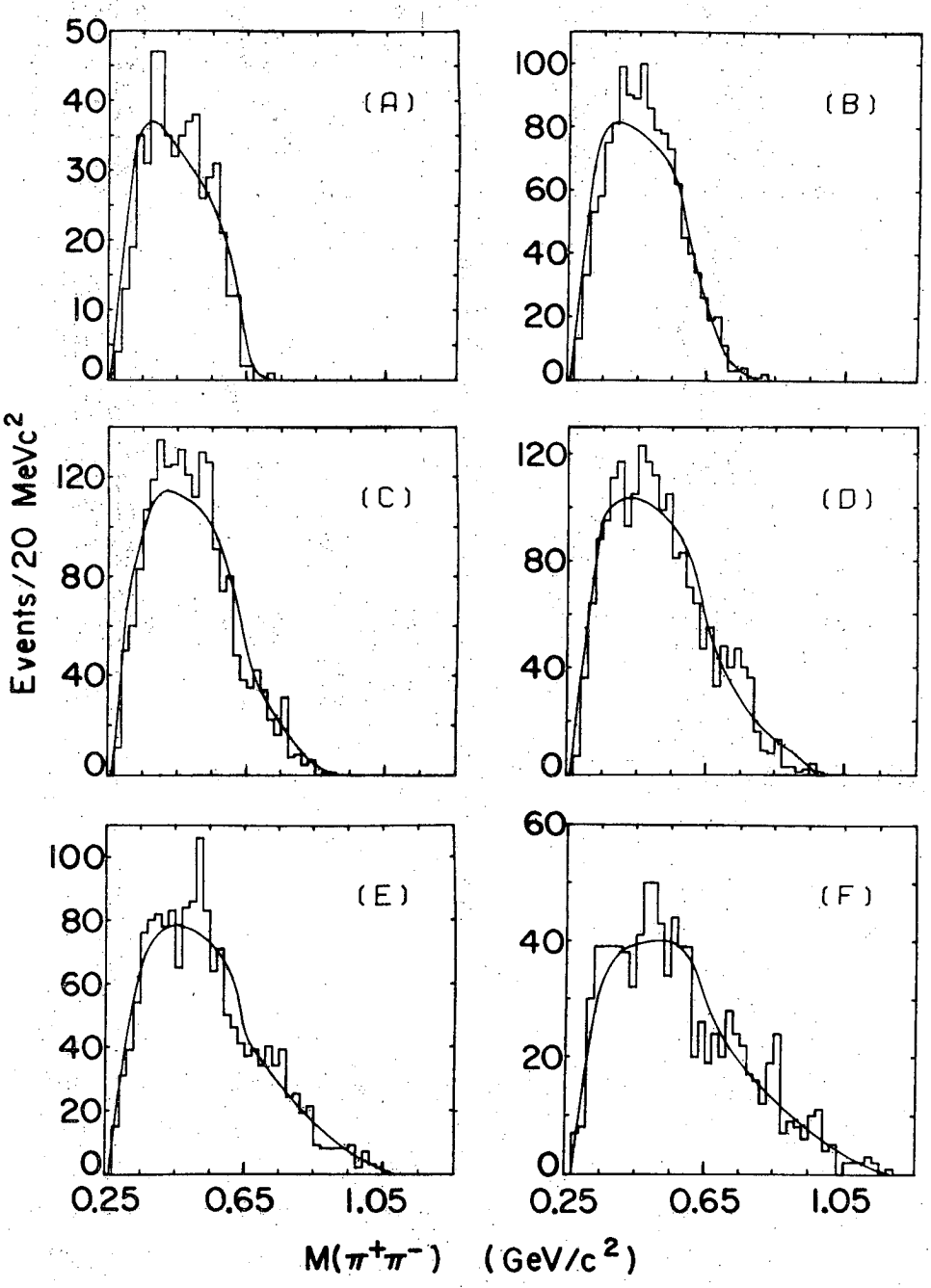

XBL 696-751

Figure 13.

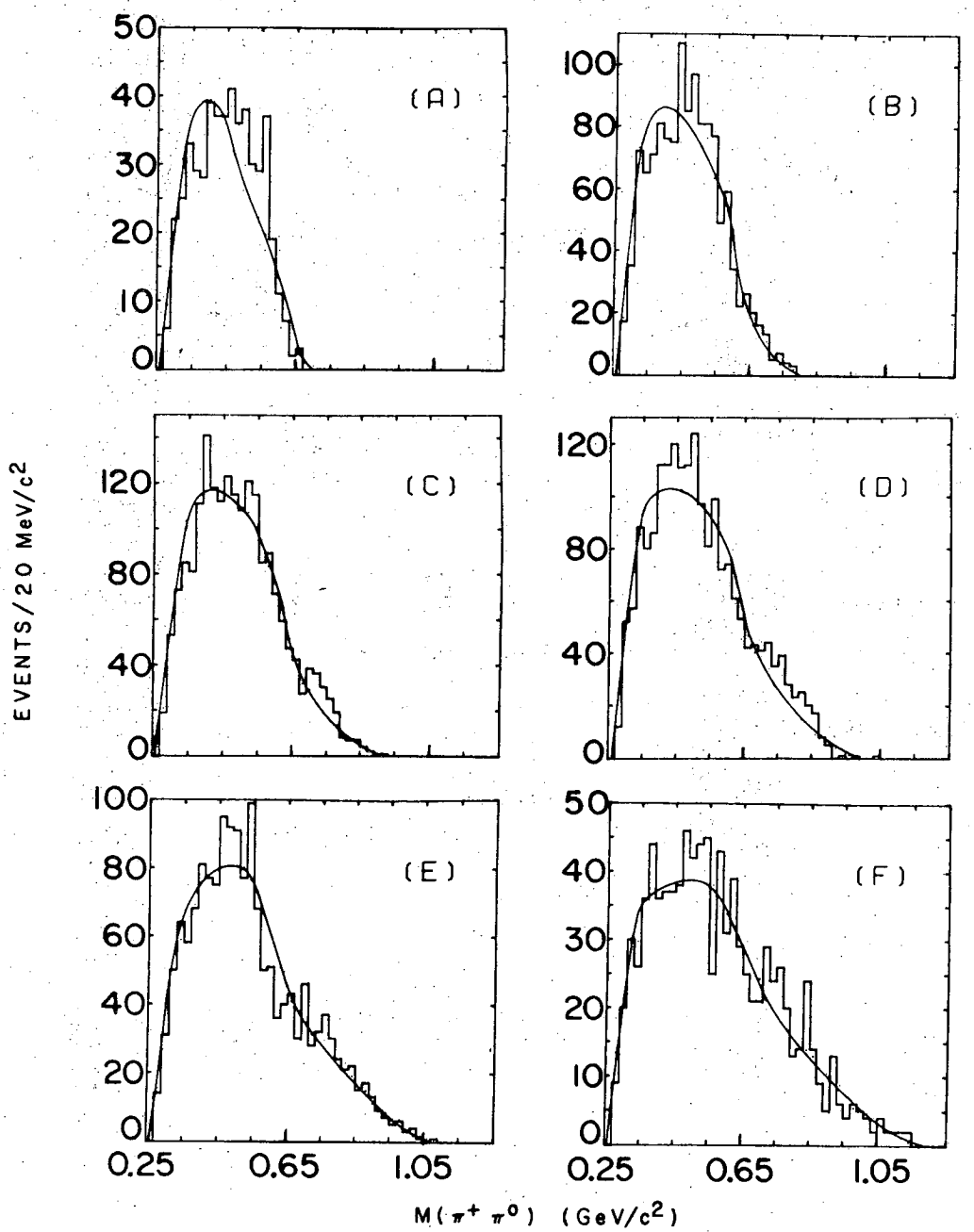

XBL 696-750

Figure 14.

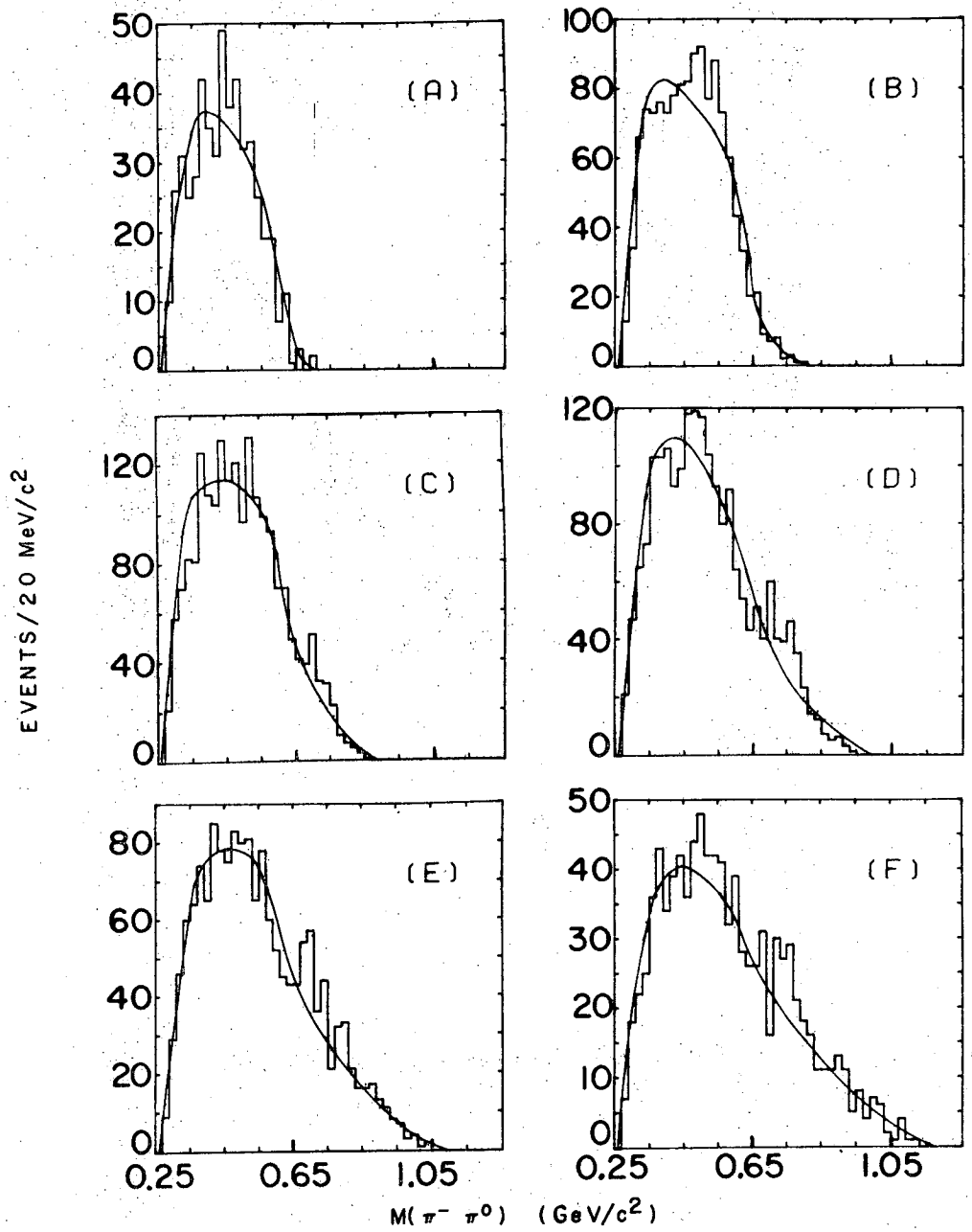

XBL 696-749

Figure 15.

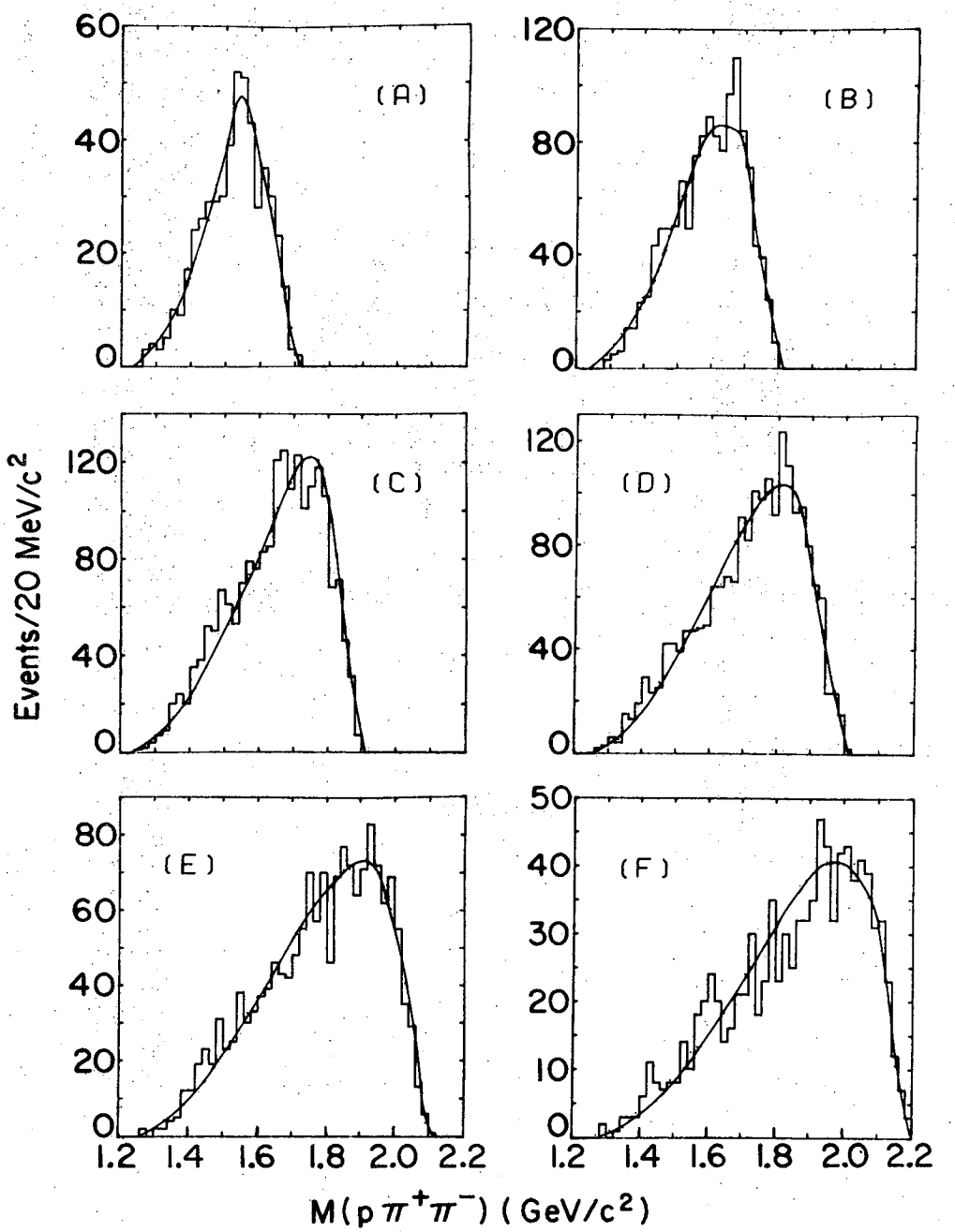

XBL 696-747

Figure 16.

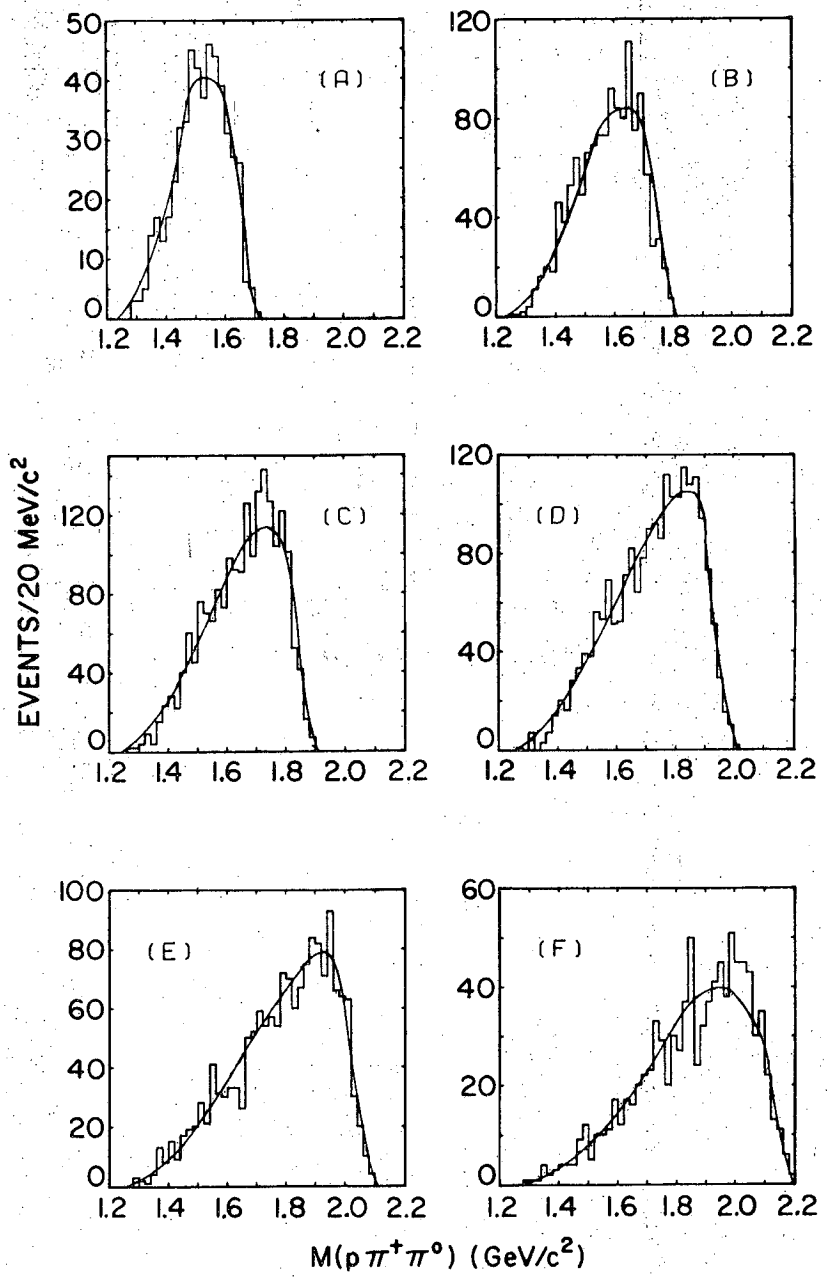

XBL 696-748

Figure 17.

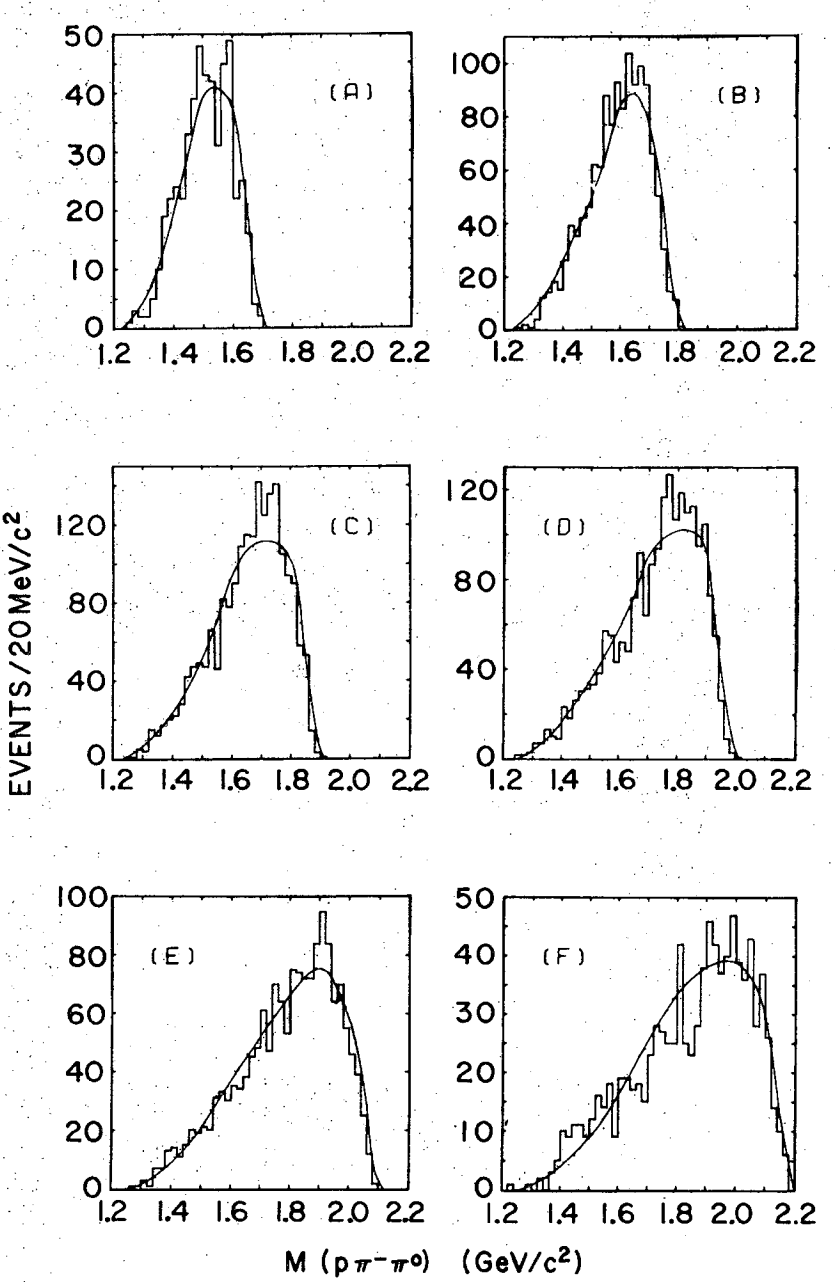

XBL 696-746

Figure 18.

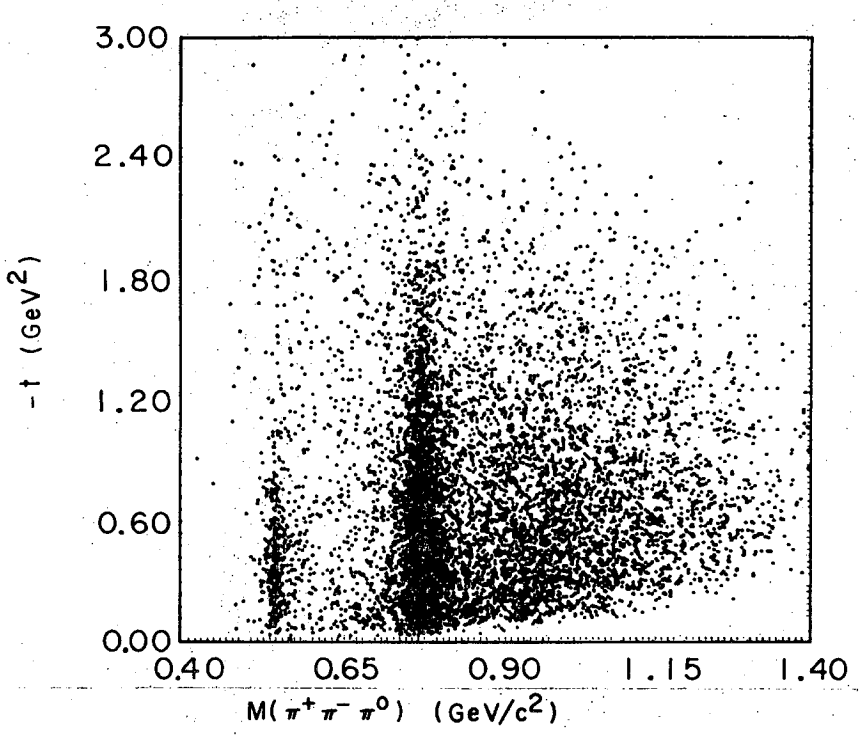

Figure 19.

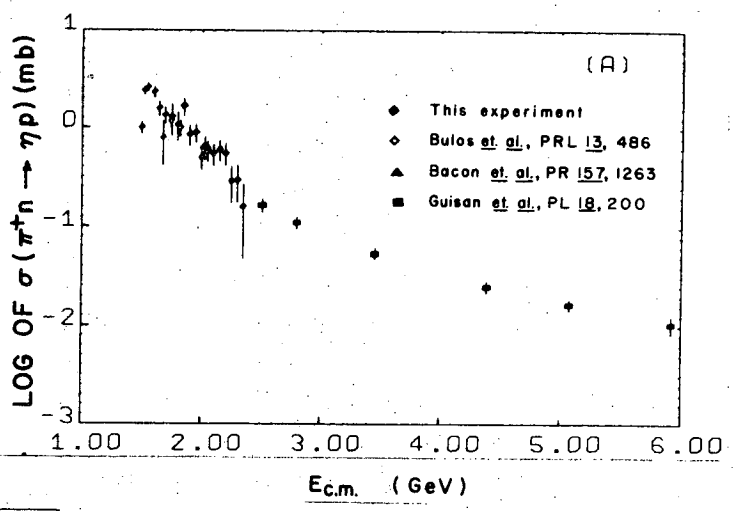

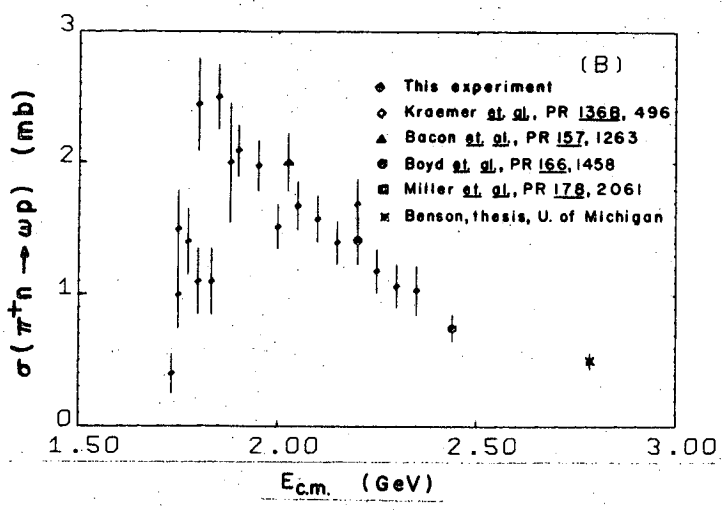

Figure 20.

XBL 694-791

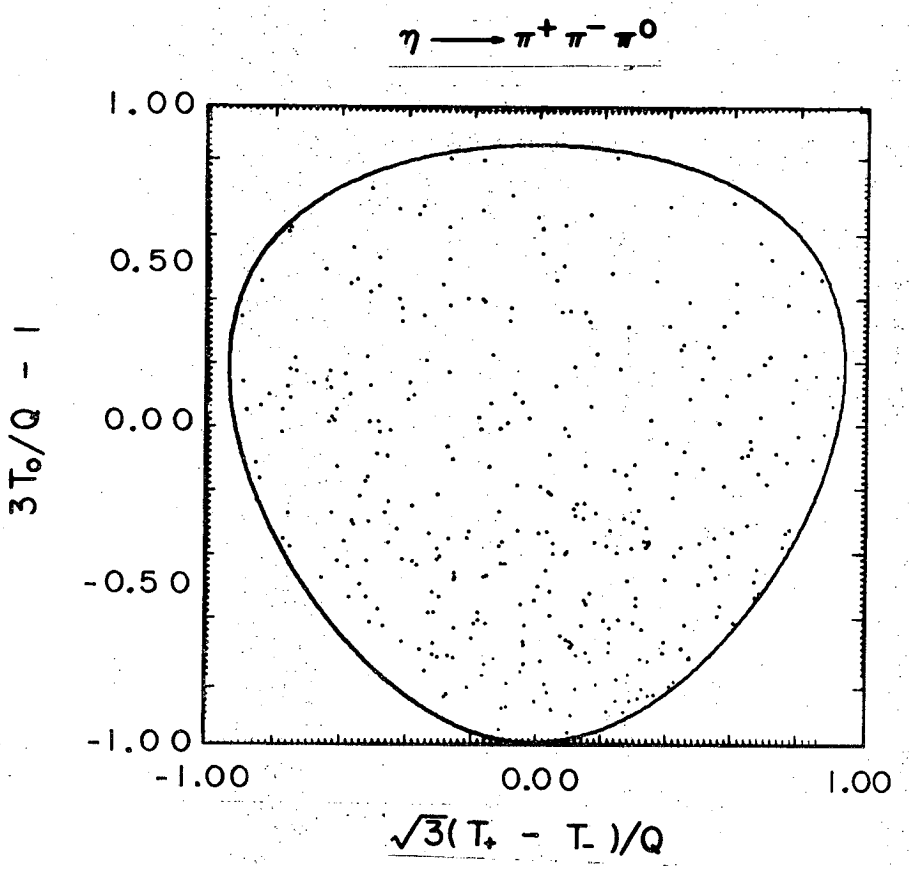

Figure 21.

XBL 696-797

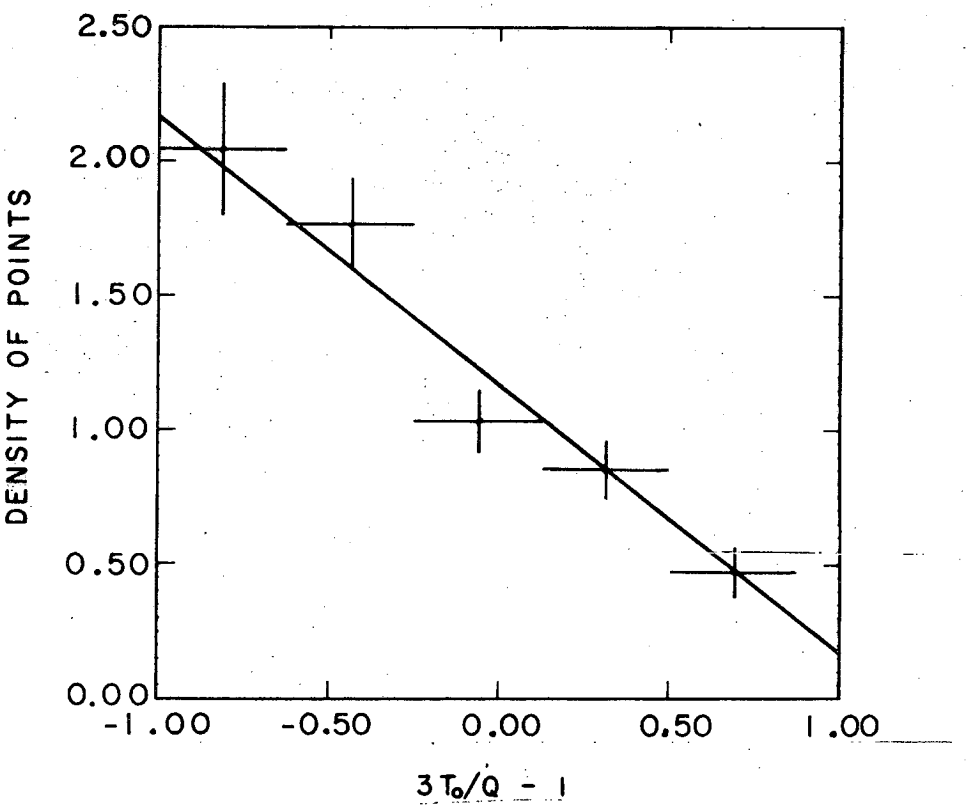

Figure 22.

XBL 696-795

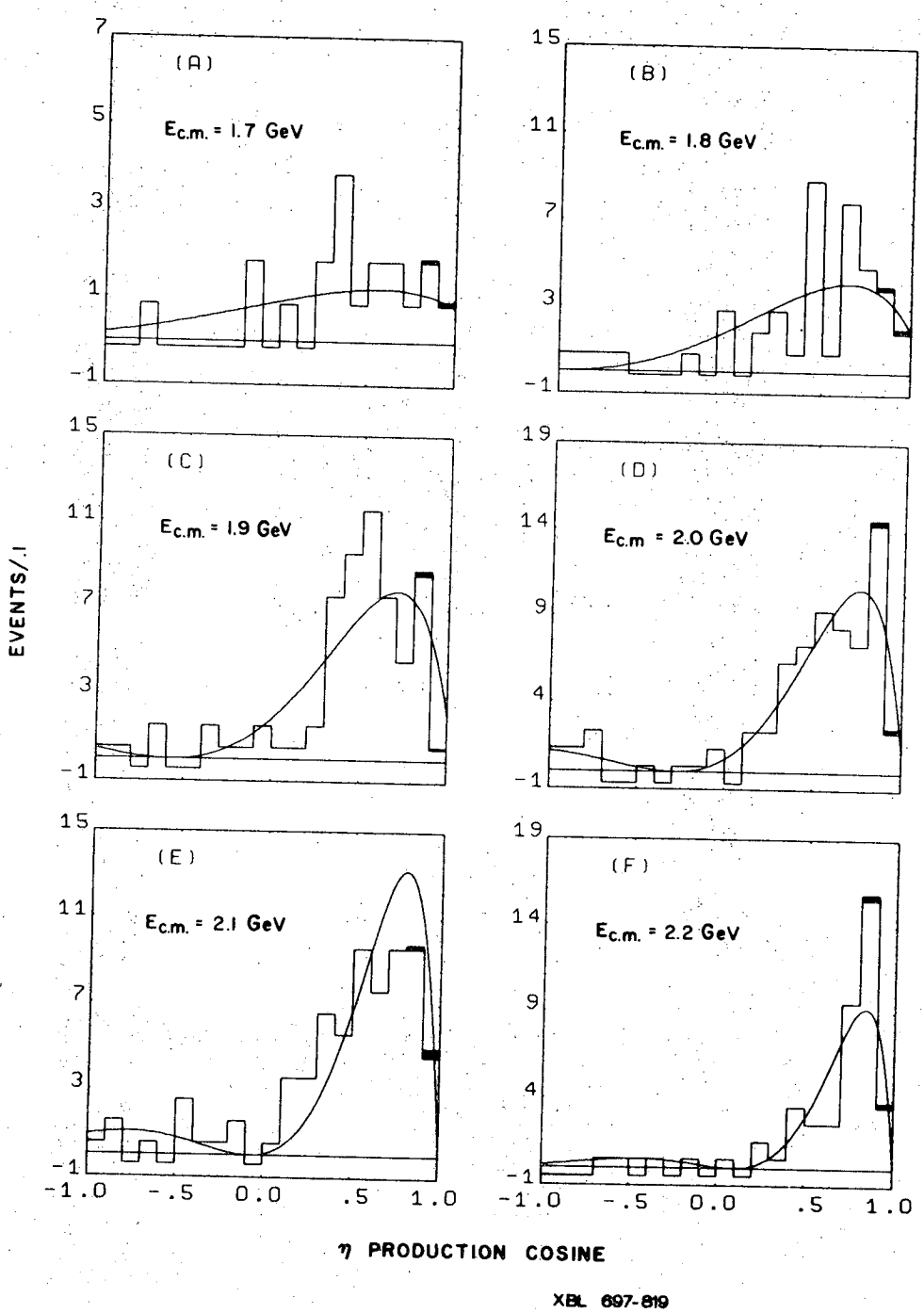
(A)
$E_{c.m.}$ = 1.7 GeV
(B)
$E_{c.m.}$ = 1.8 GeV
(C)
$E_{c.m.}$ = 1.9 GeV
(D)
$E_{c.m}$ = 2.0 GeV
(E)
$E_{c.m.}$ = 2.1 GeV
(F)
$E_{c.m.}$ = 2.2 GeV
EVENTS/.1
η PRODUCTION COSINE
XBL 697-819

Figure 23.

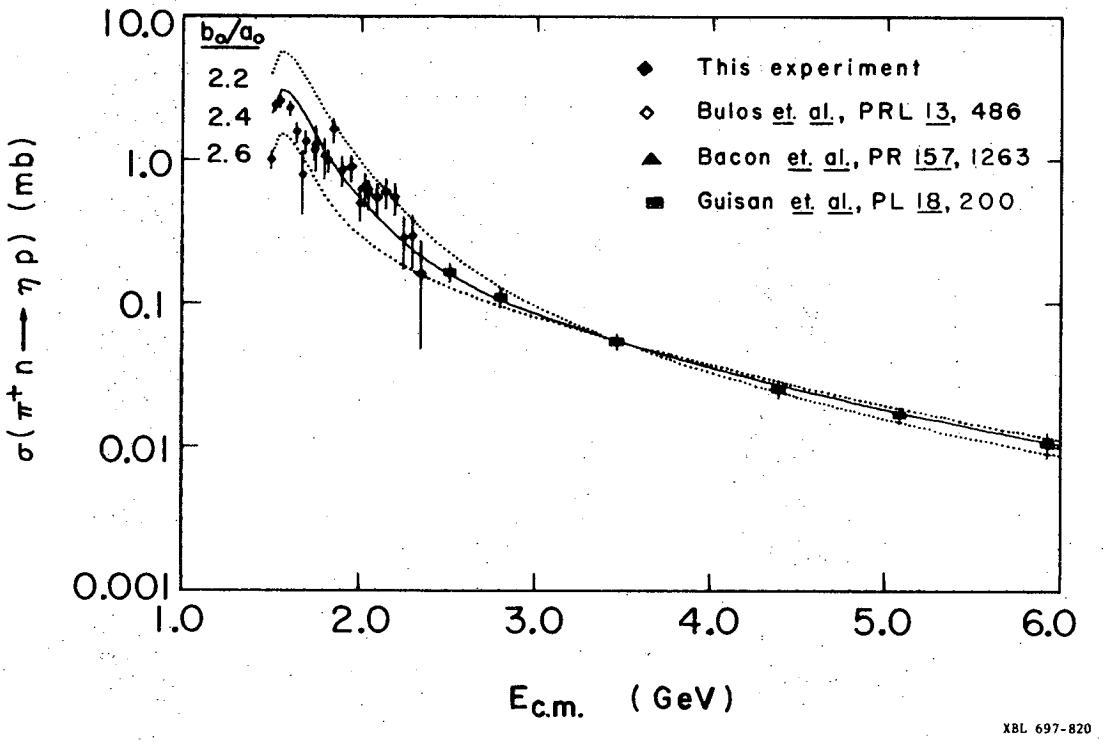
10.0
1.0
0.1
0.01
0.001
1.0
2.0
3.0
4.0
5.0
6.0
b_o/a_o
2.2
2.4
2.6
This experiment
Bulos et. al., PRL 13, 486
Bacon et. al., PR 157, 1263
Guisan et. al., PL 18, 200
$\sigma(\pi^+ n \rightarrow \eta p)$ (mb)
$E_{c.m.}$ (GeV)
XBL 697-820

Figure 24.

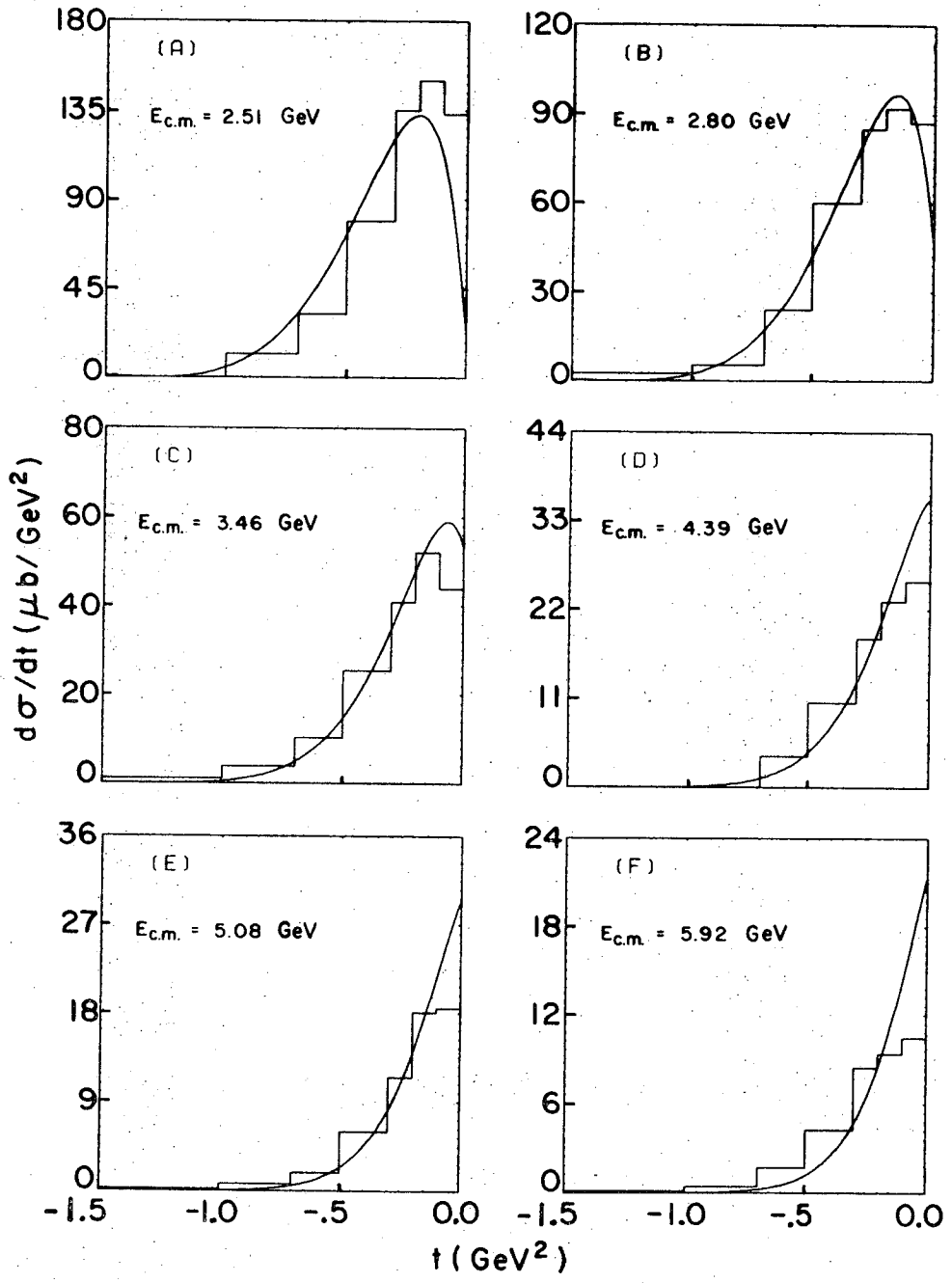
(A)
$E_{c.m.}$ = 2.51 GeV
(B)
$E_{c.m.}$ = 2.80 GeV
(C)
$E_{c.m.}$ = 3.46 GeV
(D)
$E_{c.m.}$ = 4.39 GeV
(E)
$E_{c.m.}$ = 5.08 GeV
(F)
$E_{c.m.}$ = 5.92 GeV
$d\sigma/dt\ (\mu b/GeV^2)$
$t\ (GeV^2)$
XBL 697-818

Figure 25.

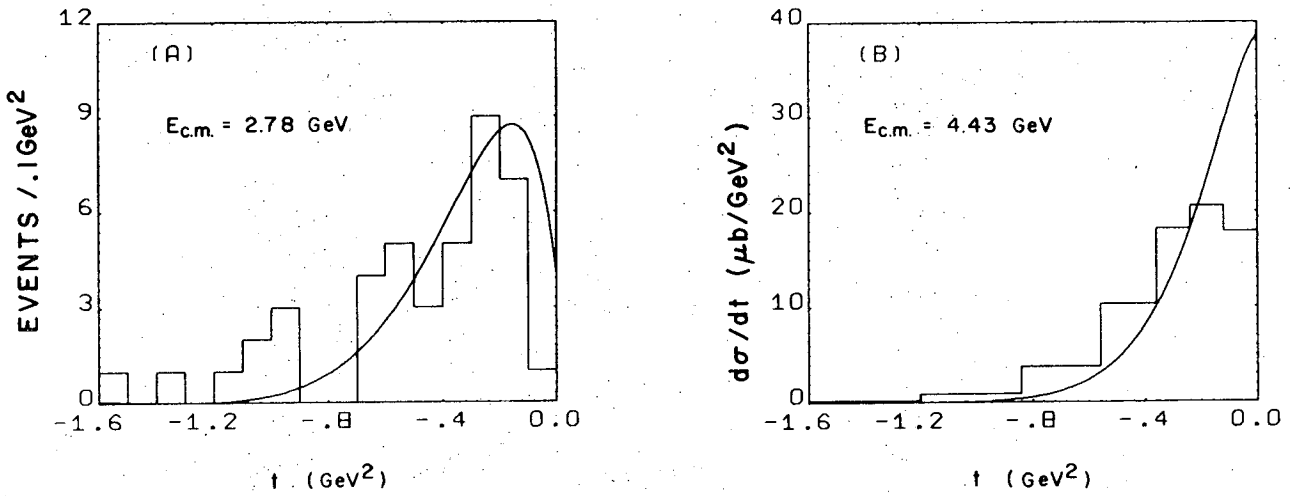

Figure 26.

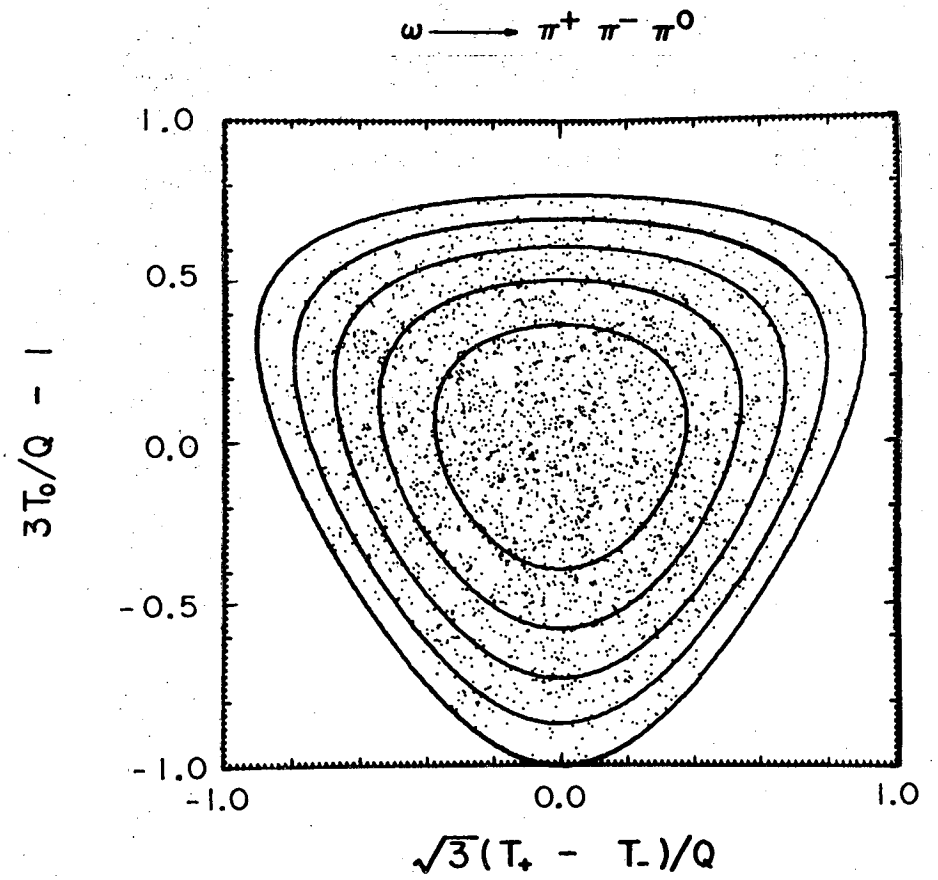

Figure 27.

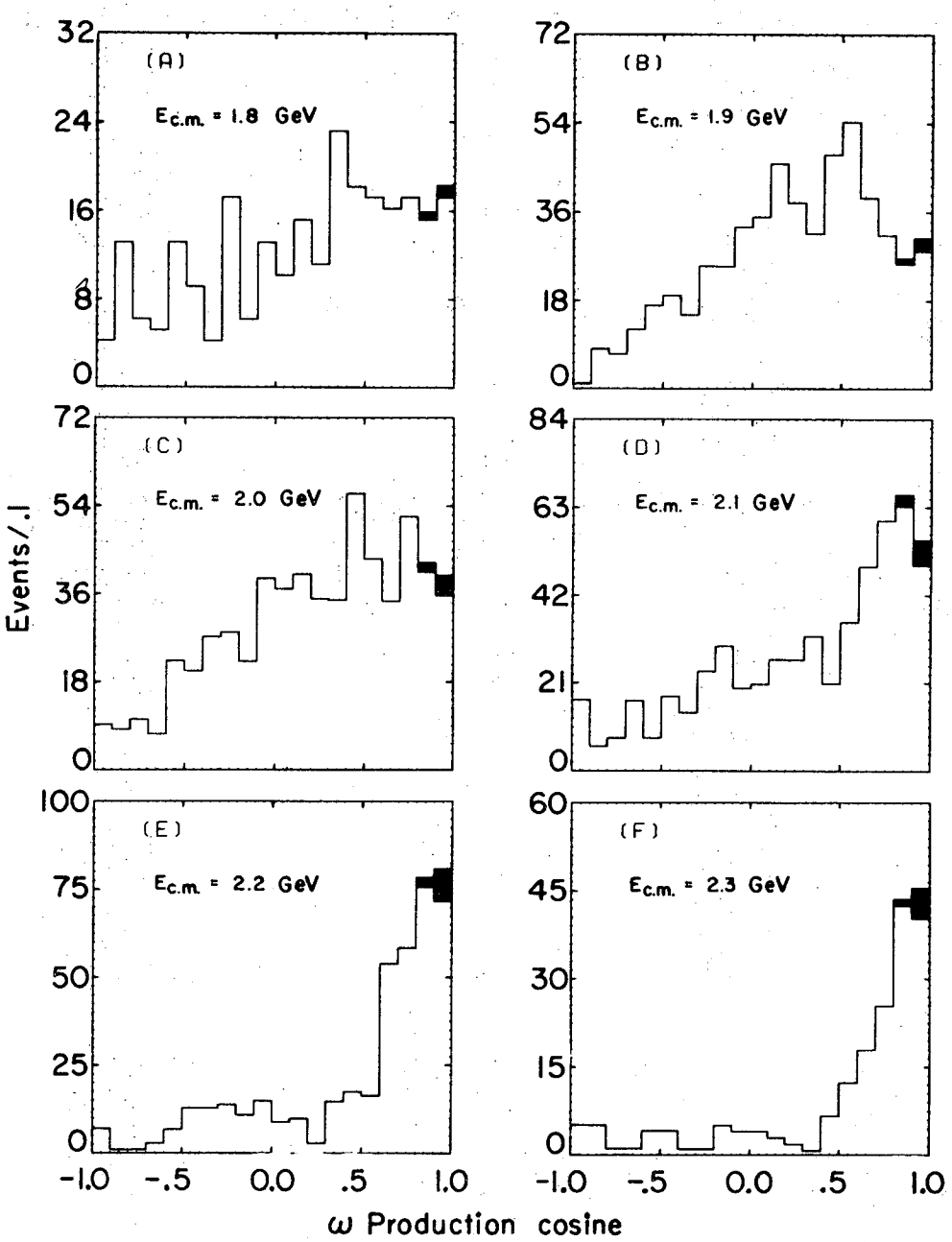
(A)
Ec.m. = 1.8 GeV
(B)
Ec.m. = 1.9 GeV
(C)
Ec.m. = 2.0 GeV
(D)
Ec.m. = 2.1 GeV
(E)
Ec.m. = 2.2 GeV
(F)
Ec.m. = 2.3 GeV
Events/.1
ω Production cosine
XBL 697-894

Figure 28.

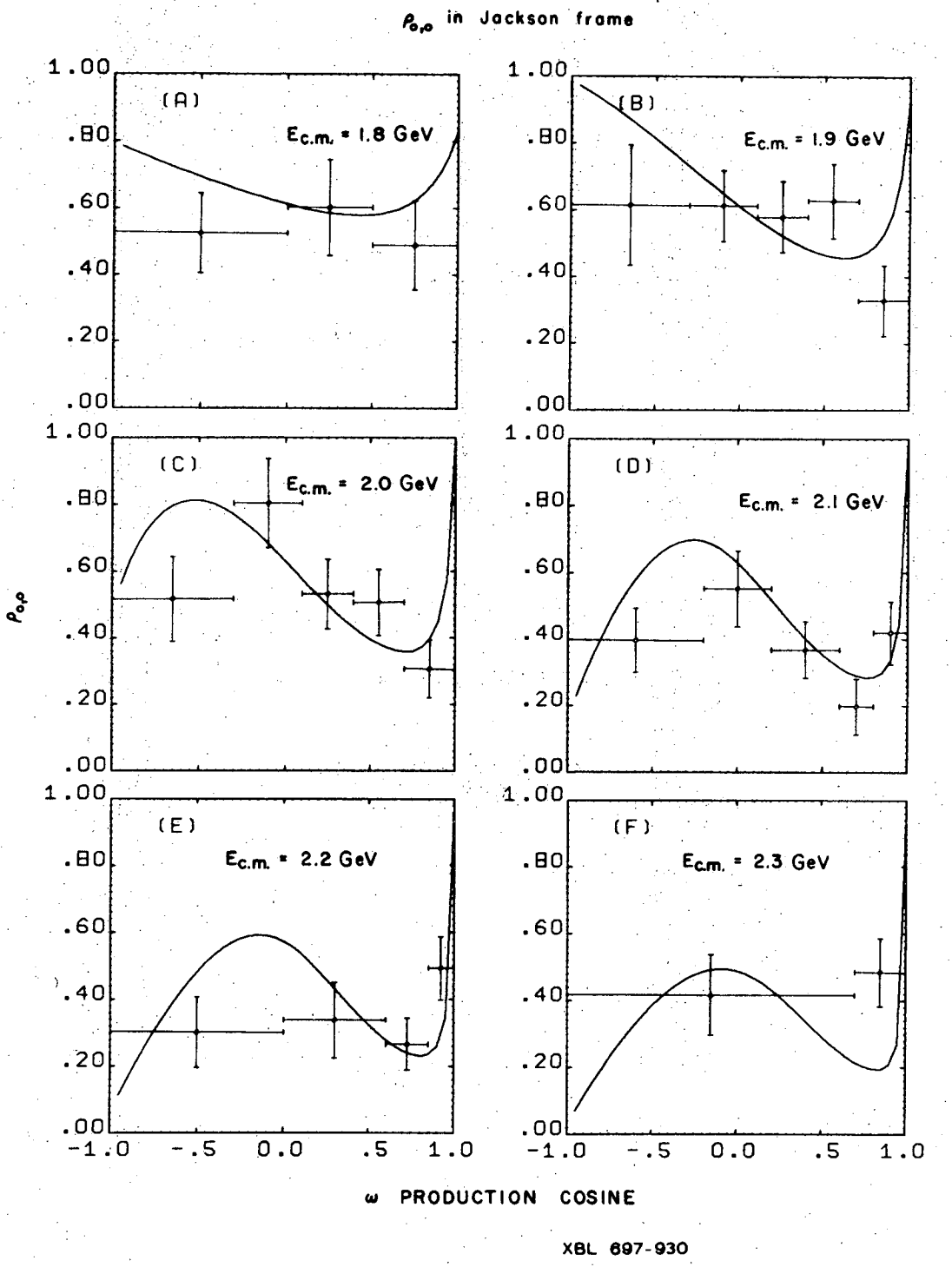
$\rho_{0,0}$ in Jackson frame
(A)
$E_{c.m.}$ = 1.8 GeV
(B)
$E_{c.m.}$ = 1.9 GeV
(C)
$E_{c.m.}$ = 2.0 GeV
(D)
$E_{c.m.}$ = 2.1 GeV
(E)
$E_{c.m.}$ = 2.2 GeV
(F)
$E_{c.m.}$ = 2.3 GeV
$\rho_{0,0}$
1.00
.80
.60
.40
.20
.00
-1.0
-.5
0.0
.5
1.0
ω PRODUCTION COSINE
XBL 697-930

Figure 29.

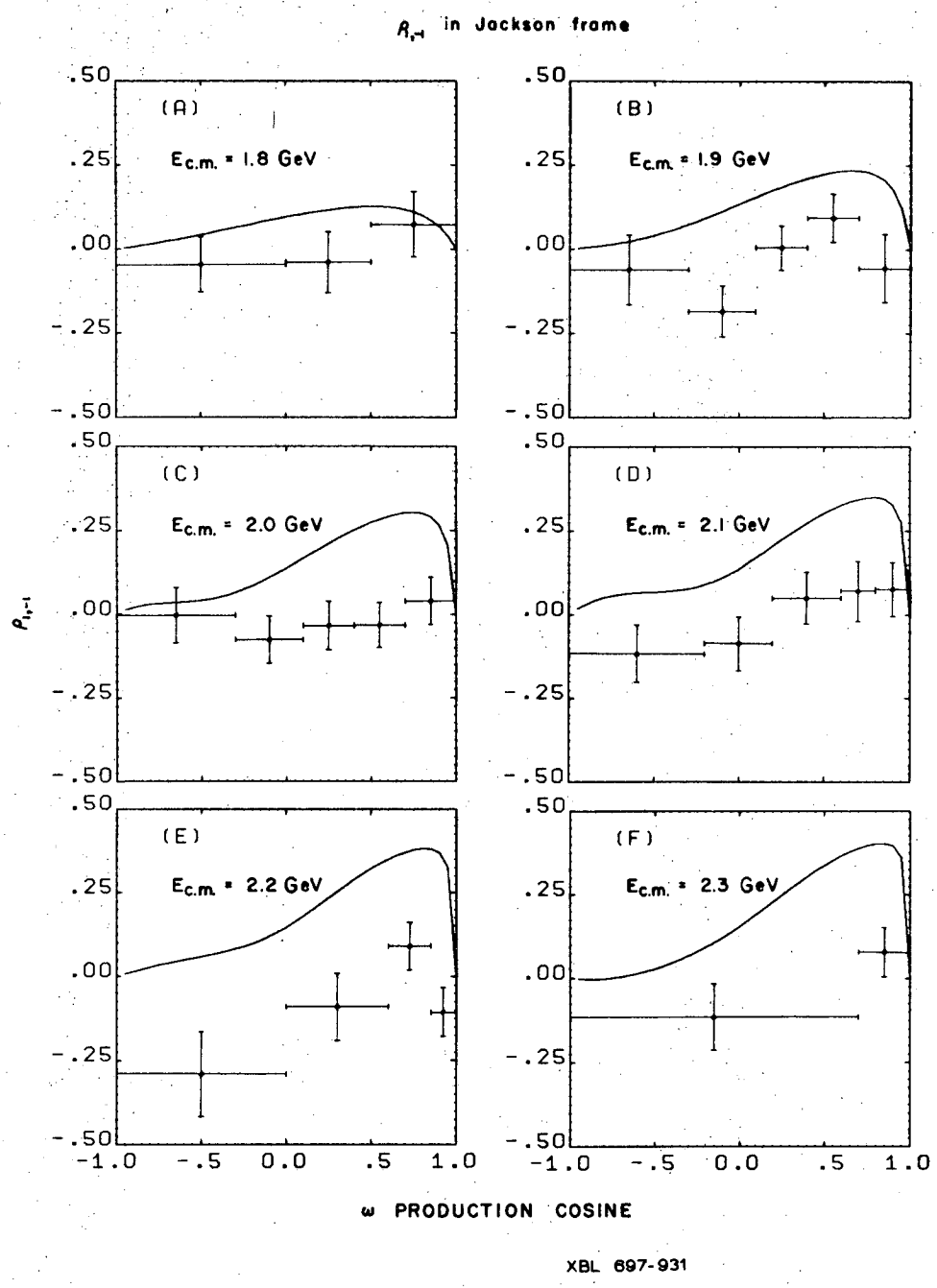
$R_{1,-1}$ in Jackson frame
(A)
$E_{c.m.}$ = 1.8 GeV
(B)
$E_{c.m.}$ = 1.9 GeV
(C)
$E_{c.m.}$ = 2.0 GeV
(D)
$E_{c.m.}$ = 2.1 GeV
(E)
$E_{c.m.}$ = 2.2 GeV
(F)
$E_{c.m.}$ = 2.3 GeV
.50
.25
.00
-.25
-.50
$R_{1,-1}$
-1.0
-.5
0.0
.5
1.0
ω PRODUCTION COSINE
XBL 697-931

Figure 30.

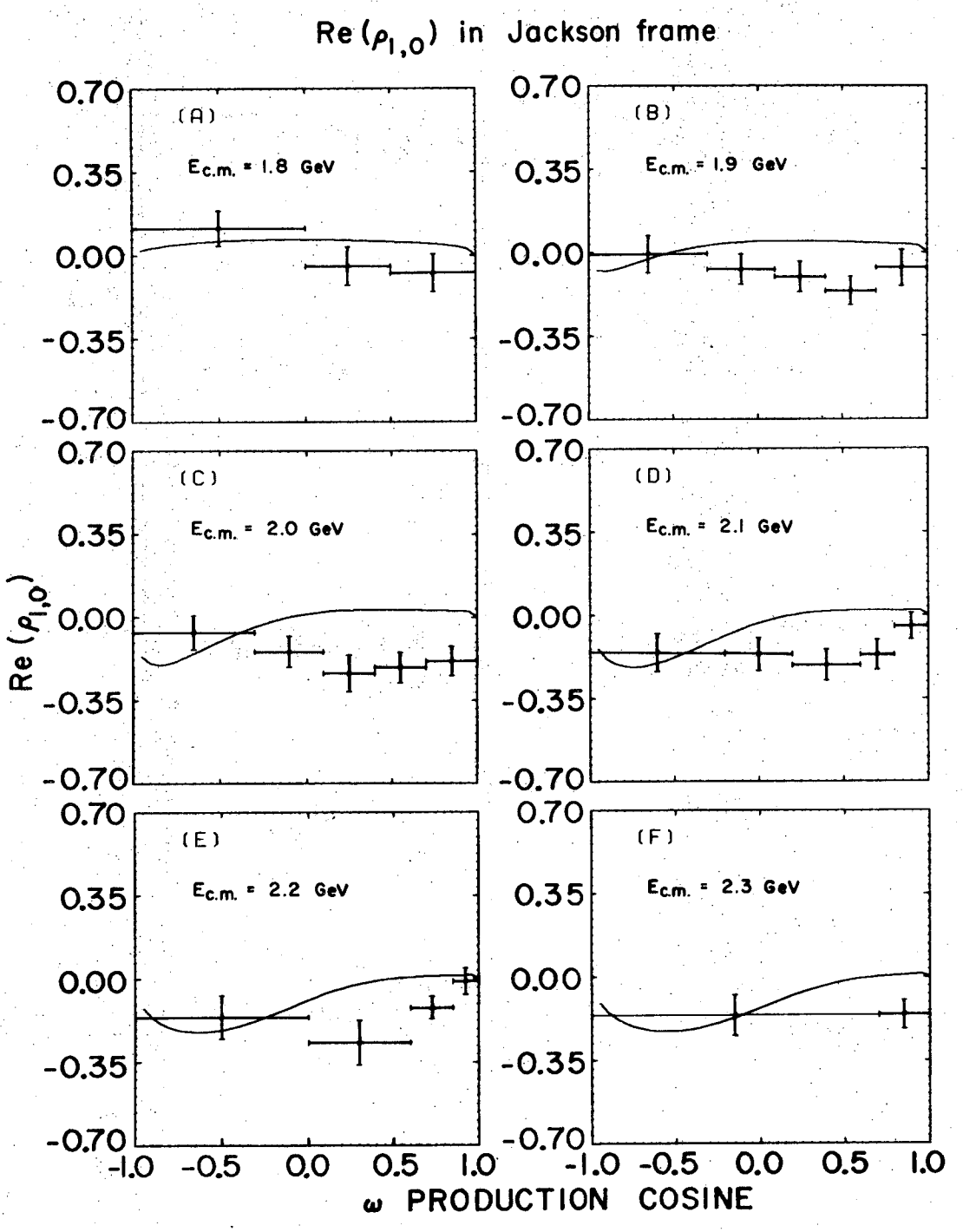
Re $(\rho_{1,0})$ in Jackson frame
(A)
$E_{c.m.}$ = 1.8 GeV
(B)
$E_{c.m.}$ = 1.9 GeV
(C)
$E_{c.m.}$ = 2.0 GeV
(D)
$E_{c.m.}$ = 2.1 GeV
(E)
$E_{c.m.}$ = 2.2 GeV
(F)
$E_{c.m.}$ = 2.3 GeV
Re $(\rho_{1,0})$
0.70
0.35
0.00
-0.35
-0.70
-1.0 -0.5 0.0 0.5 1.0
ω PRODUCTION COSINE
XBL 697-932

Figure 31.

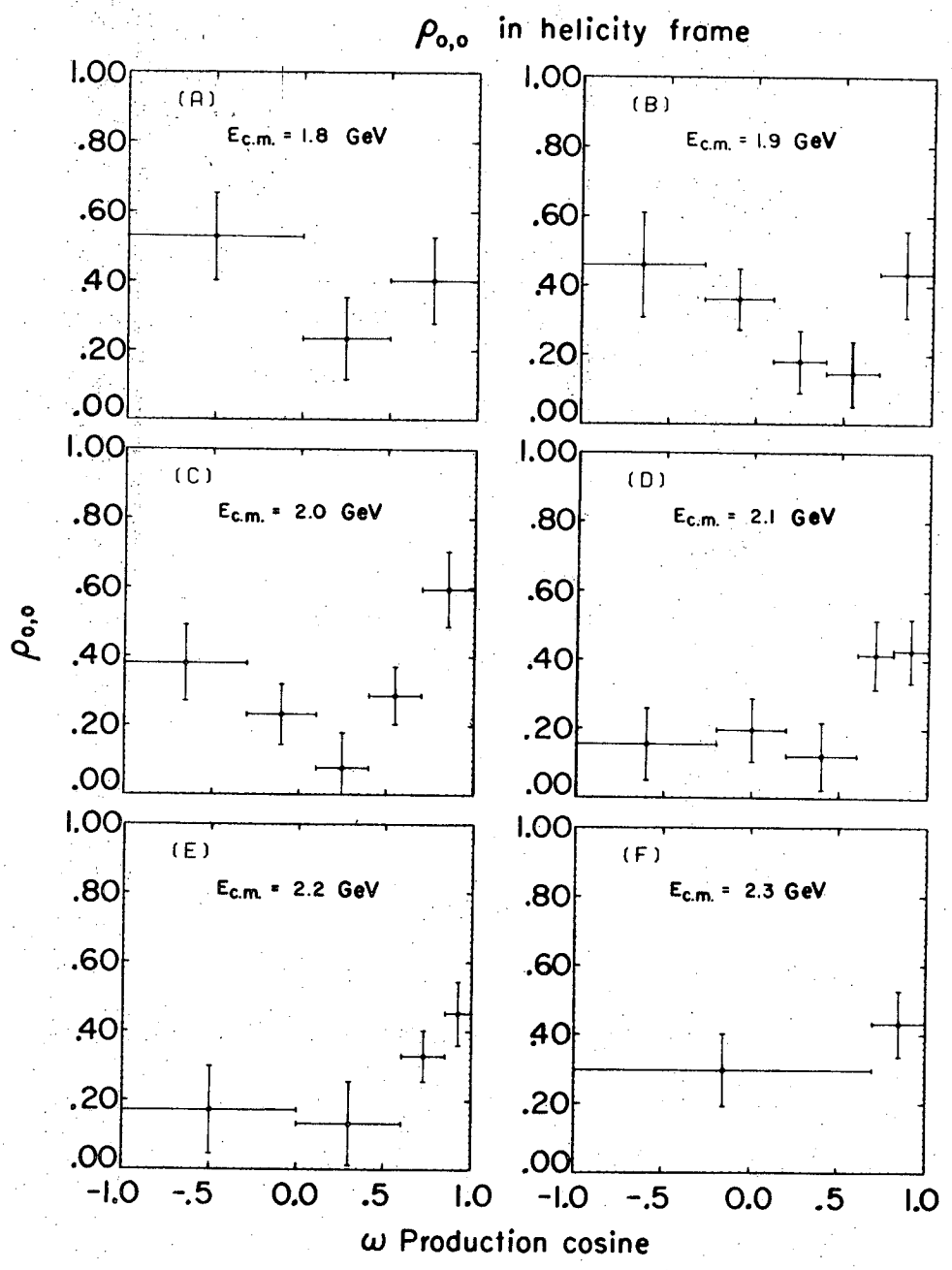
$\rho_{0,0}$ in helicity frame
(A)
$E_{c.m.}$ = 1.8 GeV
(B)
$E_{c.m.}$ = 1.9 GeV
(C)
$E_{c.m.}$ = 2.0 GeV
(D)
$E_{c.m.}$ = 2.1 GeV
(E)
$E_{c.m.}$ = 2.2 GeV
(F)
$E_{c.m.}$ = 2.3 GeV
$\rho_{0,0}$
1.00
.80
.60
.40
.20
.00
-1.0
-.5
0.0
.5
1.0
ω Production cosine
XBL 697-893

Figure 32.

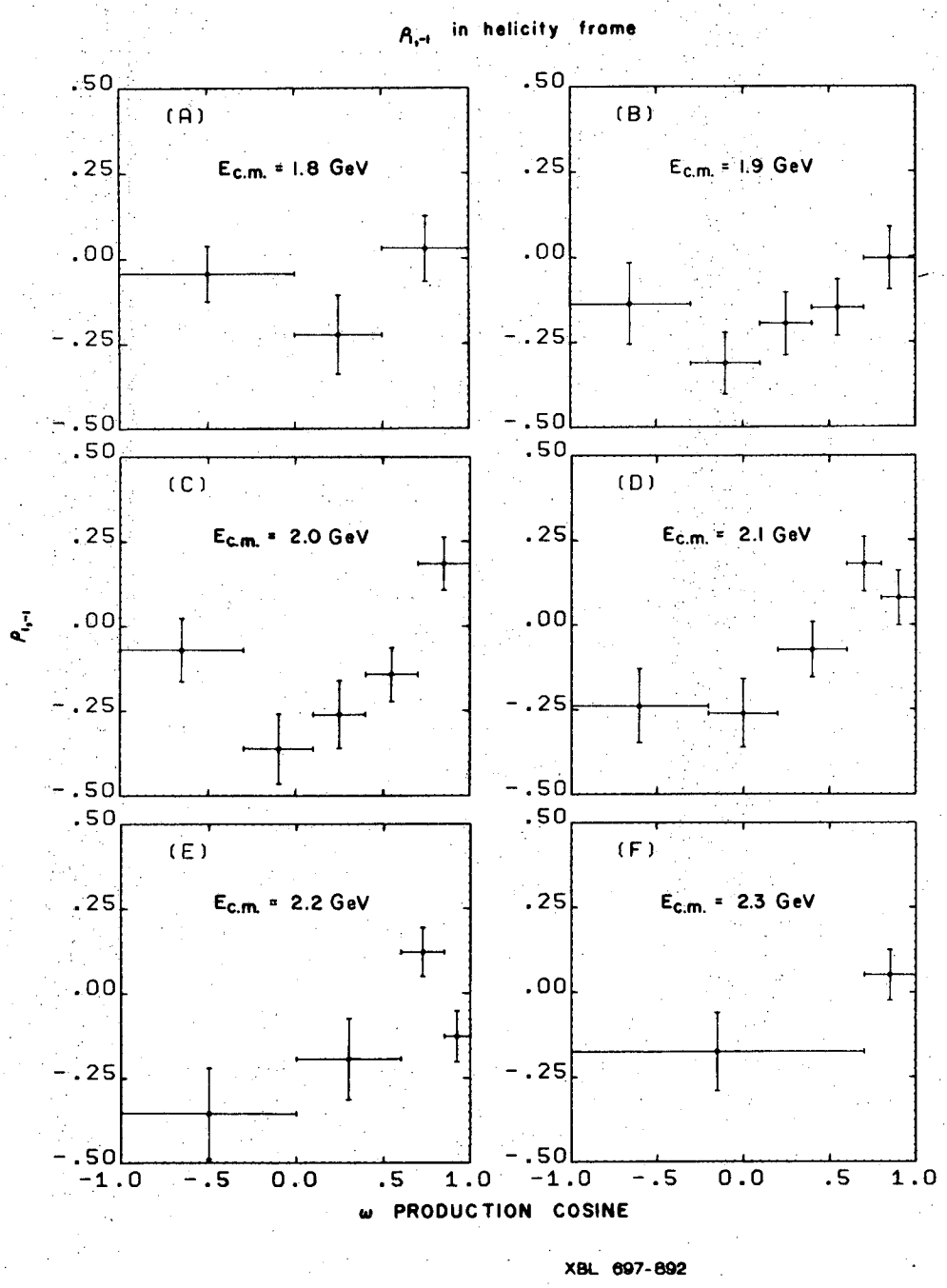
$A_{1,-1}$ in helicity frame
(A)
$E_{c.m.}$ = 1.8 GeV
(B)
$E_{c.m.}$ = 1.9 GeV
(C)
$E_{c.m.}$ = 2.0 GeV
(D)
$E_{c.m.}$ = 2.1 GeV
(E)
$E_{c.m.}$ = 2.2 GeV
(F)
$E_{c.m.}$ = 2.3 GeV
$\rho_{1,-1}$
.50
.25
.00
-.25
-.50
-1.0
-.5
0.0
.5
1.0
ω PRODUCTION COSINE
XBL 697-892

Figure 33.

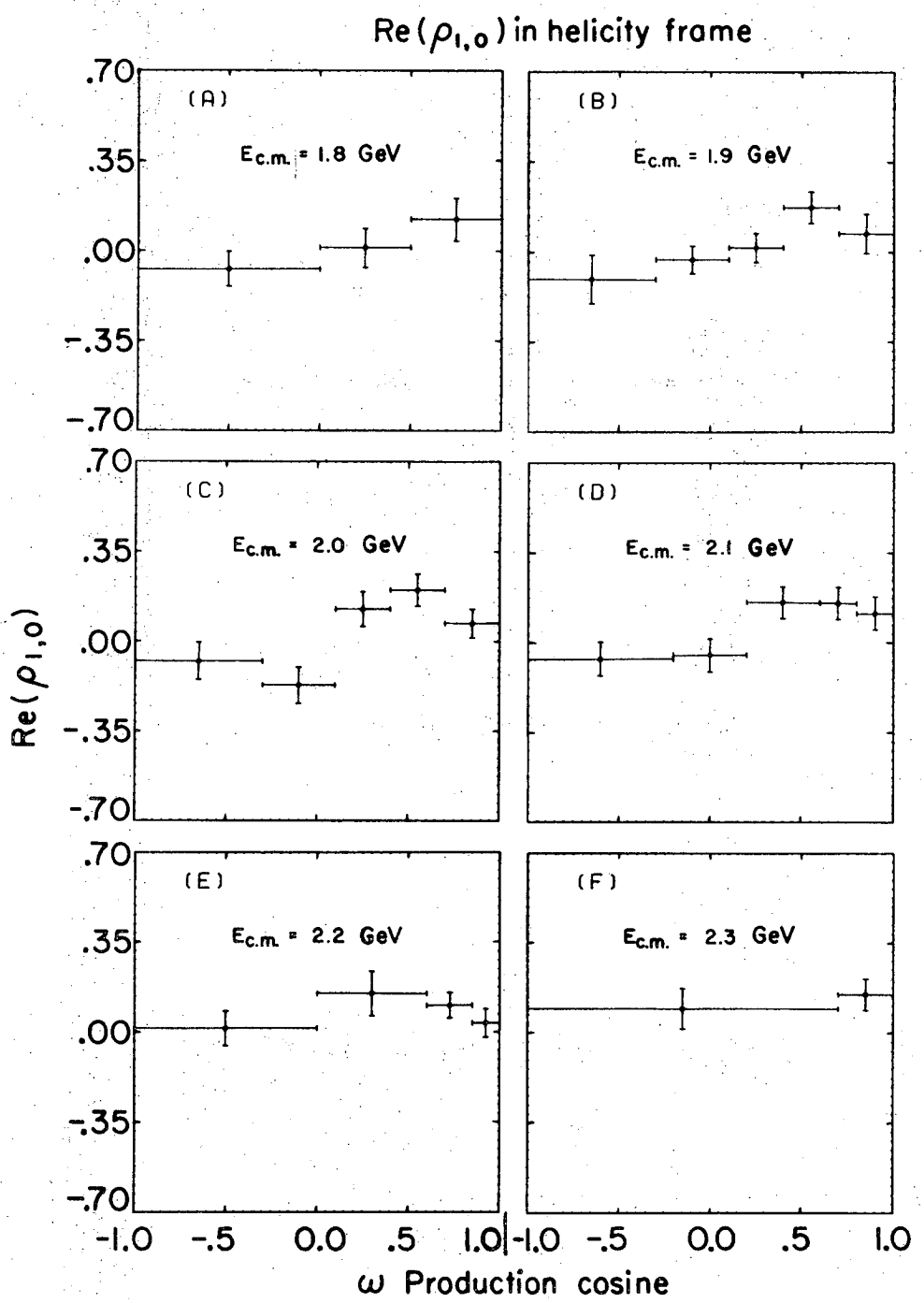
Re(ρ1,0) in helicity frame
(A)
Ec.m. = 1.8 GeV
(B)
Ec.m. = 1.9 GeV
(C)
Ec.m. = 2.0 GeV
(D)
Ec.m. = 2.1 GeV
(E)
Ec.m. = 2.2 GeV
(F)
Ec.m. = 2.3 GeV
Re(ρ1,0)
.70
.35
.00
-.35
-.70
-1.0
-.5
0.0
.5
1.0
ω Production cosine
XBL 697-891

Figure 34.

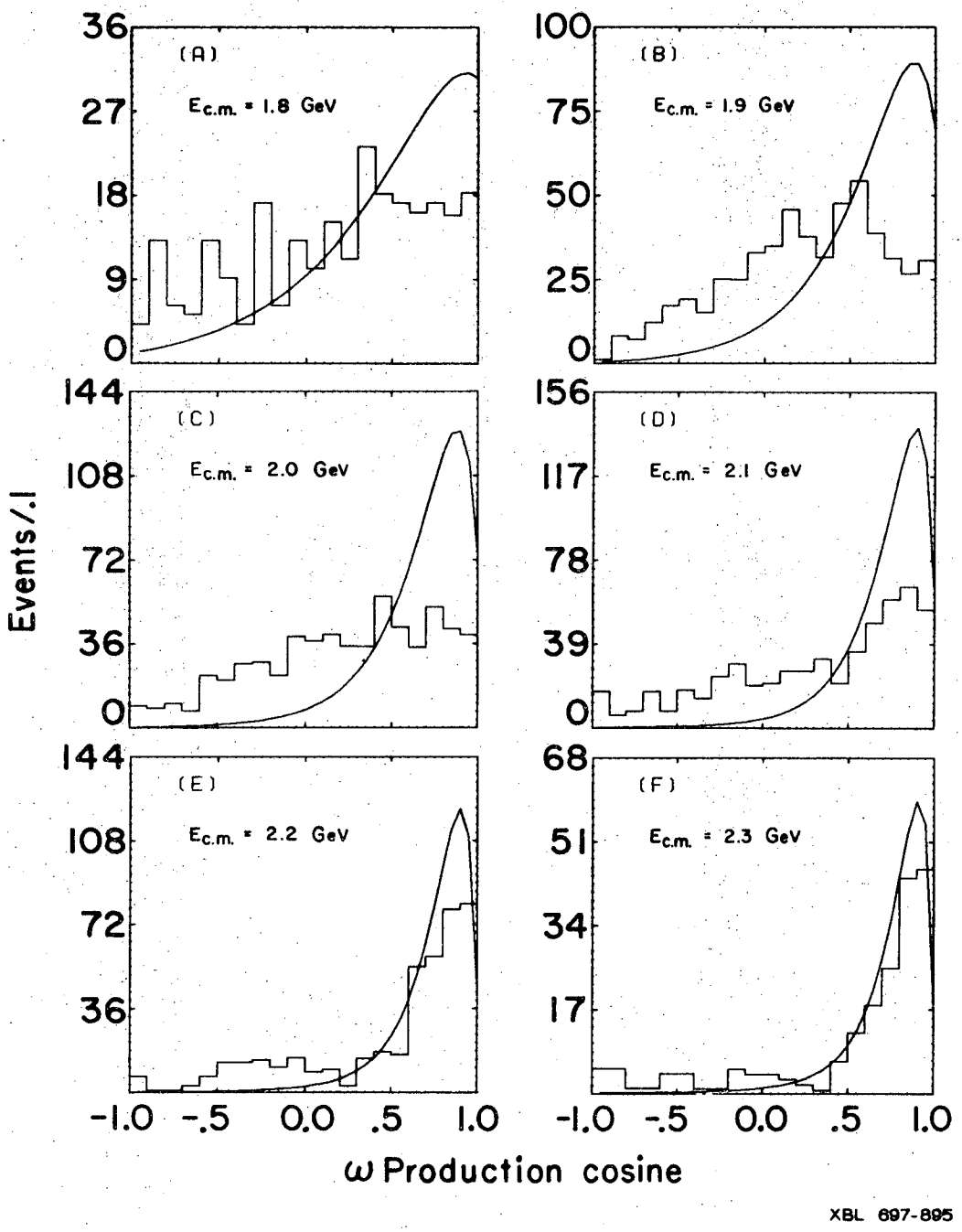
(A)
Ec.m. = 1.8 GeV
(B)
Ec.m. = 1.9 GeV
(C)
Ec.m. = 2.0 GeV
(D)
Ec.m. = 2.1 GeV
(E)
Ec.m. = 2.2 GeV
(F)
Ec.m. = 2.3 GeV
Events/.1
ω Production cosine
XBL 697-895

Figure 35.

TECHNICAL INFORMATION DIVISION
LAWRENCE RADIATION LABORATORY
UNIVERSITY OF CALIFORNIA
BERKELEY, CALIFORNIA 94720